OPEN-PIT SLOPE GEOTECHNICAL CONSIDERATIONS AND ITS EFFECTS ON MINE PLANNING

By

Bayasgalan Enkhbayar, B.S.

A Project Submitted in Partial Fulfillmetn of the Requirements

for the Degree of

Master of Science

in

Mining Engineering

University of Alaska Fairbanks

August 2020

APPROVED:

Dr. Gang Chen, Committee Chair
Dr. Il Sang Ahn, Committee Member
Dr. Sampurna Arya, Committee Member
Dr. Tathagata Ghosh, Department Chair
Department of Mining & Geological Engineering

Abstract

In open-pit mining, a stable pit slopes design is essential for safe operation and economic performance of the mine. However, a steeper pit is more desirable from an economic standpoint due to reduced overburden removal. As the mine deepens, the open-pit walls become increasingly prone to slope failure, which causes human and economic losses. Therefore, a feasible and stable slope mine design requires a serious geotechnical investigation. The optimization of this design requires steepening the overall slope angle as much as possible while maintaining mine safety for efficient and effective mining operations.

The open-pit slope geotechnical investigation calls for detailed geological and geotechnical data and advanced numerical modeling. In this study, geological and geotechnical data are collected from the Erdenet Copper Mine of Mongolia. The collected information includes data from discontinuity face mapping, geotechnical core logging, groundwater condition, geological exploration cross-sections, pit map, and rock property lab test results. The open-pit slope stability is analyzed with geotechnical numerical modeling software FLAC2D, and the variation and distribution of factors of safety (FOS) are computed and studied.

The stability of Erdenet mine's North-West open-pit is simulated by dividing the pit into ten representative cross-sections, and subsequently, FOS is calculated for each cross-section. The simulation results show that each cross-section has a higher overall FOS value than the allowable mine FOS, set at 1.5 with an earthquake magnitude of 0.165g peak ground acceleration (PGA). However, the localized high shear strain on individual benches may still occur, which can cause potential failures. Parametric studies indicate that changes in the bench angles and rock mass properties will have various degrees of impact on pit slope FOS. The effect of bench angle changes appears to be more significant. The study of pit slope design on mine planning shows that a 1° increase on slope angle will reduce excavation volume by 5 M m^3 and save $15 million in excavation cost, but will also reduce FOS by 0.12. Engineering judgment and decision will have to be made regarding this tradeoff for a safe and economical mining operation.

Practice and analysis indicate that the computer simulation alone is not sufficient to ensure the accurate estimation of slope stability. It is recommended to use a combination of slope monitoring and computer simulation to provide verification against each other to detect any potential hazards in mine. Mine pit slope movement monitoring program setup and monitoring procedure are analyzed and proposed in this study.

The above findings allow mining engineers to optimally design pit slopes under the given geotechnical conditions and minimize the risk of slope failures while improving the stripping ratio and enhancing production profit.

Table of Contents

Pages

List of Figures

List of Tables

List of Appendices

Pages

List of Abbreviations

C	Cohesion
E	Young's modulus
EMC	Erdenet Mining Corporation
FDM	Finite Difference Method
FEM	Finite Element Method
FOS	Factor of Safety
GBInSAR	Ground-Based Interferometric Synthetic Aperture Radar
GSI	Geological Strength Index
I-I North Flat1	North highwall of I-I cross-section, modified model of flat1
Lidar	Light Detection and Ranging
PF	Probability of Failure
PGA	Peak Ground Acceleration
Radar	Radio Detection and Ranging
RMR	Rock Mass Rating
RQD	Rock Quality Designation
SAR	Synthetic Aperture Radar
SRF	Strength Reduction Factor
SSR	Shear Strength Reduction
v	Poisson's ratio
Φ	Friction angle

Acknowledgments

Foremost, I would like to express my and sincere gratitude and appreciation to my advisor, Dr. Gang Chen for the continuous support of my Master's study and research. Without his guidance and persistent help, this project would not have been possible. Beside my advisor, I would like to thank my committee members Dr.Il Sang Ahn and Dr.Sampurna Arya for their encouragement and valuable advice.

My sincere thanks also goes to Erdenet Mining Corporation and Mr.Undrakhtamir Aleksandr for supporting and Department of Mining and Geological Engineering at the University of Alaska Fairbanks for providing scholarship.

Also, thanks goes to Itasca Educational Partnership and mentor Mr.Jin Wang for their support on FLAC geotechnical software.

Last but not the least, I owe my deepest gratitude to my parents for their love and sacrifices for educating and preparing me for my future. I am very much thankful to my beautiful wife Uyanga Sukhee, son Tenuun Bayasgalan, and daughter Setsen Bayasgalan for their caring, understanding, and continuous support to complete this research work.

Chapter 1

1. Introduction

This project focuses primarily on an analysis of mine pit slope stability and the determination of the critical pit slope angle that ensures a safe open-pit slope while optimizing the stripping ratio for the mine. The analysis is based on geological and geotechnical data collected from the Erdenet Mining Corporation, EMC, of Mongolia as well as data from rock sample laboratory testing. The study also contains the evaluation of the impact of pit slope optimization on mine planning and mining economics, which includes an estimation of total overburden removal and sensitivity analysis on slope angle variations.

In open-pit mining, the pit slope stability and its design are of critical importance to the mine production safety and economic performance. Pit slope failure may occur in the forms of plane failure, wedge failure, toppling failure, or circular failure. In general, the steeper the slope is, the less stable it will be. However, the necessity of overburden removal means that the slope's steepness has an opposite effect on the mine's economic performance. The steeper the slope is, the less volume of waste is removed and the better economic outcome generated. In order to simultaneously ensure a safe slope angle and optimize the stripping ratio, a comprehensive slope stability analysis based on extensive and thorough geological/geotechnical investigations is essential. In many cases, a rigorously designed and installed slope movement monitoring process is necessary to safeguard the slope stability. Failure to do so may result in slope failures that lead to severe property damages and personnel injuries or even fatalities.

Thus, the pit slope stability is the primary concern in open-pit mine design. Not only does a stable pit slope provide a safe working environment for the mining operations, but a properly designed pit also minimizes overburden removal and optimizes the stripping ratio. The study examines some serious geotechnical faults observed in the Erdenet open-pit mine, as shown in Figure 1.1.

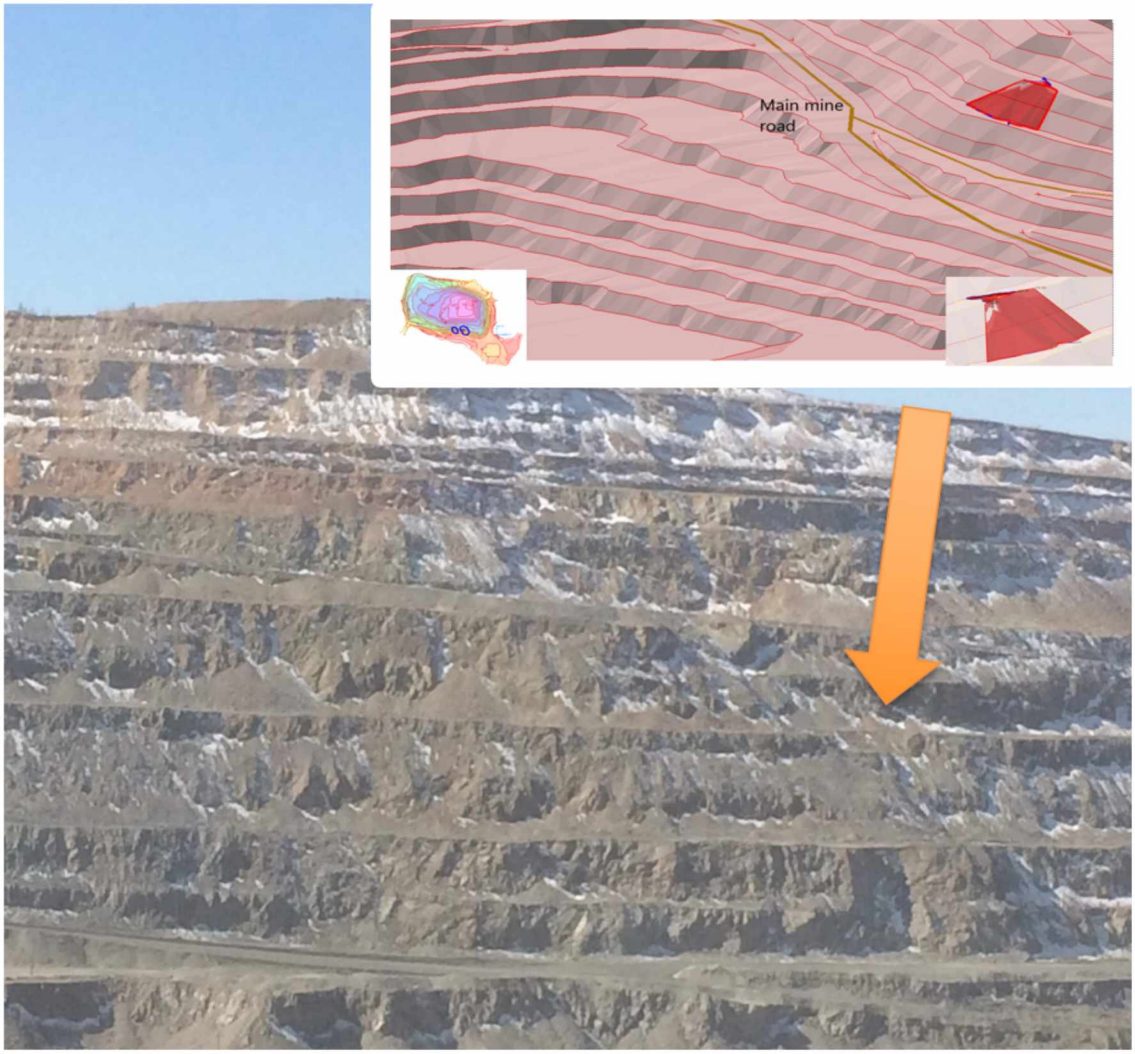

Figure 1. 1 Fault on the Erdenet open-pit mine slope

In the case of the Erdenet mine pit, the hanging wall of the fault slipped 1.5m downward and it affects 4 consecutive benches right above the main transportation road of the pit. No failure preventative action has been taken at the current time and the pit slope movement is being monitored to determine whether it is within the acceptable range. Since the fault is located just above the junction of two main roads, the analysis and monitoring of the fault conditions are of critical importance to the mine. Mine haul trucks run 24 hours daily on the main roads, and the safety of the mining operations and the lives of the miners are at stake.

In this project, the pit slope stability at the Erdenet mine is studied and the impact of slope variation on mining operations is analyzed. For the purpose of this study, several cross-sections of the pit slope are analyzed by numerical modeling with the FLAC 2D modeling software. Corresponding FOSs are calculated. The calculated FOS of each cross-section is required to have a minimum threshold FOS value of 1.50. Based on the simulation results, any critical slope have less than allowable FOS value are studied further to investigate the relation between slope geometrical dimension and corresponding FOS values. The mine slope design should be optimized by keeping the overall slope angle as steep as possible to minimize the stripping ratio while maintaining safey and well controlled mining operations.

Chapter 2

2. Literature Review

This chapter is divided into two main parts, naming slope monitoring and slope stability analysis. The former part covered different types of slope monitoring techniques, especially emphasized on radar technology and its real-time monitoring. Synthetic aperture radar (SAR) is suitable for open-pit real-time monitoring. It can stationary scan the pit continuously or mount on the vehicle or airborne to scan a better view. The latter portion reviewed the methods used to analyze the slope stability problem. Limit equilibrium method, numerical simulations, and probabilistic analyses are typical slope stability analysis methods. The limit equilibrium method calculation is based on shear strength and stress, whereas the numerical simulation uses stress-strain behavior of rock or soil. The numerical simulation method has gaining popularity in applications and have an ability to analyze a very broad range of problems. The equilibrium or numerical solution is not sufficient enough for the slope stability of the whatopen-pit. It is practical to use combinations of these techniques with probabilistic analysis due to uncertainties.

2.1 Slope Monitoring

Both natural and man-made slopes can be expected to undergo deformation /displacement, mainly due to the stress. Typically, man-made slopes tend to be more dangerous because they are located closer to other human developments such as a road excavation or an open-pit slope. All man-made slopes should be monitored regularly, regardless of what their factors of safety may be.

Slope monitoring has been performed for three primary reasons: to ensure the safety of people and the protection of equipment; to increase chances of having an early warning of possible failure and to mitigate the effects of that failure; and lastly, to enhance the understanding of slope behavior to improve designs.

There are four main types of open-pit slope monitoring:

1. Visual inspection

Walking and physical inspection of all berms, haul road, and pit perimeters to investigate any new subsidizes, tension cracks, and heaving.

2. Crack Monitors/surface extensometers

Measuring cracks width movement by connecting pegs on each side of a crack.

3. Survey monitoring

Measuring and monitoring movements of points with a conventional total station or an automated system.

4. Radar Technology (Radio Detection and Ranging)

Scanning the bench face areas continuously with a real-time control system. (Discussed below in details)

2.1.1 Radar and Lidar Technology

Radar and lidar scanner are directing radio waves, and light waves, respectively, towards the object and the wave reflection and its corresponding time are measured by the detector. The distance between objects is found by measuring the pulse speed and the difference between the transmitted pulse and received pulse. It operates in the radio and microwave portions of the electromagnetic spectrum at wavelengths ranging from a few millimeters to about a meter. The output is not a single point, but a digital elevation model (Wessels, 2009).

The main components of this technology are:

- Laser to transmit pulse
- Detector to receive scattered and reflected pulse
- Optics and Rotating Mechanism to can the object
- Timing Electronics, time measuring of transmitting and receiving the pulse
- Computer to restore the real-time data
- GPS, IMU to know it real-time location
- Mounting objects vehicle, stationary or airborne

The working principle is exactly the same in both Radar and Lidar; however, the wavelength of radio waves is 2,000 times greater than light waves. Depending on the pulse, the Lidar image has much better quality than Radar (Figure 2.1).

Radar: Radio Detection and Ranging and pulse is 3cm

Lidar: Light Detection and Ranging and pulse is 1.5 μm.

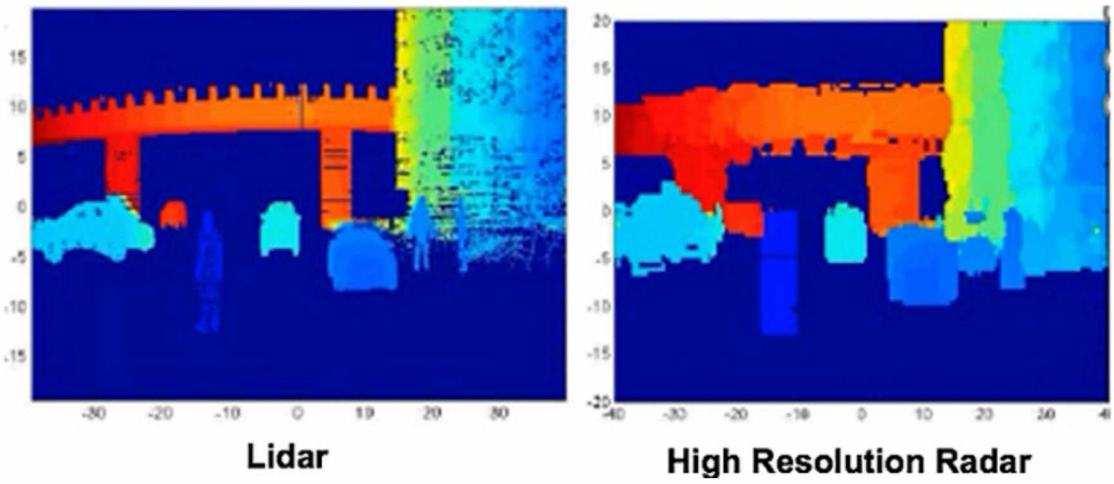

Figure 2. 1 Lidar and Radar scan quality comparison (Kashani et al., 2015)

Due to their respective wave properties, the usages of Radar and Lidar technology application are different. Table 2.1 summarizes the main differences between Lidar and Radar systems.

Table 2. 1 Summary of comparison of Lidar and Radar

	Lidar	**Radar**
Transmitting source	Light source	Radio wave
Wavelength	Shorter (1.5 μm)	Larger (3 cm)
Object detection	Small	Large
Detection range	Shorter	Longer
Working environment	Limited in harsh environment	Any harsh environment

2.1.1.1 Radar

Radar systems are mainly used in applications where the size and shape of the object are less important than the detection distance. Radar systems are primarily used in large-scale topographical or agricultural mapping, in airplanes, or military operations because of their long-range detection ability. The noticeable advantage of this technology is that it is not impaired by environmental conditions. In other words, it is reliable even in the event of heavy rain, storms, and fog, and can even penetrate through snow and water.

2.1.1.2 Lidar

Lidar uses radio or light sources to measure the distance between the object. In 1960, Lidar was first used to find the distance between the moon and the earth (Yaplee et al., 1965). Now, Lidar systems are being developed in many sectors for a variety of purposes, including slope control and self-driving vehicles.

Because of its high-precision measurement, the main applications of the Lidar are scanning 3D objects and surface scanning, such as for building and working with different terrains. In addition to its precision, Lidar has the ability to penetrate snow and water, which enables it to measure deep ocean terrain topography. The traffic police also use it daily for speed measurement of vehicles from a distance. Apart from these uses, Lidar can be used in agricultural research to find maximum yield areas for farmers.

2.1.1.3 Synthetic Aperture Radar (SAR)

Synthetic Aperture Radar is a form of radar that is used to create two-dimensional images or three-dimensional reconstructions of objects, including landscapes. SAR uses the motion of the radar antenna over a target region to provide finer spatial resolution than conventional beam-scanning radars. SAR is typically mounted on a moving platform, such as an aircraft or spacecraft, and has its origins in an advanced form of side looking airborne radar (SLAR). Typical SAR mounted on the satellite system is illustrated in Figure 2.2.

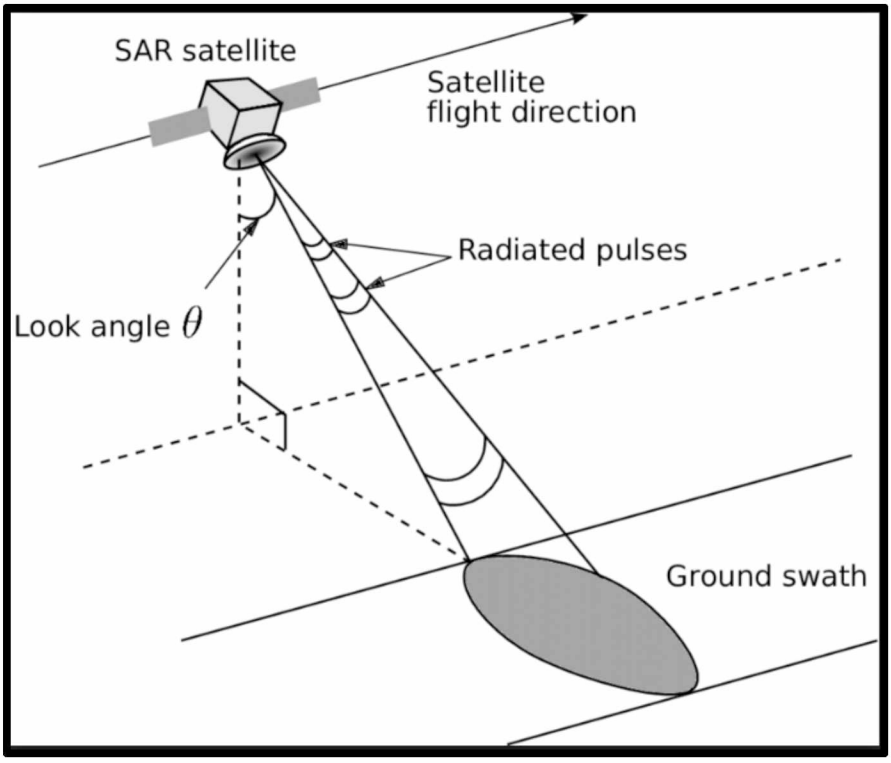

Figure 2. 2 Airborne mounted SAR (Lauknes, n.d.)

2.1.1.4 SAR In Mining Application

Discontinuous Ground Based Interferometric Synthetic Aperture Radar (GBInSAR) may be one of the best real-time wall monitoring tools for large open-pit mines. Depending on its specific purposes, GBInSAR can be stationary or mounted on a vehicle. These techniques can detect sub-mm displacement from a distance of up to 4 km in real-time, no matter what the environmental conditions are. So, any small wall movement can be detected and analyzed immediately because stationary control is scanning the pit 24 hours a day.

Still, there are some limitations to GBInSAR. The quality of the measurement depends on the distance and angle of the measuring point to an object. For a larger displacement, there will be biased deformation. Moreover, GBInSAR does not allow exactly perpendicular measurements because the transmission pulse would interrupt the line of sight.

Figure 2.3 illustrates how the soil or rock mass common failure could be noticed in GBInSAR easily. According to the distance, the brightness or tone of the image could change. The closer the object is, the darker the color has.

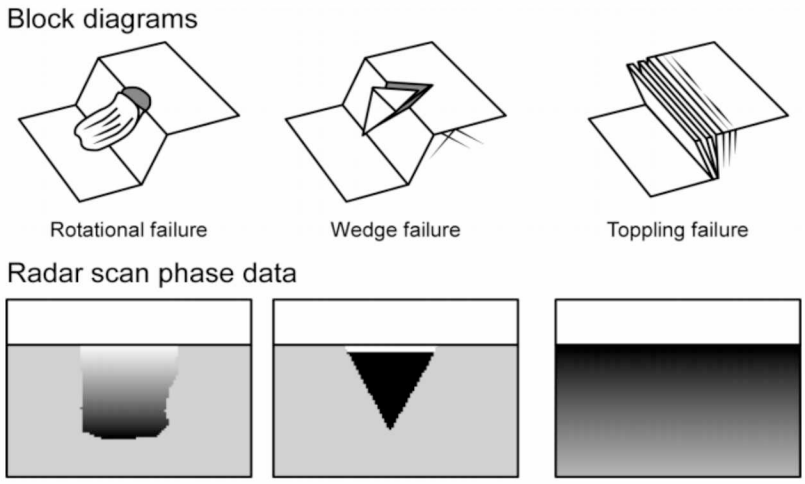

Figure 2. 3 Radar signatures possible for different failure types (McHugh et al., 2009)

Radar technology enables real-time slope monitoring (Figure 2.4) which is recommended in medium to large scale open-pit mines. The very first step of open-pit slope monitoring is scanning the wall continuously. The scan is converted to a 3D image file and inspected for changes. If there is a change, data needs to be sent to specialists for further analysis. If a potential hazard in the slope is found, the managers should take action to mitigate the effect.

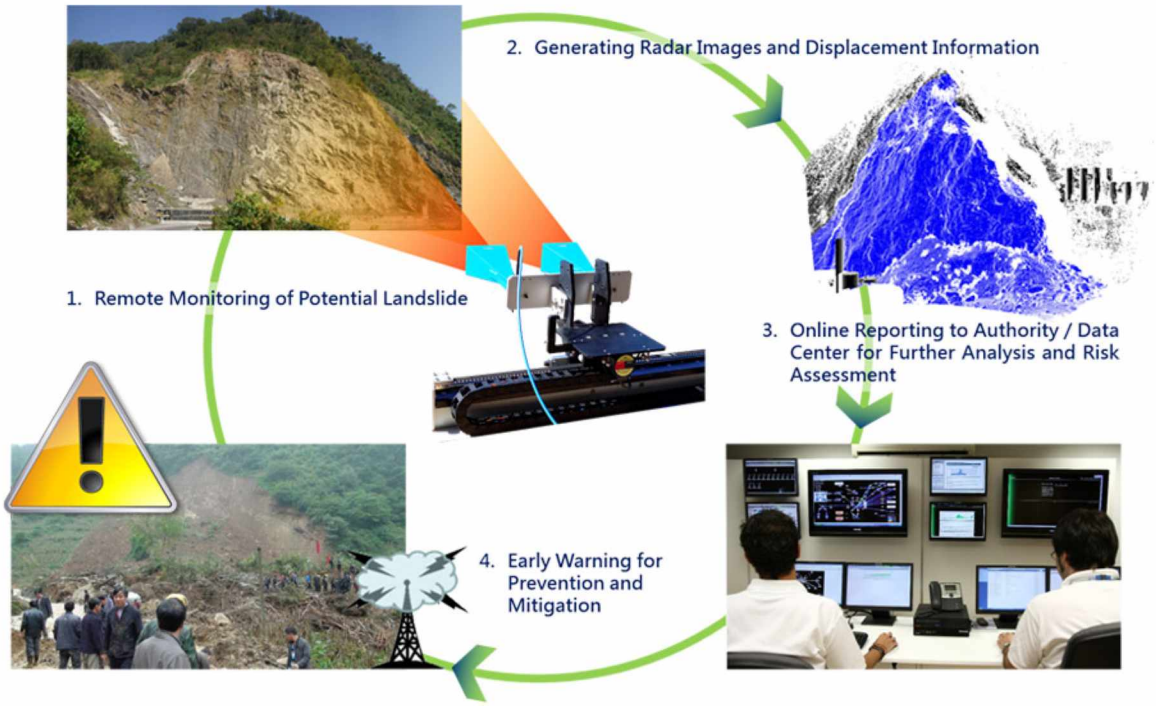

Figure 2. 4 Main cycles of the real-time controlling (airGmap Technology, 2020)

2.2 Slope Stability Analysis

Landslides occur in all 50 states and U.S. territories and cause $1-2 billion in damages and more than 25 fatalities on average each year (USGS, 2018). Man-made features are especially dangerous in terms of people's safety and the economy. Thus, rock engineers and scientists continue to devote effort to developing slope stability analysis.

The main analysis methods are limit equilibrium, numerical solution, and probabilistic analysis. The advantages and limitations of these methods are discussed below in more detail.

The information below is essential for all the slope stability analysis:

- Type of rock
- Physical properties of rock
- Laboratory test results
- Ratings RMR, RQD, and GSI.

- In-situ stress
- Groundwater condition

It is important to know the standard terminology used in open-pit mine slope design such as bench, ramp, and slope angles were illustrated in Figure 2.5. Bench face angle is measured between the crest and toe of a single bench. On the other hand, the inter-ramp angle, depends on several benches angles and bench width, is bounded by ramps and haul roads.

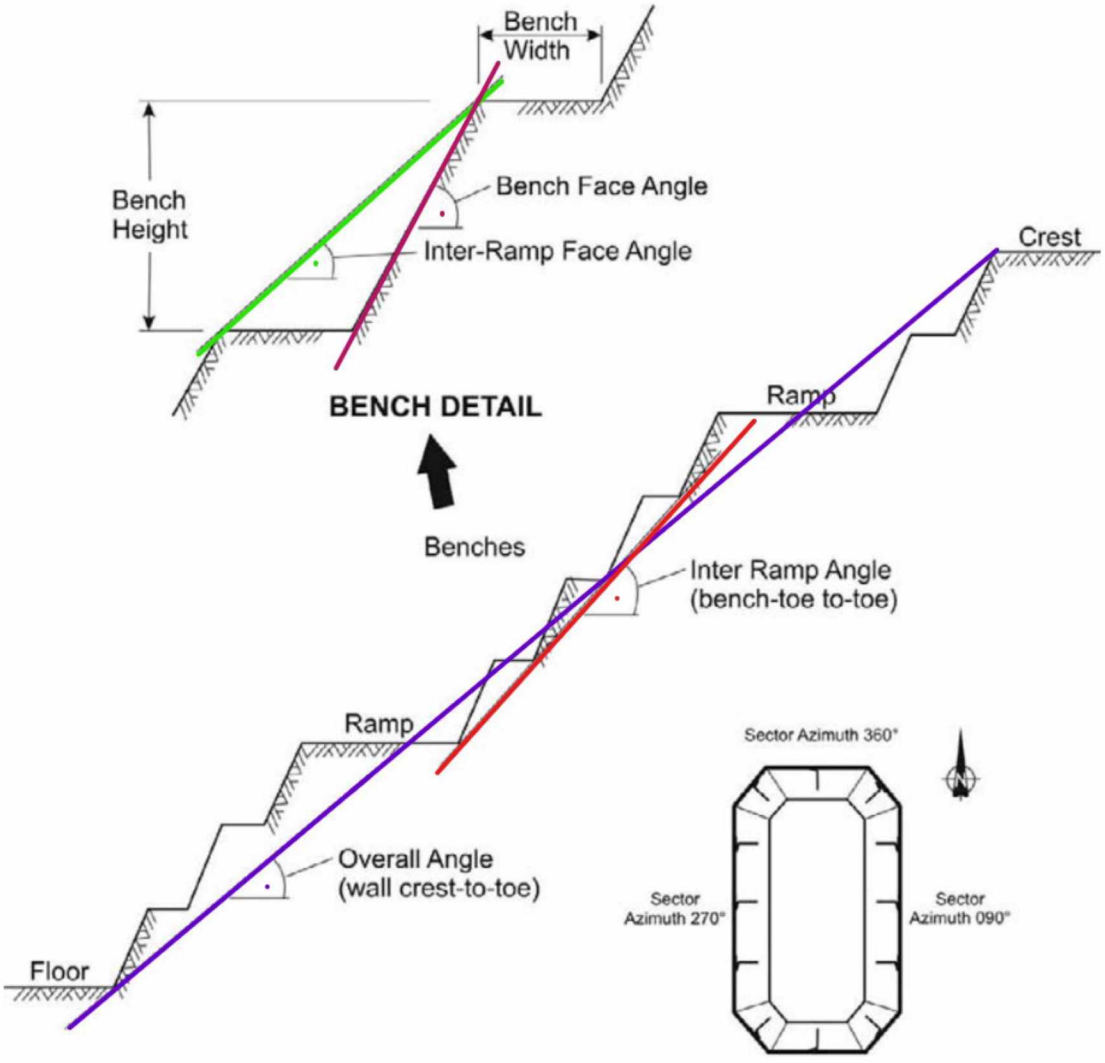

Figure 2. 5 Pit wall terminology (Read & Stacey, 2009)

2.2.1 Limit Equilibrium Method

The limit equilibrium method is the study of the equilibrium between a rigid body, such as the slope, and of a slip surface of any shapes, naming straight line, arc, circle, or logarithmic spiral, etc. Mohr-Coulomb failure criterion is preferred for limit equilibrium methods and the ratio of shear strength and shear stress illustrates the first indication of stability as the factor of safety:

$$FOS = \frac{shear\ strenght}{shear\ stress}$$

Among the various equilibrium methods, some allow the global equilibrium of the rigid body while others divide the rigid body into slices to cater for its non-homogeneity and consider the equilibrium of each of these. The slices (q), slice inter forces (E, X), and expected sliding surface with radius R calculated by the limit equilibrium method were presented in Figure 2.6.

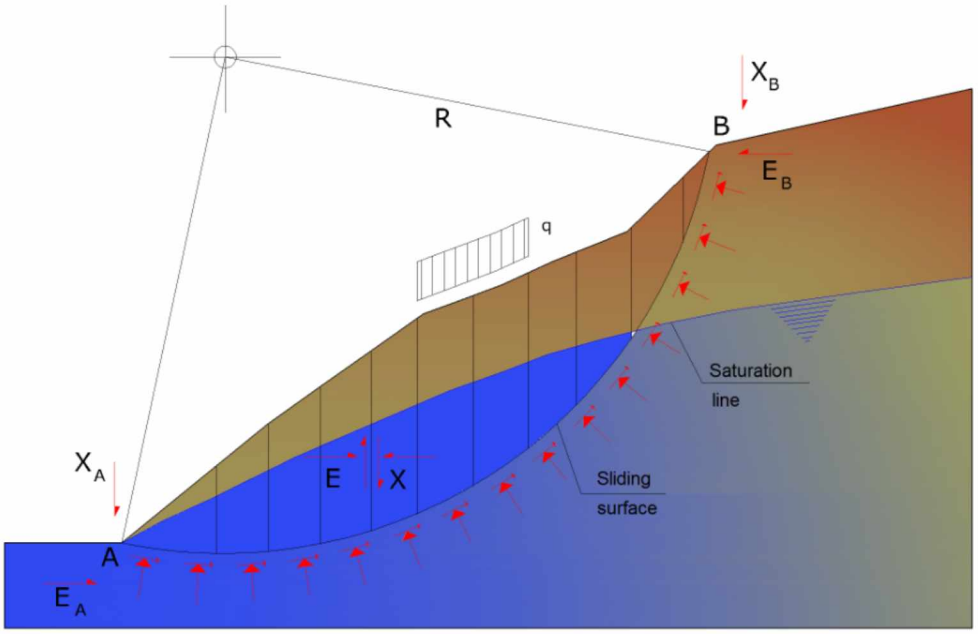

Figure 2. 6 Limit Equilibrium analysis (A New Era in Slope Stability Analysis, 2014)

However this limit equilibrium is the simplest method and it has the disadvantage that an assumption is made for a slip surface forming at a given location, which is not always the case.

2.2.1.1 Ordinary Fellenius Method (Swedish Slip Circle).

This method is also referred to as the Ordinary or Fellenius method and is considered the simplest of the limit equilibrium methods since it is the only procedure that results in a linear factor of safety equation. It is generally stated that the interslice forces can be neglected because they are parallel to the base of each slice (Fredlund & Krahn 1977). For the Swedish slip circle, important assumptions are

- Slip surface is circular
- The internal friction angle (φ) is 0. Soil strength is pure cohesion
- The slope material is homogeneous.

Factor of safety found as $FOS = \frac{Resisting\ Moment}{Driving\ Moment}$

Driving Moment (M_D): $M_D = W \cdot a$

Resisting Moment (M_R); $M_R = c \cdot l \cdot r$

Where W= weight of the slice

a= moment arm of the slice

r= radius of the slip circle

l= length of the slip circle

c= cohesion of the material (=τ)

2.2.1.2 Bishop's Simplified Method.

The simplified Bishop method neglects the inter-slice shear forces and, therefore, assumes that a normal or horizontal force adequately defines the inter-slice forces. The normal force on the base of each slice is derived by summing forces in a vertical direction.

Normal force gives:

$$P = \left[W - \frac{c'lsin\alpha}{F} + \frac{ul\ tan\ \phi'\ sin\alpha}{F}\right] / m_\alpha$$

where $m_\alpha = cos\alpha + (sin\alpha\ tan\phi')/F$

W = total weight of the slice

α = angle between the tangent to the center of the base of each slice and the horizontal

u = porewater pressure

F = factor of safety

c' = effective cohesion parameter,

ϕ' = effective angle of internal friction

The factor of safety is derived from the summation of moments about a common point. This equation is the same as since the inter-slice forces cancel out. Therefore, the factor of safety equation is the same as the ordinary method. However, the definition of the normal force is different (Fredlund & Krahn, 1977).

The FOS of the simple slope was calculated by slope stability software Slope/W employing the Simplified Bishop method. The slope was divided into 14 vertical slices, numbered left to right, where the width is 2m and height is not uniform. As seen in slice force polygon in Figure 2.7, Bishop's simplified method does not include inter-slice shear forces, but it includes inter-slice normal forces (GEO-SLOPE, 2012).

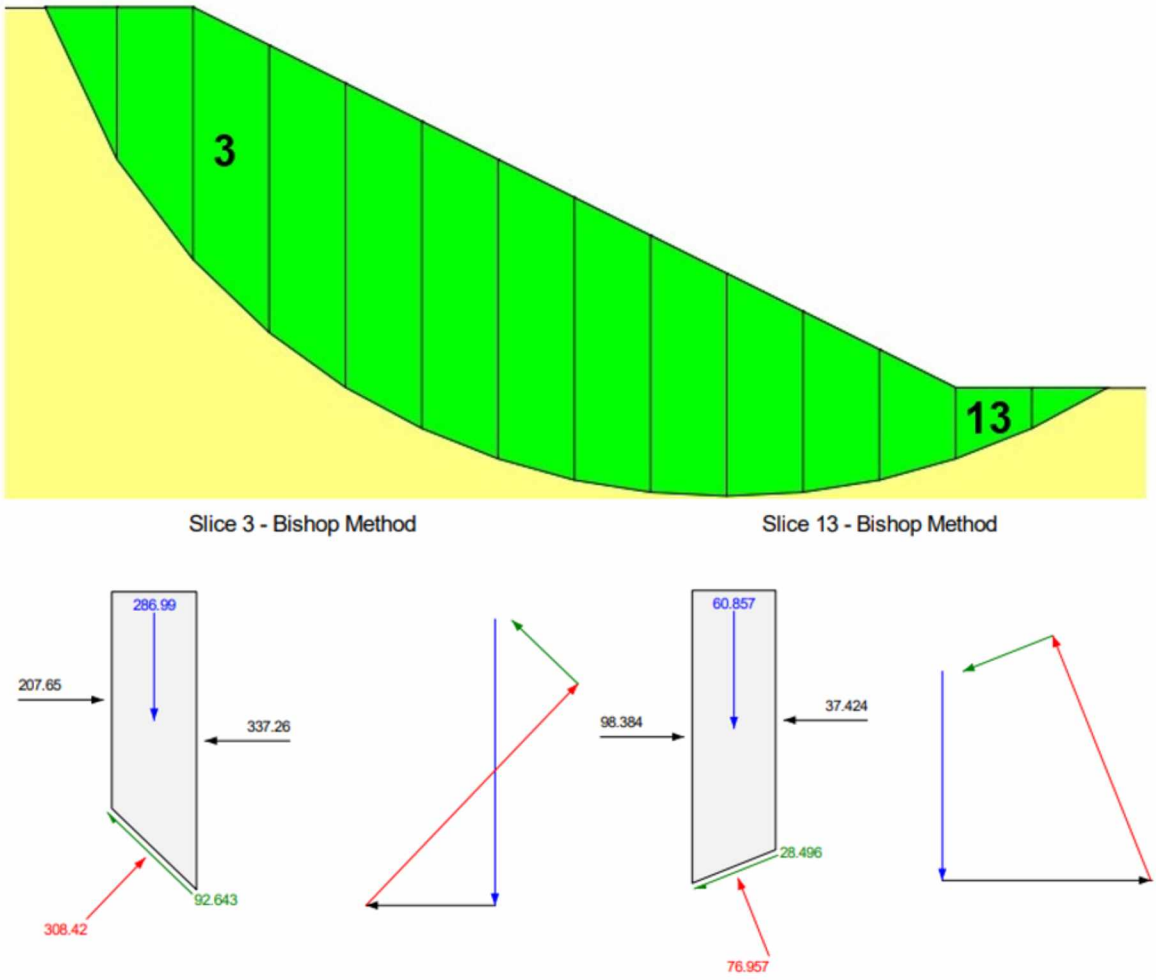

Figure 2. 7 Free body diagram and force polygon of slice 3 and 13 (GEO-SLOPE, 2012)

2.2.1.3 Janbu's Simplified Method.

Janbu has extended Bishop's method (see above) to freeform surfaces. When freeform (generic form) sliding surfaces are treated, the arm of the forces changes (in case of circular surfaces it is constant and equal to the radius of the arc), and therefore it is more convenient to evaluate the moment equation at the angle of each slice.

The factor of safety can be determined by the below equation

$$F\ iterative = \frac{\Sigma\grave{\imath}[ci \cdot bi + (Wi - ui \cdot bi + \Delta Xi) \cdot tan\varphi i] \cdot [sec^2 \alpha i/(1 + tan\alpha i \cdot tan\varphi i/F)]}{\Sigma\grave{\imath} Wi \cdot tan\alpha i}$$

Detailed parameters of narrow slices and forces acting on them are shown in Figure 2.8.

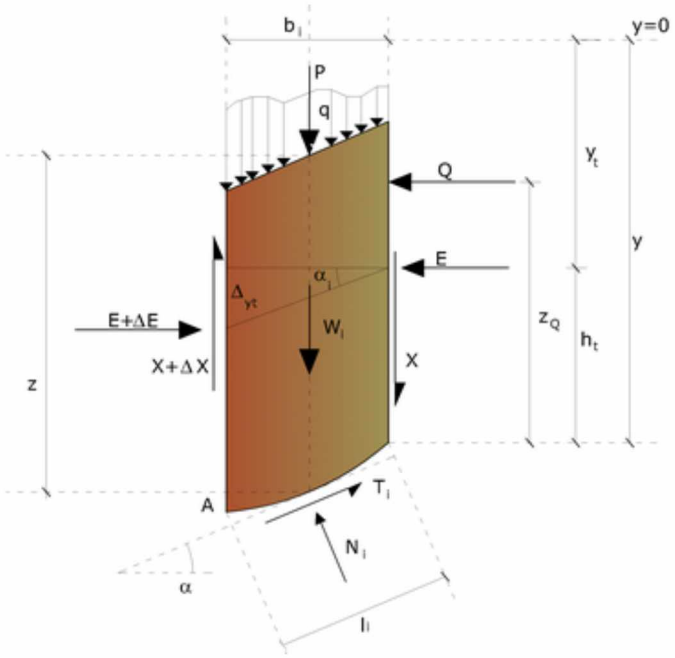

Figure 2. 8 Janbu's parameters (A New Era in Slope Stability Analysis, 2014)

Assuming ΔXi = 0 is obtained by the ordinary method. Janbu also proposes a method for the correction of the safety factor obtained by the ordinary method according to the following:

$$F_{corrected} = f_0 \cdot F_{iterative}$$

where, f_0 empirical correction factor, depends on the shape of the sliding surface and the geotechnical parameters. This correction is very reliable for slightly inclined slopes. For convenience, this correction factor can also be calculated according to the following formula:

$$f_0 = 1 + b1 * \frac{d}{L} - 1.4\left(\frac{d}{L}\right)^2$$

where b1 varies according to the soil type:

Ø = 0 soils: b1 = 0.69

C = 0 soils: b1 = 0.31

C>0, Ø>0 soils: b1 = 0.5 (Abramson et al., 1996)

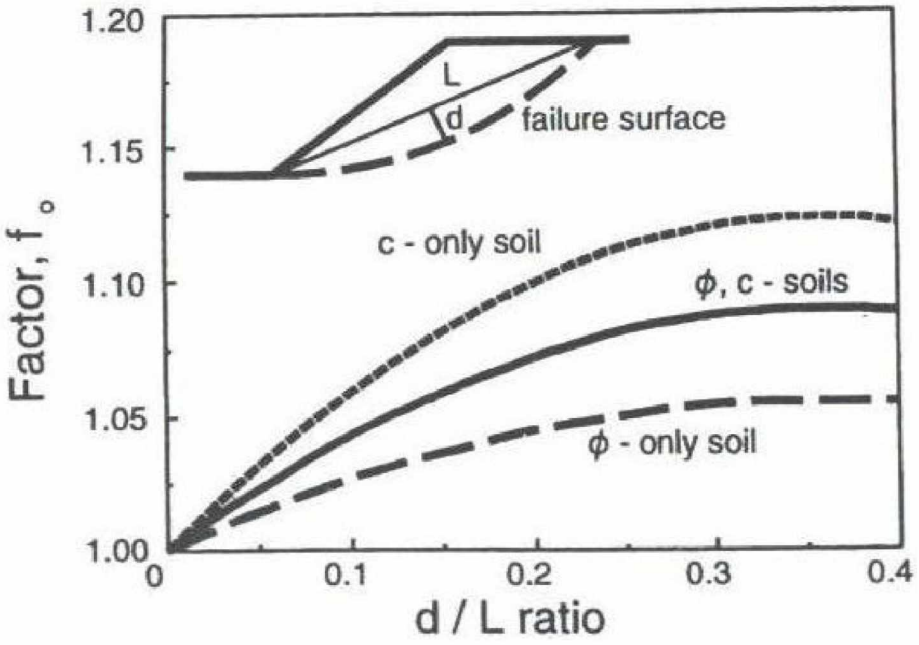

Figure 2. 9 Janbu's correction factor for the simplified method (Abramson et al., 1996)

The limit equilibrium methods, Ordinary Fellenius, Bishop's Simplified, Janbu's Simplified, and Juanbu Generalized, are compared by their equation of statics and inter-slice force in Table 2.2.

Table 2. 2 Limit equilibrium method comparison (GEO-SLOPE, 2012)

Method	Moment Equilibrium	Force Equilibrium	Inter-slice Normal	Inter-slice Shear
Ordinary Fellenius	Yes	No	No	No
Bishop's Simplified	Yes	No	Yes	No
Janbu's Simplified	No	Yes	Yes	No
Janbu Generalized	Yes (by slice)	Yes	Yes	Yes

Ordinary Fellenius and Bishop's Simplified method calculations are based on the moment equilibrium and neglect force equilibrium. On the contrary, Janbu's Simplified method uses force equilibrium instead of moment equilibrium. The Janbu's Generalized method is updated to deal with both moment and force equilibrium conditions and normal and shear forces in inter-slices.

2.2.2 Numerical Simulations

The numerical methods are widely accepted for analyzing stress and strain around rock excavations. They require significantly more computation than the limit equilibrium method, but they also need fast computers to make just one factor of safety calculation. The development of the processing speed of computers allowed numerical solutions to gain popularity in the application. Compared to the conventional limit equilibrium method, numerical methods have an ability to analyze a very broad range of problems, including stress-pore pressure variation and stress paths of different materials across different shapes of bodies.

The limit equilibrium method needs to assume a failure plane. If the assumed failure plane is not correct, the limit equilibrium analysis will produce a wrong answer. Whereas, numerical analysis is a stress analysis.

The overlaying rock weight creates compression stress on the rocks below. Depending on this stress, stages, and rock type, there are different stress-strain zones, namely elastic, plastic, strain-softening or hardening zone, and residual zone (Figure 2.10). In lower stress (between O to A in Figure 2.10) range, rock deforms elastically and when the stress is released, rock can return to its original shape. Conversely, in higher stress, up to breaking point (B), rock deforms plastically. In this zone, rock is irreversibly altered and will not return to its original shape.

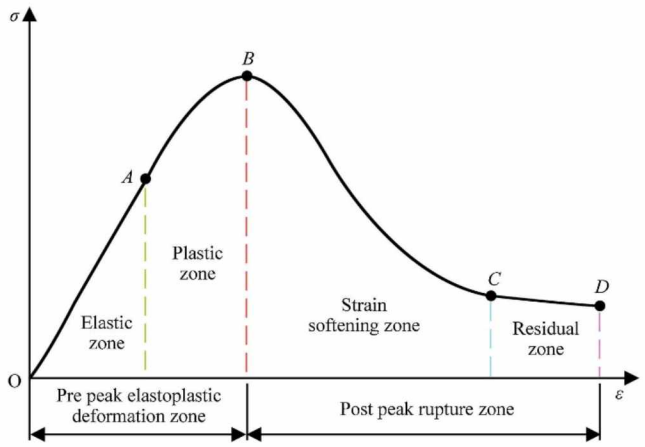

Figure 2. 10 Stress-strain curve of rock (Ruijie et al., 2018)

The Shear Strength Reduction (SSR) technique has been often used in mine ground control and slope stability studies. Cala, et al. (2004) highlighted that the SSR technique is a popular numerical method of slope stability analysis. In the SSR procedure, the FOS of a soil slope is defined as the number by which the original shear strength parameters must be divided to bring the slope to the point of failure.

The biggest advantage of calculating the factor of safety is that it is calculated globally and accordingly, gives critical failure surface automatically. The factor of safety is calculated by shear strength reduction (SSR) techniques (FLAC online manual, 2020).

For Mohr-Coulomb material shear strength reduced by a factor of safety, FOS can be determined from

$$\frac{\tau}{FOS_i} = \frac{C'}{FOS_i} + \frac{tan\phi'}{FOS_i}$$

The equation can be re-written

$$\frac{\tau}{F} = C_i + tan\phi_i$$

$$where \qquad C_i = \frac{C\prime}{FOS_i} \quad and \quad \phi_i = arctan\,(\frac{tan\phi\prime}{FOS_i}),$$

FOS_i, i=1,2,…, are series of strength reduction factors.

The FOS index is defined as the ratio of any relevant problem parameters (such as force, stress, and moments of inertia, etc.) to corresponding calculated parameters. Those parameters depend on slope height, bench width, water level, applied load, and strength property (FLAC online manual, 2020). FOS is calculated by strength reduction techniques with the Mohr-Coulomb failure criterion and requires a series of simulations known as FOS_i, which reduce the cohesion (C), and friction angle (Φ) until the failure occurs. When the slope is in a critical equilibrium state (on the verge of failure), the FOS_i will be considered as the FOS (Yang et al., 2019).

Moreover, the SSR technique eliminates the arbitrary assumptions regarding the inter-slice forces. As well, the method can automatically monitor the development of failure zones, from localized areas all the way to total slope failure. This is particularly important in the analysis of high slopes, such as those found in large open-pit mines, and the impact of slope excavation on nearby structures.

As a general rule for simple slopes, FOS obtained from SSR is usually the same as FOS obtained from Limited Equilibrium Method. A 10-m high homogeneous silt clay embankment with 45° slope angle, 20kN/m^3 unit weight, 12.38 kPa cohesion, and 20° friction angle has FOS of exactly 1.0 calculated by analytical solution (Chen, 2007, as cited in FLAC 8 Basics, 2015) as shown in Figure 2.11.

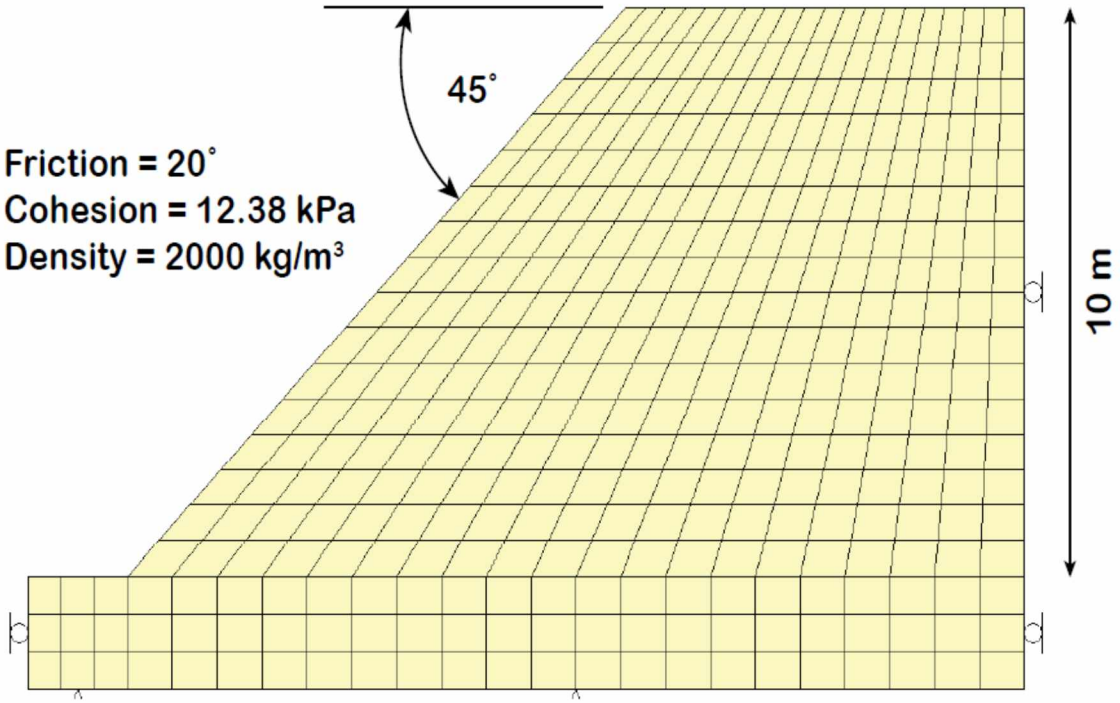

Figure 2. 11 The embankment with FOS of 1.0 (FLAC 8 Basics, 2015)

The same problem is solved by numerical simulation software FLAC and the factor of safety is found to be 1.01 using the strength reduction method. In addition to the FOS calculation, numerical modeling determines the embankment's failure surface, velocity vectors, and shear strain, presented in Figure 2.12. The FOS approaches 1.0 when finer meshes used in the model.

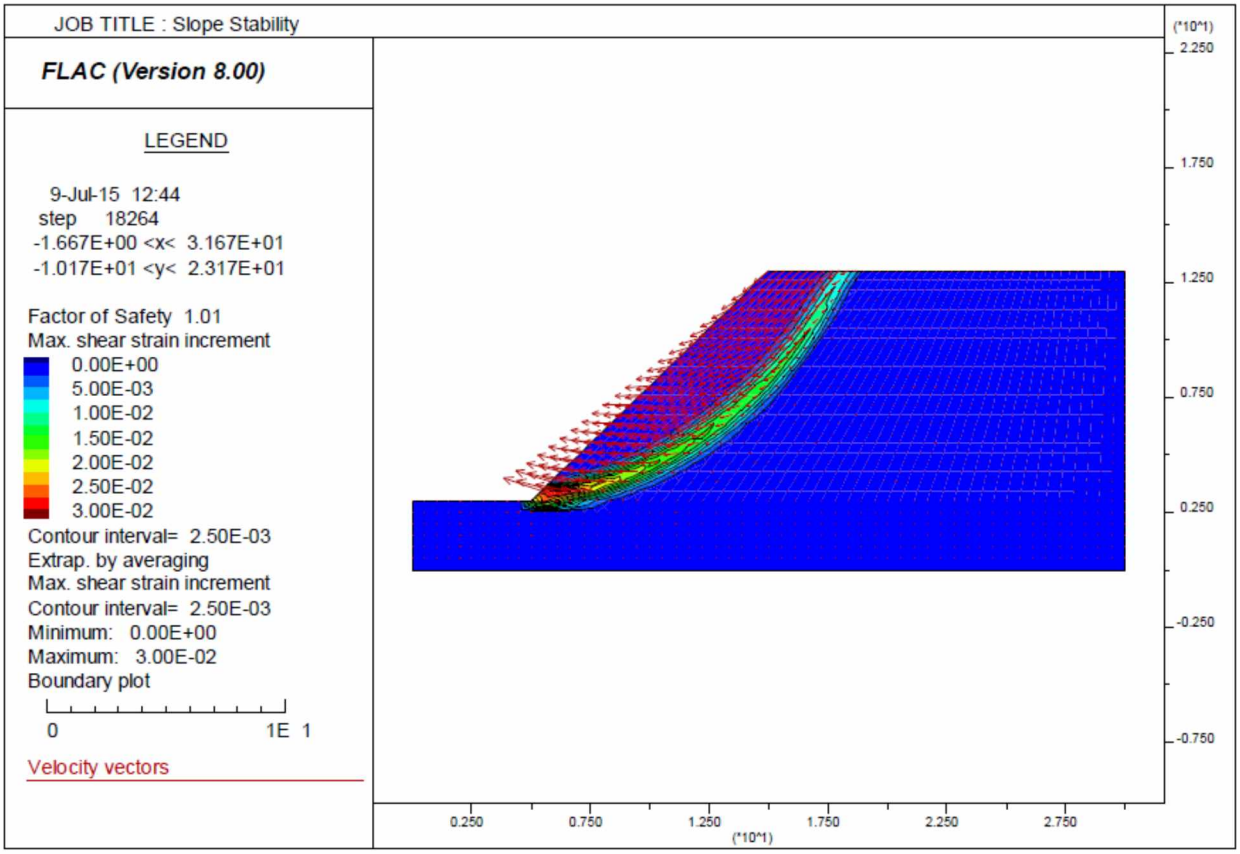

Figure 2. 12 The embankment FOS simulated by FLAC (FLAC 8 Basics, 2015)

The two most common numerical simulation methods, which could provide more reliable geotechnical results, are the Finite Element Method (FEM) and Finite Difference (FDM). (Discussed below in details)

2.2.2.1 Finite Element Method

The finite element method (FEM) is applicable for any geometry and topography of the slope. The derived factor of safety in the FEM is believed to be more accurate than the limit equilibrium method since there is no need of finding the failure surface. The shear strength reduction (SSR) method is used for FEM slope stability analysis. The finite element method solves problems by dividing the geometry into small elements, each with a shape that is easy to

calculate and calculates the stresses and strains in those elements before assembling them back using the theory of superposition. Some of the 3D limit equilibrium methods have restrictions regarding the shape of the slip surface.

2.2.2.1.1 RS2 Finite Element Program

RS2, formerly known as RS^2 or Phase2, is a versatile 2D elasto-plastic finite element stress analysis program for designing underground and surface excavations. The software is developed by Rocscience.

One of the major features of Phase2 is finite element slope stability analysis using the shear strength reduction method. This aspect of the program is fully automated and can be used with either Mohr-Coulomb or Hoek-Brown strength parameters. The analysis parameters can be customized if required. Slope models can be imported from Slide and computed in Phase2, allowing easy comparison of limit equilibrium and finite element results (RS2, 2019). An example result of a failed slope simulated by RS2 program was presented in Figure 2.13.

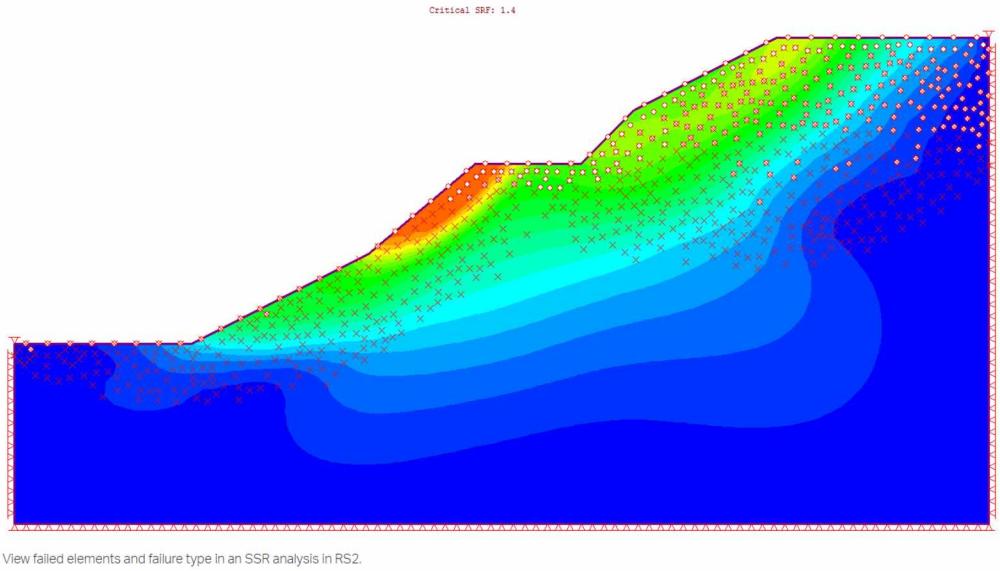

Figure 2. 13 View failed elements and failure type in a SSR analysis in RS2 (Rockscience, 2019)

2.2.2.2 Finite Difference Method

Finite difference method (FDM) is another popular scheme for stress analysis of continuum. The geotechnical simulation software FLAC2D is one of the popular tools used in numerical modeling studies. The Shear Strength Reduction (SSR) technique has been often used in mine ground control and slope stability studies. Cala, et al. (2004) highlighted that the SSR technique is a popular numerical method of slope stability analysis. In the SSR procedure, the factor of safety (FOS) of a soil slope is defined as the number by which the original shear strength parameters must be divided to bring the slope to the point of failure.

2.2.2.2.1 FLAC Finite Difference Program

FLAC, Fast Lagrangian Analysis of Continua, is two-dimensional numerical modeling software for advanced geotechnical analysis of soil, rock, groundwater, and ground support. *FLAC* is used for analysis, testing, and design by geotechnical, civil, and mining engineers. It is designed to accommodate any kind of geotechnical engineering project that requires continuum analysis.

FLAC utilizes an explicit finite difference formulation that can model complex behaviors, such as problems that consist of several stages, large displacements, and strains, non-linear material behavior, or unstable systems (even cases of yield/failure over large areas, or total collapse). The finite difference method offers lots of favors compared to FEM, but two disadvantages should be noted:

- Linear (elastic) simulations run more slowly with *FLAC* than with equivalent FEM programs; *FLAC* is most effective when applied to nonlinear or large-strain problems, or to situations in which physical instability may occur.
- FLAC is less efficient in modeling certain problems (e.g., beams, represented by solid elements rather than structural elements, or problems that contain large disparities in elastic moduli or element sizes).

2.2.2.3 Comparison of Numerical Simulation Methods

In an investigation of geotechnical and rock engineering applications, limit equilibrium is the most common method for slope stability analysis. However, slope stability numerical methods have been gaining popularity in open-pit mining and landslide studies over limit equilibrium methods due to mechanical instability of rock mass and in-situ stress. The comparison of numerical analysis and limit equilibrium methods is outlined by Lorig and Varona (2004), as shown in Table 2.3.

Table 2. 3 Comparison of numerical and limit equilibrium analysis methods (Wyllie & Mah, 2004)

Analysis result	**Numerical solution**	**Limit Equilibrium**
Equilibrium	Satisfied everywhere	Satisfied only for specific objects, such as slices
Stresses	Computed everywhere using field equations	Computed approximately on certain surfaces
Deformation	Part of the solution; yield condition	Not considered; failure allowed only
failure	satisfied everywhere; slide surfaces develop "automatically" as conditions dictate	on certain predefined surfaces; no check on yield condition elsewhere
Kinematics	The "mechanisms" that develop satisfy kinematic constraints	A single kinematic condition is specified according to the particular geologic conditions

The main drawbacks of the numerical method compared to limit equilibrium are that it requires longer computational time and a qualified analyst to run a specific computer software program. Still, there are several reasons why geotechnical engineers prefer the numerical method in slope stability-related problems.

- The resultant stress and displacement of the rock mass can be fully represented by the numerical method. Any critical area of monitoring slope displacement could be compared with simulated displacement.
- It is powerful enough to analyze any problems with geological complexity.
- There is no need failure surface assumption in the numerical method. The shape and location are found automatically by computing shear stress in the rock mass.

2.2.3 Probabilistic Analysis

Of all the geotechnical subjects, slope engineering is perhaps the one most dominated by uncertainty. Geological discontinuities, subsurface stratigraphy, anomalies, inherent spatial variability of soil and rock properties, scarcity of representative data, changing environmental conditions, unexpected failure mechanisms, simplifications and approximations adopted in geotechnical models, and human mistakes in the design are all factors that contribute to this uncertainty. The effects of these uncertainties on the probability of slope failure are often significant, and insight on these effects is integral to understanding failure mechanisms and designing slope remedial measures. A conventional deterministic analysis is based on average or measured single values of natural variabilities in rock mass properties and does not consider any statistical variability. Without considering uncertainty, the factor of safety (FOS) alone can give a misleading sense of stability. The FOS alone is an insufficient safety indicator without any probabilistic approach. Probabilistic slope stability analysis (PSSA) was first introduced into slope engineering in the 1970s, and significant more work still needs to be done in this area (EI-Ramly et al 2002).

Calderon compared the slope FOS of two cases which have different material properties and geometry. The first slope has a FOS of 1.2 with a standard deviation of 0.1, and the other slope has a higher FOS value and standard deviation, 1.5 and 0.5, respectively (Figure 2.14). The probability density function of FOS is assumed to be a normal distribution function and the shaded area on the left side of the FOS=1.0 vertical line represents failure probability. According to this model, the first slope has lower FOS value; its probability of failure is less than the other slope (Calderon, n.d.).

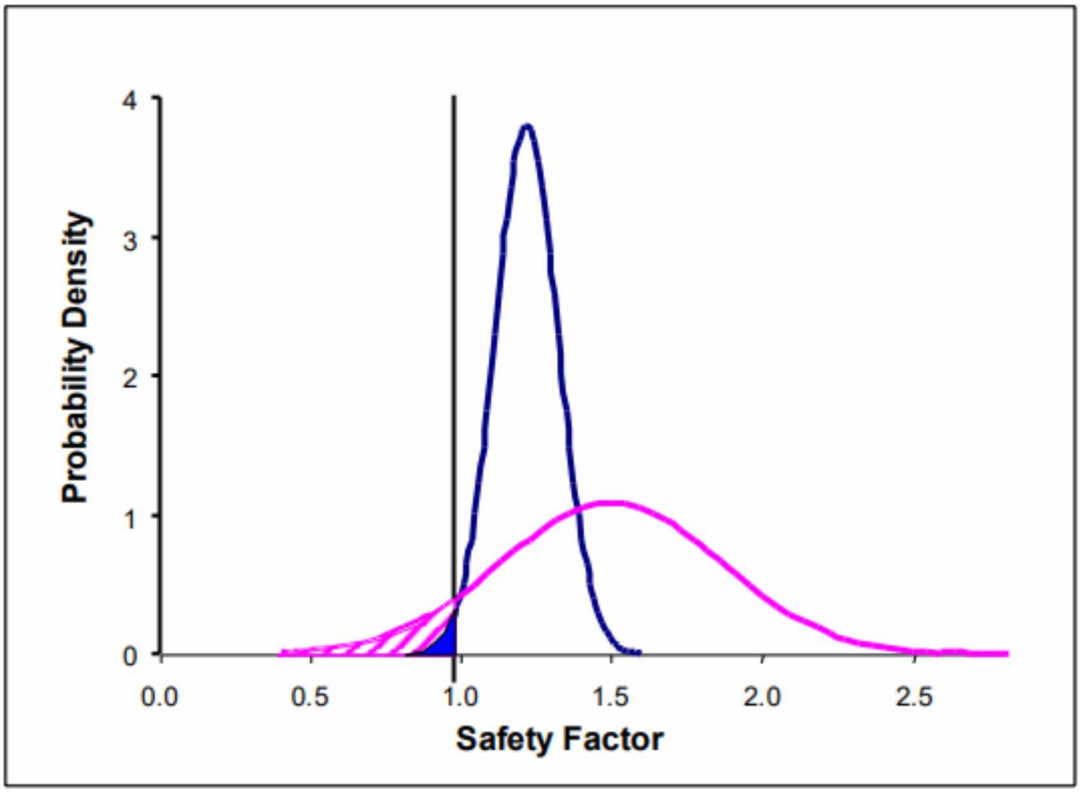

Figure 2. 14 FOS Probability density curves of two different slope (Calderon, n.d.)

- There several techniques available to overcome the complexity of math:
- Monte Carlo simulation – use random number generators to create a large number of simulations
- The First Order Second Moment (FOSM) method – use the first terms of the Taylor series for estimation.
- The Second Order Second Moment (SOSM) method – use the Taylor series up to the second order.
- The Point Estimate method – evaluate the performance function at a set of specific points
- The Hasofer-Lind method – an improvement of FOSM, use a reliability index and an iteration process
- The Stochastic Finite Element Method (SFEM) – for complex structures when no simple performance function can be defined and no global random process to be studied, SFEM can be employed. (Chen, 2019)

2.2.3.1 Monte Carlo Simulation

Monte Carlo Simulation (MCS) method has been widely used in probabilistic analysis of slope stability, and it provides a robust and simple way to assess failure probability. However, the MCS method does not offer insight into the relative contributions of various uncertainties (e.g., inherent spatial variability of soil properties and subsurface stratigraphy) to the failure probability. Furthermore, it is known for prone to a lack of resolution and efficiency at small probability levels.

Basically, the MCS is a method that provides randomized inputs for a wide range of problems in engineering and scientific disciplines, as well as for other areas of study. A large number of trials with randomized inputs are repeated until a statistically significant outcome is achieved (Chen, 2019).

Chapter 3

3. Erdenet Mine Slope Stability

Erdenet Mine Slope StabilityThe orebody being extracted at Erdenet Mine is the Erdenetiin-Ovoo deposit, which is a big porphyry copper-molybdenum ore deposit located north of the center of Mongolia, 241km from the capital city of Ulaanbaatar. Watanabe and Stein (2000), and Gerel and Munkhtsengel (2005, 2018) stated that (as cited in Kim et al., 2018, p. 659) "The Cu-Mo mineralization in the Erdenetiin Ovoo ore district is associated with the Erdenet porphyry complex consisting of quartz-diorite, granodiorite porphyry, and granite porphyry, and the ore-bearing stockwork intrudes the Selenge intrusive complex, including granodiorite, granite, and quartz-syenite".

The mine has two open-pits next to each other, named the North-West Pit and Central Pit, which have been mined since 1978 and 2011 respectively. After 42 years of continuous operation, North-West Pit depth has reached over 320m, and it extends about 2.5km long and 1.5km wide. The mine is designed for a 15m ledge height and 30m bench height and truck-shovel combination. The annual production has been increasing dramatically since 2011. And in 2018, 36.6M tons of ore was mined from both pits. There are three sets of main faults, striking N-S, NW-SE, and NE-SW were shown green in color in Figure 3.1.

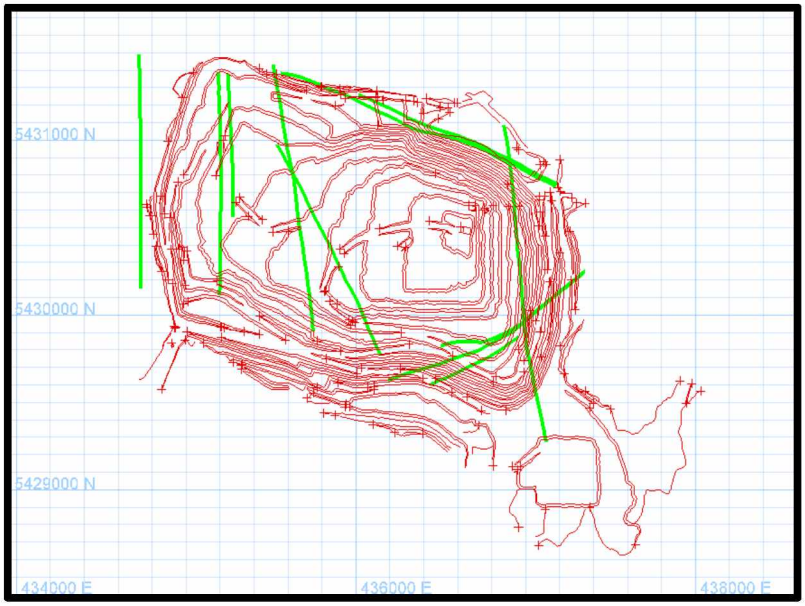

Figure 3. 1 Mine Layout and Main Faults

Taking account of discontinuity sets, major faults, and rock properties, the pit slope is to be divided into geotechnical domains that have similar geotechnical properties and inter-ramp angles in each group. Optimizing the pit slope section by section and the corresponding inter-ramp will be more efficient in improving the overall stability of the pit slope and maximizing savings in overburden excavations. Analysis of pit slope variation has a huge effect on mine planning and mine economic performance. Sensitivity analysis on pit slope variations will be carried out to investigate their impact on overall excavation production and mine planning. The analysis will be conducted with the help of Maptek Vulcan 3D mining software. This analysis enables visualization of how the earth-work is sensitive to the pit slope's inter-ramp angle. In the model, each domain may have its optimum slopes, some of which could be more effective in reducing the volume of overburden removal, and as a result, in generating significant cost savings.

The average slope angle of different sides and benches of North-West pit are measured from the mine map with the help of Vulcan 3D software and listed in Table 3.1. The planned inter ramp angle (IRA), overall angle, and depth of North-West and Central pit are presented in Table 3.2.

Table 3. 1 Slope Angles in North-West Pit at Different sides and benches

Bench	**Slope angle (degree °)**							
level	**N**	**NE**	**E**	**SE**	**S**	**SW**	**W**	**NW**
1205	40.5	46.4	49.4	46.7	44.6	43.1	44.1	45.1
1220	41.7	42.6	41	43.1	43.6	41.4	41.4	42
1235	40.5	44.7	40	40.9	42.4	40.5	45.1	43.5
1250	39.7	43.6	45.6	45.6	41.7	46.1	42.6	46.6
1265	40.8	48	39.5	43.73	44.6	41.8	45.7	43.8
1280	39.7	48.1	37.9	40.4	41.2	48.2	41.8	45
1295	40.2	52.1	40.5	44.3	51.9	40.7	45.6	48
1310	47.3	51.4	46.4	44.2	53.7	44.7	46.3	43
1325	45.8	47.1	44.5	52	43.4	49.4	51.6	47.6
1340	60.8	44.1	50.5	48.1	46.4	40	54.1	47.9
1355	53.6	48.7	45.9	49.7	51.6	46	53.8	51.1
1370	53.9	48.6	45.8	55.4	48.6	52		
1385	49.5	46.6	52.3	53.7	44.5	43.8		
1400	45.9	51.4	57.5	58.8	53.9	56.3		
1415			40	49.8	39			
1430			51.8	47.1	46.2			
1445			45.1		44.1			
1460					47.3			
1475					45			
mean	45.71	47.39	45.51	47.72	45.98	45.29	46.55	45.78
std	6.63	2.98	5.43	5.24	4.24	4.80	4.58	2.72
IRA	34.56	39.3	22.22	19.8	20.5 (37.8)			

Table 3. 2 Open-pit design parameters (Erdenet Mining Corporation, 2018)

	North-West pit		Central pit	
	East	**West**	**East**	**West**
IRA (°)	33	36	40	
Overall slope angle (°)	23	29	25	29
depth (m)	447.6	524		303.7

3.1 Blasting

Australian Orica Exel nonelectric detonators and water-resistant emulsion explosives have been used for blasting at Erdenet Mine. Depending on the strength of the rock, burden and spacing vary between 7m to 9.5m. All blast-holes have a diameter of 250mm and the buffer row has a depth of almost half of the ledge height. The near-surface layer of the barrier wall is loosened up to several meters due to production blasting. This layer is unstable and in the end, it forms talus cones sloping 40 (Valenta et al., 2018). Erdenet mine production blasting damage to the host rock is presented in Figure 3.2.

Figure 3. 2 Blasting damage

3.2 Maptek Terrestrial Laser Scanner usage

Since Erdenet mine possesses a Maptek I-Site XR3 long-range terrestrial laser scanner, it could be used as a main slope monitoring device. However, there are difficulties associated with the problems below:

1 The laser scanner alone is not sufficient to monitor slope stability. It is recommended to use with Geotechnical Module of Maptek PointStudio software.
2 The laser scanner is barely used at mining site, instead it is used in tailing dam deformation and minor stockpile volume calculations.
3 XR3 model works only a few minutes in cold ambient temperature outside.
4 Slope stability monitoring stations in the edge of the pit need be prepared. Also, the highwalls need to be scanned in more detail by mounting it on the vehicle.

3.2.1. Solution of Problem 1

Maptek PointStudio software was developed in 2000 as a set of desktop tools of a laser scanner to process large point cloud data mainly from a large geographical area survey and geotechnical analysis over the highwall. Maptek PointStudio continues the logical progression to a new generation 3D platform for modeling, analysis, and reporting. Laser scanning has now become an accepted and common technique for obtaining precise measurements and 3D visualization of large scenes.

The PointStudio Geotechnical module is the main tool of the slope stability monitoring and geotechnical kinematic analysis and it should be purchased. Working directly on laser scan data ensures accurate and informative geotechnical reporting to guide mine planning and operational decisions. The important features why Geotechnical Module is essential for the Erdenet Open-pit are listed below:

- Discontinuity solids and shape, size and spacing
- The volume of wedge failure
- Customizable and interactive stereonet
- Display drilling blind zones on stereonet

- Kinematic analysis
- Dynamic dip and strike
- Stability analysis
- Automated cell mapping
- Interactive stereonet
- Full 3D visualization

3.2.2. Solution of Problem 2

It is more related to the company management and availability of the PointStudio dongle key. The laser scanner usage efficiency should be increased by purchasing an additional dongle key or connecting dongle key on the company network so that all the surveyors and geotechnical engineers could use both PointStudio software and the laser scanner more efficiently. For the field measurements, the XR3 laser scanner is fast enough to be used only a few hours for any task and it kept in an office rest of the day. Thus, it is highly suggested that the equipment be used for pit slope monitoring in addition to regular usage for tailing dam monitoring.

3.2.3 Solution of Problem 3

The average temperature of the coldest months are December, January, and February with temperatures of -15.5°C (4.1°F), -17.9°C (-0.2°F), and -15.2°C (4.6°F), respectively at Erdenet mine site. In those months, the XR3 scanner is able to work only a few minutes outside and the battery dies quickly. The best solution is to upgrade to a cold climate XR3 scanner which redesigned to operate at temperature down to -20°C, with a limited operating time below that. The new laser scanner has released in March 2019 with the improvement of very low charge acceptance of batteries. The battery pack has been redesigned and insulated to keep the unit at a stable operating temperature. Other built-ins such as a generator, hydraulics, and electrical systems were adapted to maintain energy-efficient and cost-effective operation. Also, a

removable neoprene jacket for the scanner provides extra protection against wind chill. (Lidar magazine, 2019)

The first successful Maptek laser scanner in cold region test was done in, Diavak Diamond Mine, 220 km south of the Arctic Circle, Yellowknife, Canada in December of 2006. Maptek I-Site 4400 was able to operate at -50°C with cold-weather jacket. After the useful feedback from the site operators, a heated battery was developed and used successfully (Maptek I-Site, 2008).

neoprene jacket for the scanner provides extra protection against wind chill. (Lidar magazine, 2019)

The first successful maptek laser scanner in cold region test was done in, Diavak Diamond Mine, 220 km south of the Arctic Circle, Yellowknife, Canada in December of 2006. Maptek I-Site 4400 was able to operate at -50°C with cold weather jacket. After the useful feedback from the site operators, heated battery was developed and used successfully (Maptek I-Site, 2008). Figure 3.3 illustrates the protective jacket and the location of the test.

Figure 3. 3 I-Site 4400 scanner with protective jacket to keep out the cold (Maptek I-Site, 2008)

3.2.3. Solution of Problem 4

Slope stability monitoring stations at the edge of the pit should be prepared. In order to monitor the whole open-pit, at least two stations are necessary, proposed positions (A and B in Figure 3.4), and views are sketched on the figure. The views from stations A and B are estimated by considering a laser scanner scan window (-40° below horizontal), range, and the face azimuth angle relative to the stations. In Figure 3.4, yellow and pink lines illustrate the range and monitoring area of the pit from the station points A and B, respectively. The images of east, south, and west highwal are shown in Appendices Figure A.1, A.2, and A.3, respectively, for better visualization of scanning pit highwall.

Figure 3. 4 Continuous slope monitoring positions (A&B) and their view range

Station A is already prepared and served as a primary location. Station A position was specifically chosen to monitor:

- North highwall which has the major fault (Figure 1.1)
- South-West highwall which has the highest failures occurred
- Station A is designed for slope monitoring and other detailed survey
- Easy to access and just next to the Open-pit dispatcher room

Similarly, Station B should be installed in the indicated location to monitor North highwalls. The proposed Stations A and B elevations are 1460 and 1430 m.a.s.l, respectively.

Also, the highwalls should be scanned in more detail by mounted on the vehicle. Even after the detailed scan from the two different stations, there are always some spots not scanned and some faces need to be scanned in more detail again for geological and geotechnical purposes. Even for the open-pit survey and stockpile volume calculation, drive mode could be useful.

If the fixed stations are not the preferred choice, the other costly application might be purchasing a cold climate sentry mobile system. The XR3 scanner is the main part of the sentry, which has some additional features to keep the battery warmer. The main advantage of this choice is that a sentry system is installed and run to watch multiple areas and deploy the monitoring systems in a targeted way, and a screening tool is employed for detecting and recording surface changes.

3.3. Failure Prediction

The challenge in rock science is the prediction of the failure, including the amount and time of rock failure. Once continuous movement or potential hazard is found, the failure may occur over time. An early prediction of the potential failure could give enough time for effective control and consequently enable authorities to estimate the failure date as closely as possible. By doing so, any equipment loss and mine site employee safety issues could be minimized.

On the 17th of November 2016, an unexpected slope failure occurred in an undisclosed copper open-pit mine. As shown in Figure 3.5, months of satellite InSAR spanning data and ground-based radar measurement data from just before the failure are compared. Interestingly, although ground-based radar measurement is more accurate, it did not detect any potential failure. This was possibly due to ground-based radar position selection. Most of the significant movements

were recorded on the crest of the pit. However, from the same or lower elevation, the crest could not be precisely measured because of the stepping angle. The preferred stepping angle is 90 degrees, and a 180 degree angle is impossible to measure. It is believed that at least two measurements are needed to minimize occluded parts and accurately visualize the pit.

On the contrary, satellite InSAR gave more warning results before the failure took place. The largest displacement occurred around the failure area and at the top of the crests near the failure.

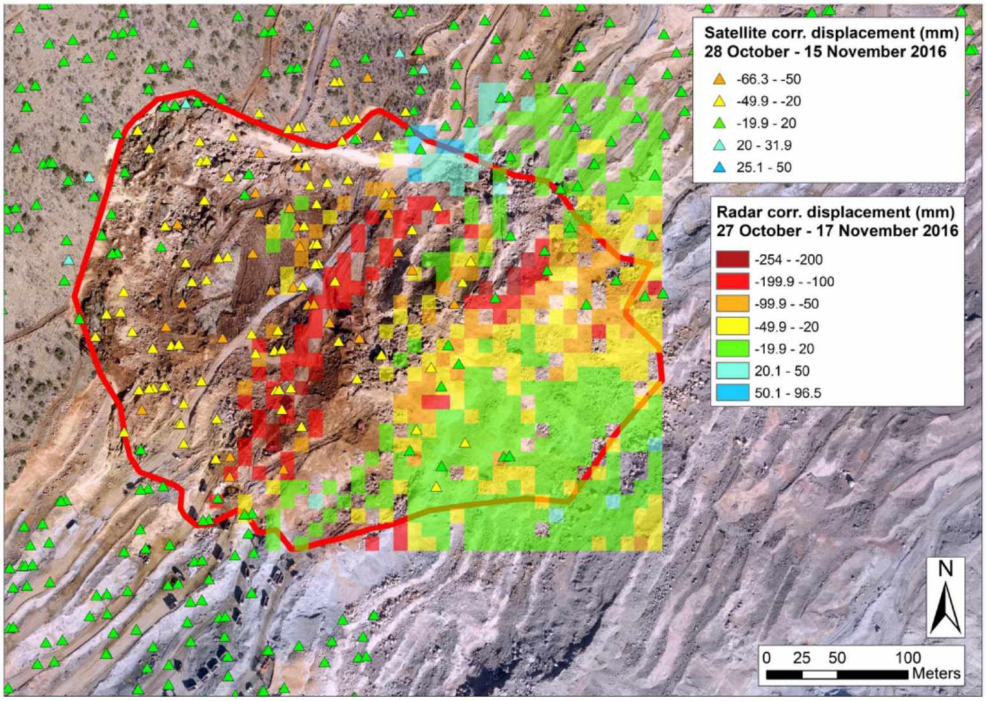

Figure 3.5 Comparison between satellite InSAR and resampled radar data (Carlà et al, 2018)

There, even though ground-based radar measurement is more reliable in terms of precision, it has some limitations regarding the size of the covered area. More specifically, ground-based radar was unable to detect the displacement on the top of the crest, but satellite sensors detected much longer displacements than ground-based radar and predicted the potential failure.

The collected data from the slope monitoring which include velocity, displacement, and acceleration should be compared with numerical simulation results to ensure the pit slope response. Tracking of monitoring data and their comparison with numerical simulations will result in early detection of potential instability. The potential failure could be predicted by its strain and displacement, which are discussed in detail below.

3.3.2. Failure Prediction with Strain

Newcomen and Dick (2016) plotted the correlation between RMR and strain of slope failures by using collected the database of pit highwall wedge and planar failures from a total of forty-eight slope failures, as shown in Figure 3.6. However, since each slope behaves differently depending on the climate and geological environments, they suggested general guidance regarding the strain threshold for the mining activities that do not have the historical monitoring data and experience, like EMC.

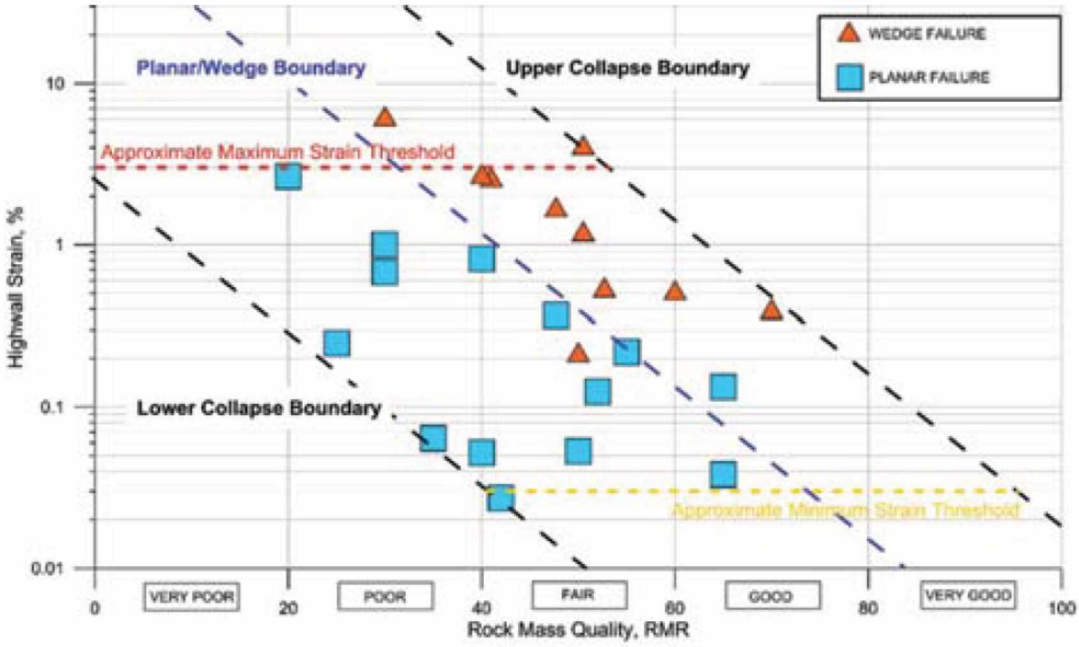

Figure 3. 6 Strain vs RMR for planar and wedge failures (Newcomen & Dick, 2016).

Planar and wedge failures are expected from the simulations. Figure 3.6 shows that planar failures have a lower strain threshold and wider strain range than the wedge failures. The absolute strain reached 6%, and higher values were counted as an outlier. The results suggest that poor-fair RMR rock mass may have a 3% maximum and 0.03% minimum strain threshold for planar and wedge failure.

The other suggestions (Manga & Wang, 2015) are based on shear strain rather than total strain. Permanent deformation was noticed in the range of 0.01-0.1% and failure occurs at 1% and

greater. Wessels (2009, p.61) stated that "Zavodni (2001) suggests that once 0.5% strain has been exceeded, displacement rates start to accelerate. Once slope strain exceeds 1 – 2% the displacement results in collapse. Small and Morgenstern (1991) found that at a strain of between 0.6 to 1%, a failure becomes progressive." (Table 3.3)

Table 3. 3 Suggested strain level comparison (Wessels, 2009)

	North Wall	Brox and Newcomen (2003)	Zavodni (2001)	
Highwall Stability Stage	**Threshold Strain Level, %**	**Threshold Strain Level, %)**	**Highwall Stability Stage**	**Threshold Strain Level, %**
Tension Cracks	Planar : 0.2 Toppling: 0.3–0.4	~ 0.1	Regressive movement	< 0.5
Progressive Movement	Planar: 0.5-0.6 Toppling: 1-1.5	~ 0.6	Increase in movement rates	> 0.5
Imminent Failure/Collapse	Planar: 0.5 - 0.7 Toppling : >1.7	>2.0	Slope acceleration (results in collapse)	1.0 - 2.0

3.3.3. Failure Prediction with Displacement

The most common graph, which shows the trend of displacement, is slope stability monitoring displacement vs time. This graph is suitable for the early stages of displacement, which are small and have an almost constant velocity. If the moving rock slope is monitored regularly and the slope displacement trend changes, the displacement rate or acceleration vs time graph can be prepared for further investigation. According to Chen (2019), if acceleration is observed in the slope creeping curve, failure will occur. Once the open-pit highwall is unstable, there is no economical way to stop it, although the failure impact should be reduced by predicting the failure date and taking necessary actions suggested in Table 3.4.

Table 3. 4 Displacement rate thresholds and related actions and/ or descriptions (Wessels, 2009)

Author	Movement thresholds	Actions Description
Martin (1993)	0.1mm/day (0.004 mm/hr)	Initial rock mass response
	0.2 to 2 mm/day (0.008 to 0.08 mm/hr) Strain hardening	Strain hardening
	10 - 100 mm/day (or more) (0.4 - 4.1mm/hr)	Progressive failure
Flores and Karzulovic (2001)	Less than 10mm/day (0.4mm/hr)	Conditions normal; no indication of instability
	10 - 30mm/day (0.4 to 1.25mm/hr)	More detailed monitoring required, Appearance of cracks
	30 - 50mm/day (1.25 - 2.1mm/hr)	Potential for instability (if ongoing for longerthan 2 weeks)
	More than 50mm/day (2.1mm/hr)	No mining allowed
Zavodni (2001)	0.1mm/day (0.004 mm/hr)	Initial response
	Less than 17mm/day (0.71 mm/hr)	No failure expected within 24hrs
	Less than 15mm/day (0.63 mm/hr)	No failure expected within 48hrs
	More than 50mm/day (2.1 mm/hr)	Indicates progressive failure (total collapse expected within 48 days)
	More than 100mm/day (4.2 mm/hr)	Clear mining area (Progressive geometry and progressive velocity)
	150mm/day (6.25 mm/hr)	Clear mining area (Regressive geometry)
Naismith and Wessels (2005)	84 mm/day (3.5mm/hr) 120 mm/day (5 mm/hr) 240 mm/day (10 mm/hr)	Alert : Increase monitoring assessments Alarm : Inform operations Scram : Pit evacuation
Roux, Terbrugge and Badenhorst (2006)	0.1 mm/day (0.004 mm/hr) for 3 days ; downward vertical movement	Red alert
	0.2mm/day (0.008 mm/hr)	Evacuate
	0.5 mm/day (0.02 mm/hr) for 10 days; horizontal movement	Orange alert
	1.0 mm/day (0.04mm/hr) for 3 days; horizontal movement	Red alert
	2.0 mm/day (0.08mm/hr) horizontal movement	Evacuate
Sullivan (2007)	0.1 - 0.25 mm/day (0.004 - 0.01 mm/hr)	Definite movement of slope related to shear of displacement on structures
	0.25 - 0.5 mm/day (0.01 - 0.02 mm/hr)	Likely to fail sometime in future
	1 mm/day (0.04 mm/hr)	High chance of failure
	More than 1.0 mm/day (>0.04 mm/hr)	Pre-failure collapse movements

There are some methods for predicting when the expected failure will take place. The case study done by Carla et al. 2018 predicted the pit slope failure precisely using the inverse velocity method, illustrated in Figure 3.7.

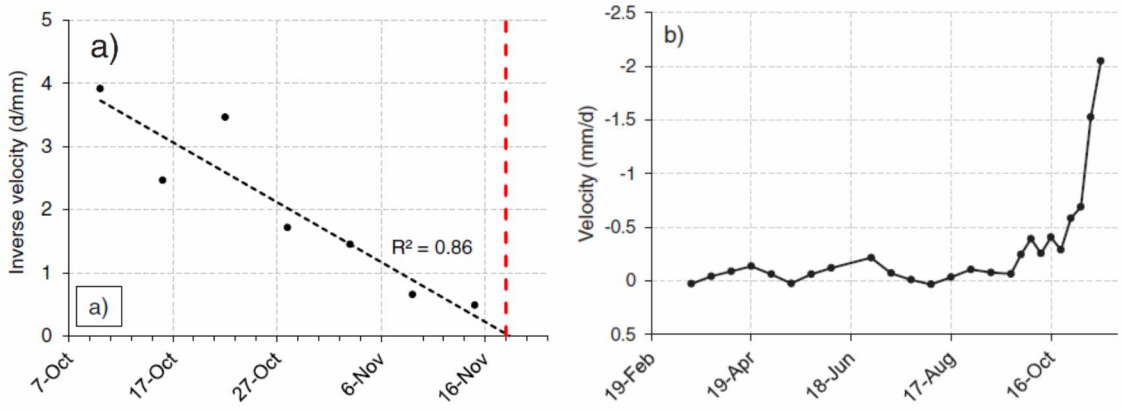

Table 3. 5a) Inverse velocity analysis and prediction of failure (red dashed line) b) Corresponding velocity when the acceleration creep is captured

The summary of displacement thresholds, actions, and trigger levels were shown in Table 3.5, and the movement thresholds vary depending on different cases, geological environments, and pit geometries. This general guidance might be beneficial for the mines which do not have initial monitoring data.

Chapter 4

4. Numerical Simulation Analysis and Results

Erdenet mine's North-West open-pit slope stability is evaluated based on the FOS, which is defined as resisting force over the driving force ratio of the rock mass. The pit is divided into ten slope cross-sections, and each cross-section's FOS is calculated by the FLAC2D simulation program. The minimum acceptable FOS for each cross-section is set to be 1.5 by considering mine life and recent monitoring results. The slopes which have lower values of FOS than 1.5 need to be inspected. Estimation of stability of high slopes will be biased if it is represented by only one FOS value. Thus, the FOS contour helps to analyze the entire slope stability in detail. Generally, high slopes may have different ranges of FOS, and the region which has the minimum FOS will be the most critical and should be paid more attention. The FOS contour of the cross-section I-I North (I-I cross-section of the north side of the pit) in Figure 4.1 is composed of three major parts, i.e., blue, green, and red colored. Top three benches, red in color, have the lowest FOS values.

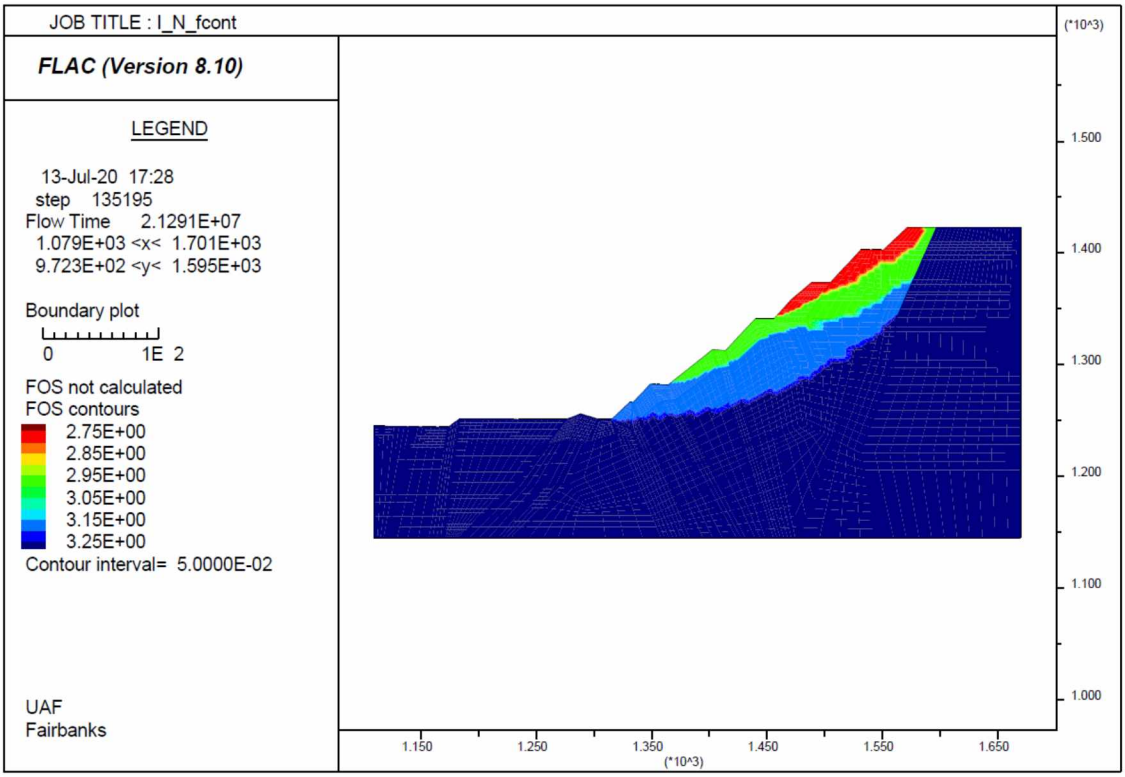

Figure 4. 1 Factor of safety contour of I-I North cross-section

Other than a prediction of slope stability, estimation of the potential failure, which could be predicted by the computer simulation, is crucial for engineering purposes. The shape and size of the potential failure could affect the mine design and optimization.

4.1 FOS

Depending on the safety regulations and the slope function, size, and effect of the failure, the minimum allowable FOS values vary in engineering slope projects. Several acceptable FOS recommendations could be found depending on the importance of the slope criteria. Priest and Brown (1983) suggested the allowable slope FOS guideline based on the consequence of failure, and they stated that FOS should range between 1.3 and 2.0 in mining application, depending on the consequence of failure, as presented in Table 4.1. They emphasized on any permanent or semi-permanent slope with moderate failure impact should have an acceptable FOS of 1.6. Another suggestion (Wesseloo & Read, 2009) states that slope stability should individually be designed for each slope scale, namely bench height, inter-ramp angle, and overall angle. Both allowable FOS and the probability of failure (PF) values depending on the failure consequence level should be provided, as shown in Table 4.2. Accounting for the consequence of failure, life of the mine, characteristics of the monitoring technique, fact that current pit is a semi-permanent slope, the acceptability criterion for Erdenet mine open-pit slope stability should have an overall FOS greater than 1.5, with a simulated 0.165g earthquake.

Table 4. 1 Allowable FOS guideline (Priest & Brown, 1983)

Consequence of failure	Examples	Acceptable values
Not serious	Individual benches; small (<50 m), temporary slopes, not adjacent to haulage roads	1.3
Moderately serious	Any slope of a permanent or semi-permanent nature	1.6
Very serious	Medium-sized (50-100 m) and high slopes (>150 m) carrying major haulage roads or underlying permanent mine installations	2.0

Table 4. 2 Typical design acceptance criteria for open-pit slopes (Wesseloo & Read, 2009)

Slope scale	Consequence of failure		
	Low	Medium	High
Bench	FOS ≥1.1 PF≤ 25-50%		
Inter-ramp	FOS ≥1.15-1.2 PF≤ 25%	FOS ≥1.2 PF≤ 20%	FOS ≥1.2-1.3 PF≤ 10%
Overall	FOS ≥1.2-1.3 PF≤ 15-20%	FOS ≥1.3 PF≤ 5-10%	FOS ≥1.3-1.5 PF≤ 5%

4.2 Simulation Model

Five different cross-sections of the North-West open-pit are chosen from the geological exploration cross-sections, as shown in Figure 4.2 for the investigation of the slope stability, i.e.: A-A, I-I, XVIII-XVIII, IX-IX, and X-X as shown in Figure 4.3. The selected cross-sections are distributed evenly in the open-pit and each cross-section is divided into South (S) and North (N) subsections. Only the A cross-section, which extended laterally, is composed of East (E) and North (N) subsections. In total, five cross-sections or ten different slope stabilities are simulated in terms of FOS with FLAC2D geotechnical software. Geological cross-section images are georeferenced and the features are redrawn by AutoCAD 2018 program, redrawn A-A cross-section is shown in Appendices Figure A.4, then used in FLAC modeling.

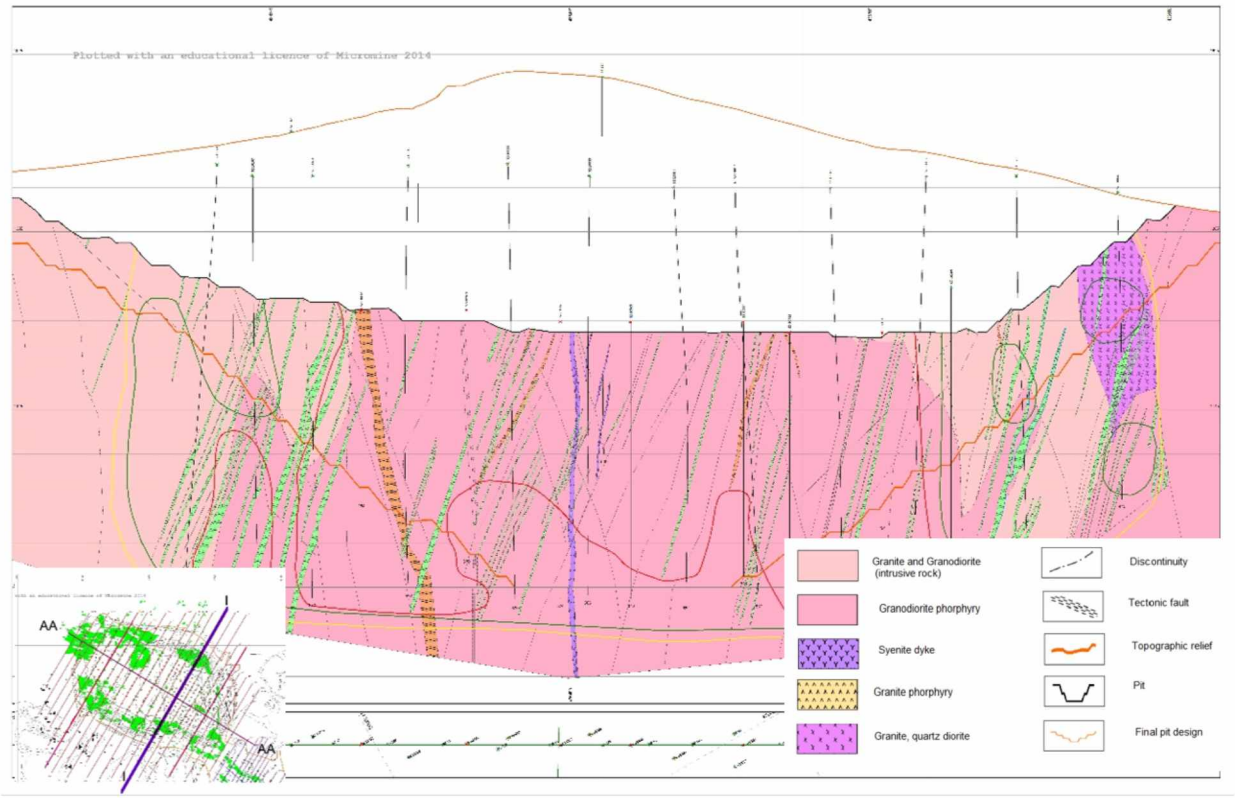

Figure 4. 2 The I-I geological exploration cross-section

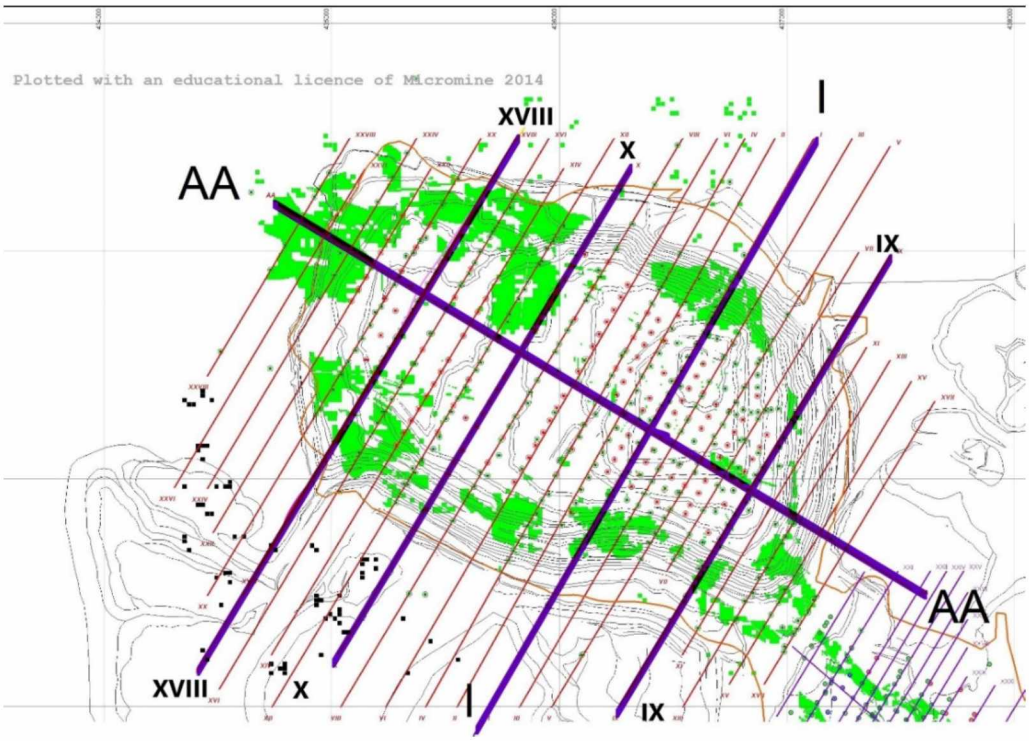

Figure 4. 3 The highlighted geological cross-sections used in the numerical method

A representative computer model of I-I North is illustrated in Figure 4.4. The I-I North cross-section is one of the deepest cross-sections in the computer simulation modeling, which has 560 m in length and 278 m in height (178 m of slope height). The model is composed of two different rock masses with the following properties respectively (see in Figure 4.4):

- Property I: inside 2a (Blue colored): Main host rock, strong
- Property II: face 2b (Green colored): Rock mass near the face, weakened by blasting

The majority of the potential failure is expected in the weak rock mass, near the face and thus finer cell size (maximum 2.5 m) is chosen for "face 2b" rock mass to examine individual bench stability in detail. On the other hand, stronger rock mass "inside 2a" has a relatively coarser cell size. In the I-I North cross-section model, the black lines are the interfaces of the major joints and tectonic faults, as presented in Figure 4.4.

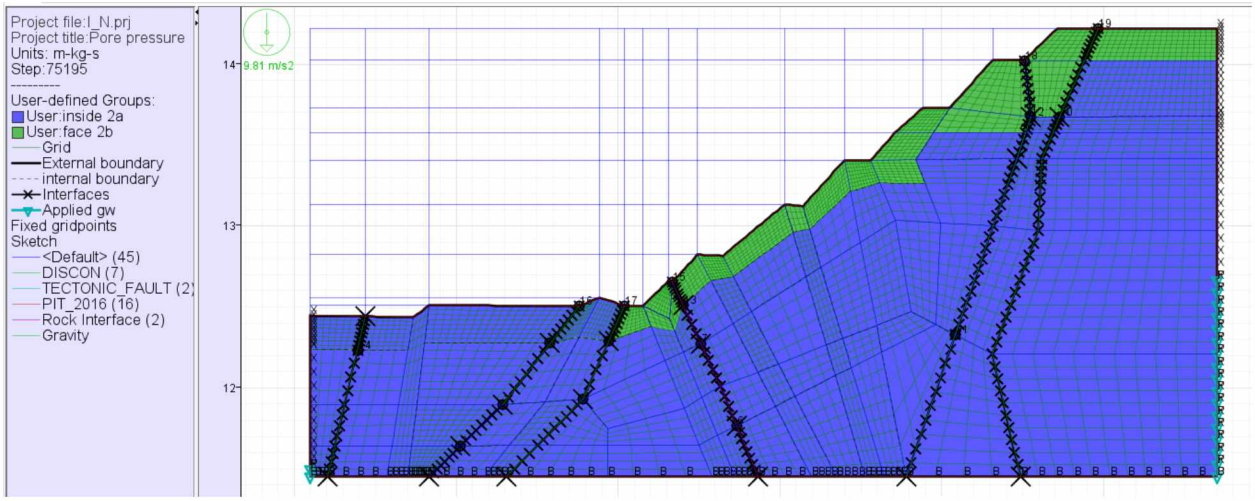

Figure 4. 4 Representative computer model of I-I North cross-section

As shown in Figure 4.5, the boundary of the simulation model extends 100 m extra to the right of the slope and 100 m extra to the bottom of the pit. This is to reduce boundary effects in the simulation. Roller supports are applied to the left and right sides of the simulation model, allowing only vertical (y) direction deformation. The bottom boundary is fixed. In the model, the slope is formed by simulating the excavation of the light green colored region as shown in Figure 4.5, to accurately calculate the actual displacement and strain along the slope.

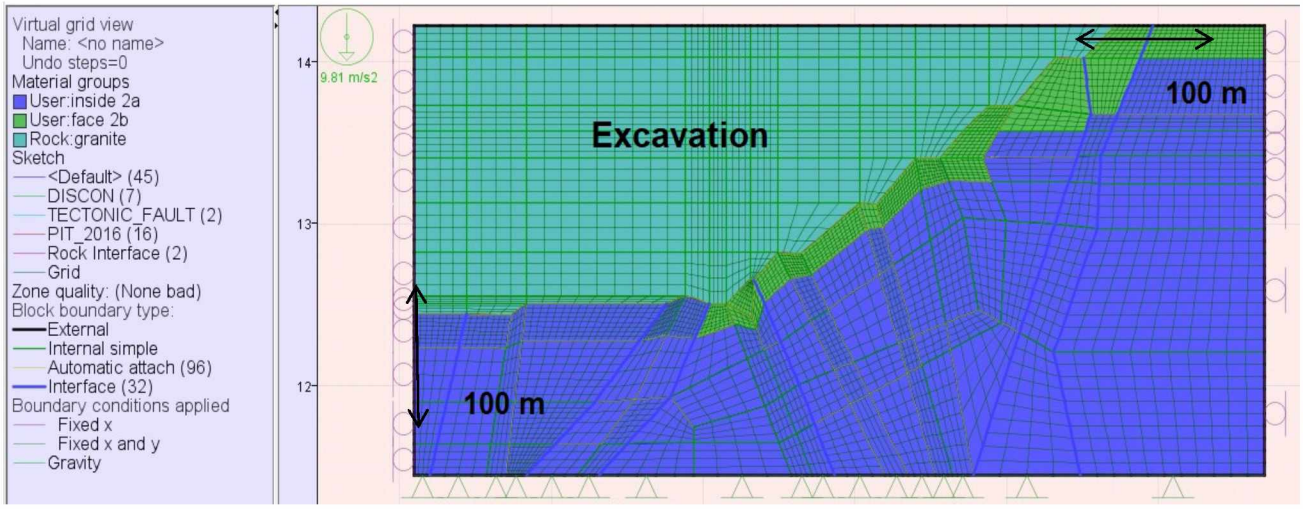

Figure 4. 5 Boundary conditions and excavation of I-I North cross-section

4.2.1 Rock and Rock Mass Parameters

In order to define rock and rock mass properties of the North-West pit, GEOtest performed diamond core drilling, highwall face-mapping, and rock sample laboratory tests (2018).

Based on rock grades defined in Table 4.3, Table 4.4 summarizes the rock grades of core samples from diamond core drilling boreholes, BH-5, 6, 7, and 8. As illustrated in the table, rock grade has a direct relation to the depth. It is obvious that the boreholes located at pit edges (BH-1, BH-5, and BH-6) have weaker rock near the surface, as shown in Table 4.4.

The corresponding rock grade's description, field identification, and approximate UCS are shown in Table 4.3.

Table 4. 3 Rock classification (ISRM, 1981b, as cited Wyllie & Mah, 2004))

Grade	*Description*	*Field identification*	*Approx. range of uniaxial compressive strength (MPa)*
R6	Extremely strong rock	Specimen can only be chipped with geological hammer.	>250
R5	Very strong rock	Specimen requires many blows of geological hammer to fracture it.	100–250
R4	Strong rock	Specimen requires more than one blow of geological hammer to fracture it.	50–100
R3	Medium strong rock	Cannot be scraped or peeled with a pocket knife, specimen can be fractured with single firm blow of geological hammer.	25–50
R2	Weak rock	Can be peeled by a pocket knife with difficulty, shallow indentations made by firm blow with point of geological hammer.	5.0–25
R1	Very weak rock	Crumbles under firm blows with point of geological hammer and can be peeled by	1.0–5.0

Table 4. 4 Rock classification in various depths of boreholes

Grade	depth (m)				
	BH-1	BH-5	BH-6	BH-7	BH-8
R0		6	4		
R3	150.2		96		128
R4		30 255		28.4 501	490
R5	200		303	47.5	500

The majority of the rock mass is granodiorite. This classification was made based on diamond drill rock core sample grade (Table 4.4), geological strength index (GSI), and the effect of blasting, among other things. The rock core samples collected from the EMC mine site had been brought to be tested for direct shear strength of different discontinuities. However, laboratory works were canceled due to Covid-19 pandemic. Instead, the rock mass properties of North-West pit produced by GEOtest, are used in the numerical simulation (Table 4.5).

Table 4. 5 Strength and deformability parameters for rock mass used in numerical model (GEOtest, 2018)

Parameter	Symbol	Unit	Rock Mass (Inside)	Rock Mass (Near Face)	Discontinuity
Mass-density	ρ	kg/m^3	2570	2520	2200
Young's modulus	E	MPa	5000	1500	300
Poisson's ratio	v	-	0.22	0.16	0.3
Cohesion	C	kPa	456	100	24
Tension	T	kPa	48	48	16
Friction angle	φ	°	39	45	42
Dilation angle	ψ	°	0	0	0

As stated above, two different rock mass properties are used in the model, i.e. inside rock mass, and near face rock mass. Rock mass near the face is relatively weak due to blasting damage and weathering.

The simulation used the most common and simplest stress-strain model, called linear elasto-perfectly-plastic, which is sufficient for slope FOS calculation. The shear stress is defined by the Mohr-Coulomb criterion, cohesion, and friction angle. The material behavior is described by the stress-strain relationship, represented by Young's modulus (E) and Poisson's ratio (v). The tensile strength of the rock mass is calculated by RocData 5.0 of RocScience software, presented in Appendices (Figure A.5). The calculated tensile strength is verified by the rule of thumb which states that rock mass tension strength is approximately equal to 10% of the cohesion.

It is impossible to include all discontinuities in the simulations. Only the major joints and faults that are presented in the geological exploration map are modeled explicitly. The other discontinuities noticed in face mapping and core samples are included implicitly in rock mass properties. Joint normal (Kn) and shear (Ks) stiffness represent the elasticity of the discontinuity.

4.2.2 Discontinuity Property

Apparent stiffness could be found following equation:

$$\text{Max}\left[\frac{(K+\frac{4}{3}*G)}{\Delta Z_{min}}\right] = \text{Max}\left[\frac{(7.35*10^8+\frac{4}{3}*6.46*10^8)}{3.5}\right]=4.56*\ 10^8$$

Where Bulk moduli, B=$7.35*10^8$ Pa

Shear moduli, G=$6.46*10^8$Pa

The smallest width in the normal direction ΔZ_{min}= 3.5 m (FLAC manual, 2020)

Normal stiffness, K_n, and shear stiffness, K_s, are estimated by a good rule-of-thumb, which states that they are ten times higher than stiffness of the stiffest neighboring zone. Extreme higher values of stiffness can result in no movement or very slow response along the interface. In contrast, lower stiffness is associated with small interface deformation (FLAC manual, 2020).

The normal and shear stiffness of the interface is found to be:

K_n= K_s=10*4.56e8=$4.56*10^9$ Pa/m

4.2.3 Earthquake

Earthquake occurance and groundwater increase are the main natural phenomena that cause slope failure. Due to seismic load induced by blasting and earthquake, shear stress increases, and thus FOS drops. However, the possibility of an earthquake seems low, it should be taken account of FOS calculation. According to the research done by the Global Earthquake Model (GEM) in 2018, an earthquake in the Erdenet area with a peak ground acceleration (PGA) of 0.08-0.13 g has a 10% possibility of occurring in 50 years. Also, PGA reaches 0.13-0.20 g at a point 30 km north of the Erdenet Mine (Pagani et al., 2018).

The peak ground acceleration during earthquakes and its probability near the Erdenet Mine area is presented in the seismic hazard map (Figure 4.6).

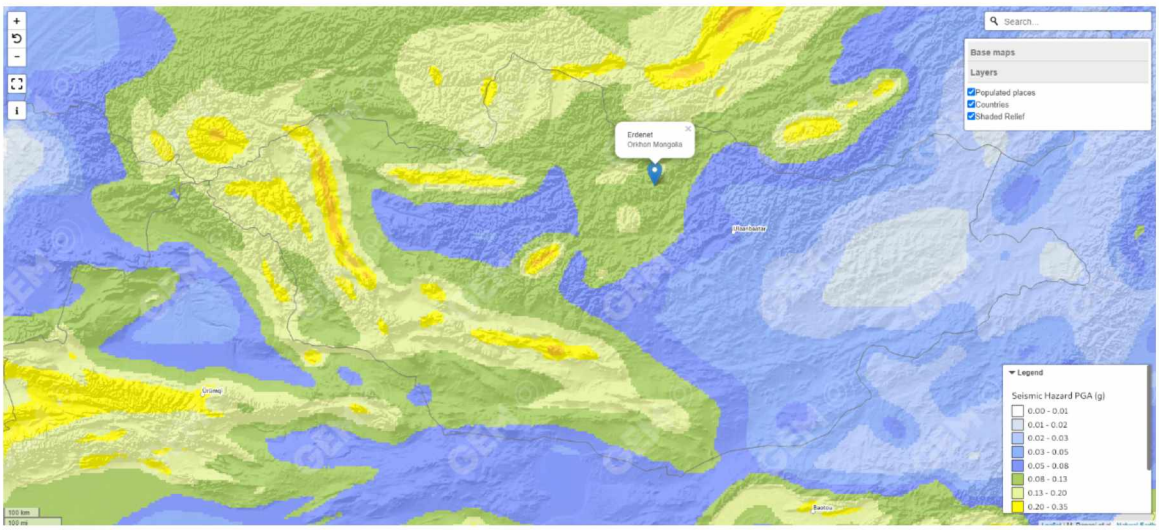

Figure 4. 6 Seismic Hazard Map of Erdenet Mine region (Pagani et al., 2018)

The mean value of the most likely and the most unlikely scenario PGA i.e. 0.105g (1.03m/s^2) and 0.165g (1.62m/s^2) respectively, are separately modeled in the computer simulations. The stability of slope under seismic activities is estimated by pseudostatic analysis with the assumation of an earthquake with constant horizontal acceleration. The vertical acceleration coefficient, k_v, is set zero and horizontal acceleration coefficient, k_h, is set 0.105 and 0.165. Pseudostatic acceleration coefficients, k_h and k_v, magnitude represent the severity of the earthquake. Gravitational vector is adjusted by introducing horizontal acceleration component of a_h ($a_h=k_h*g$) which towards the pit center.

4.2.4 Underground water

In September 2018, the lowest level of underground water level was measured at 1140 m, which was about 100m below the lowest operation bench level of 1235 m (Figure 4.7).

Underground water level is slightly inclined towards the center of the open-pit, and water is collected in the sump (1220 m), which is located at the lowest bench level. The collected water is pumped out of the pit continuously.

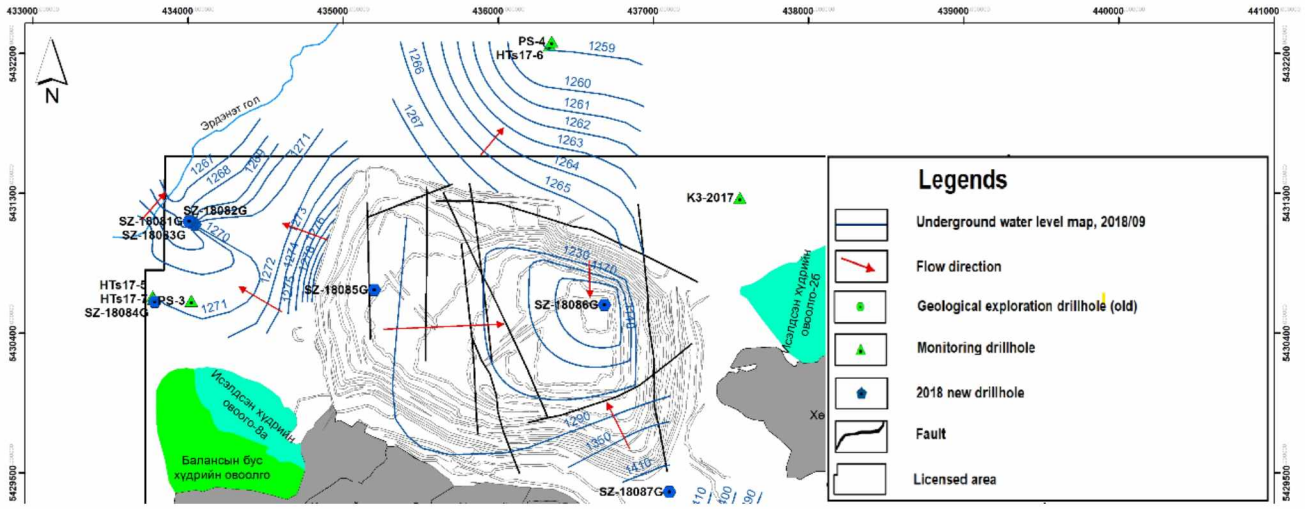

Figure 4. 7 Underground water level map (EMC, 2018)

Pore water pressures in each cross-sections are separately calculated for use in the computer simulation. The following is the calculation of I-I North cross-section's pore pressure:

Groundwater (I-I North)

g_w=9.81 kN/m^3

Pore pressure range (right side)

Depth of water table, h_w= 1265-1145=120 m

Pore water pressure, p_s= g_w* h_w=9.81*120=1177.2 kPa

Pore pressure range (left side)

Depth of water table, h_w= 1150-1145=5 m

Pore water pressure, p_s= g_w* h_{w1}=9.81*5=49.05 kPa

The calculated underground water pore pressure, as shown in Figure 4.8, may have a significant effect on the slope stability, depending on the depth of the mine underground water level.

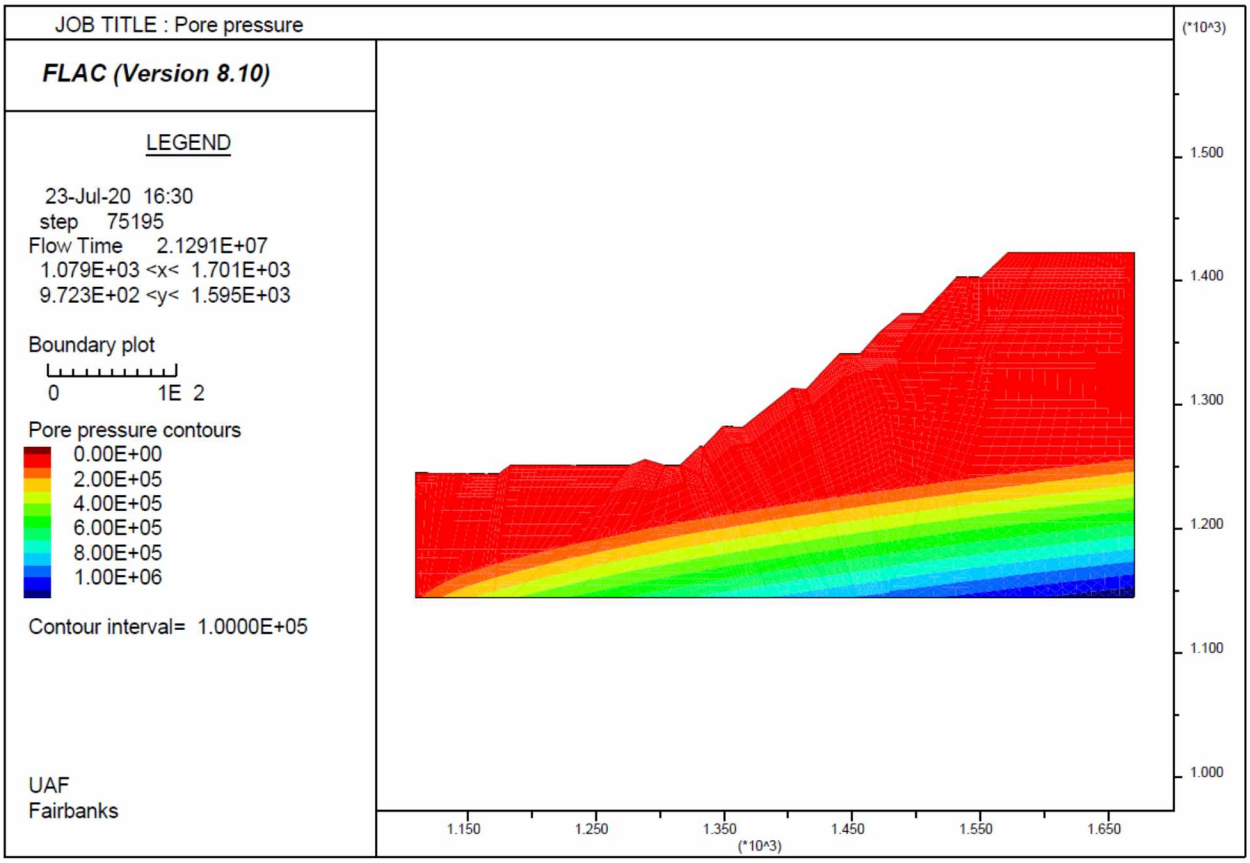

Figure 4. 8 Pore pressure of I-I North cross-section

4.3 Simulation Result

Each cross-section is individually simulated by FLAC software and they are stable and no severe yielded region noticed in the simulation. The actual displacement of I-I North cross-section, as illustrated in Figure 4.9, has a maximum displacement of 12 cm at the bottom of the pit. This should have no impact on slope stability because the major part of actual displacement is Y-displacement, presented in Appendices Figure A.6, which is resulted from a huge weight release of pit excavation (see X-displacement in Figure A.7).

The FLAC slope stability simulation of I-I North cross-section provides FOS value as 2.17 and shear strain contour, shown in Figure 4.10. In the cases 0.105g and 0.165g earthquake, FOS drop to 1.78 and 1.57, respectively. Every small cell (mesh) is checked whether yielded or not. If a cell is yielded, the plasticity indicator tells more about how it is yielded.

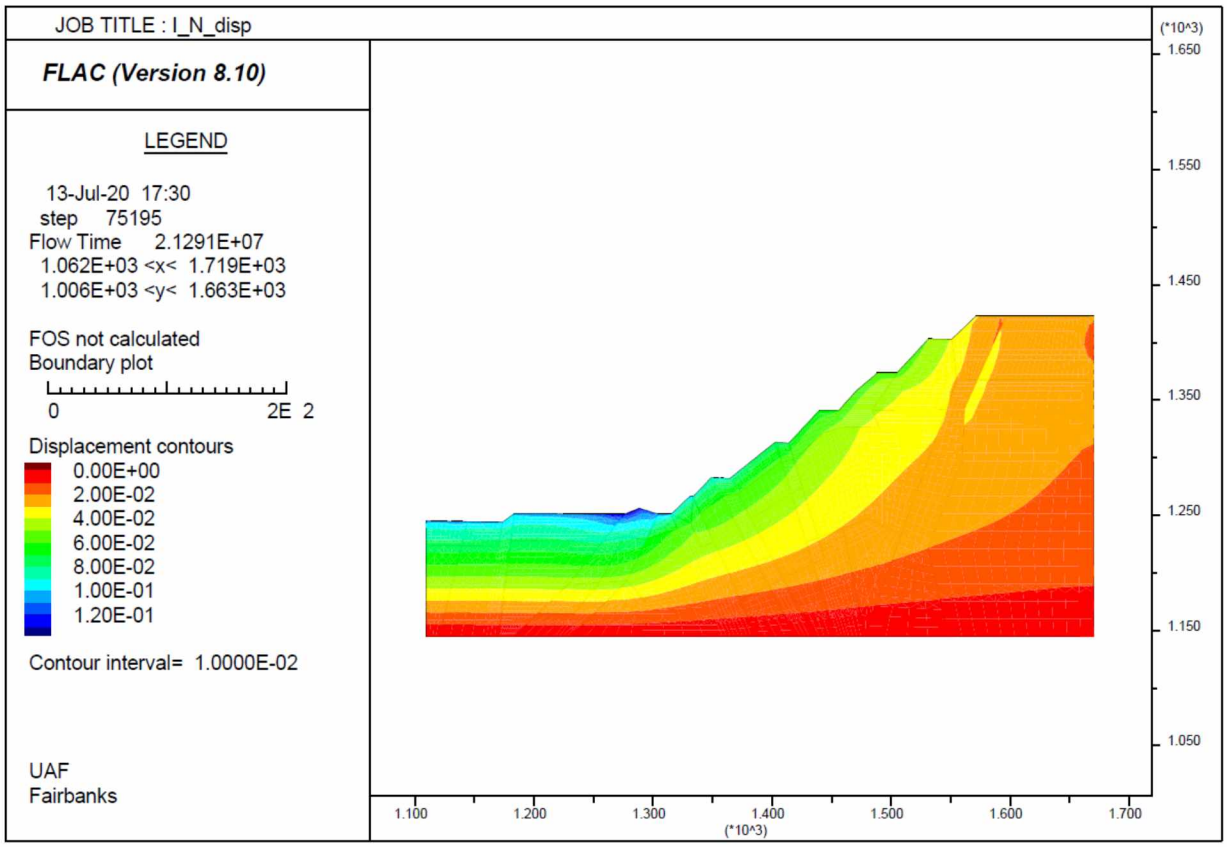

Figure 4. 9 Actual displacement of I-I North cross-section

From the shear strain contour and plasticity indicator, the failure surface is expected in top three benches, yellow colored region in Figure 4.10 has yielded by shear and top surfaces of the benches are yielded by tension. The effect of the potential failure surface could be seen by the contour of displacement at failure, as shown in Figure 4.11, and the second and third benches and the first and forth benches from the top have up to 1.4 m and 1.0 m displacement at failure, respectively.

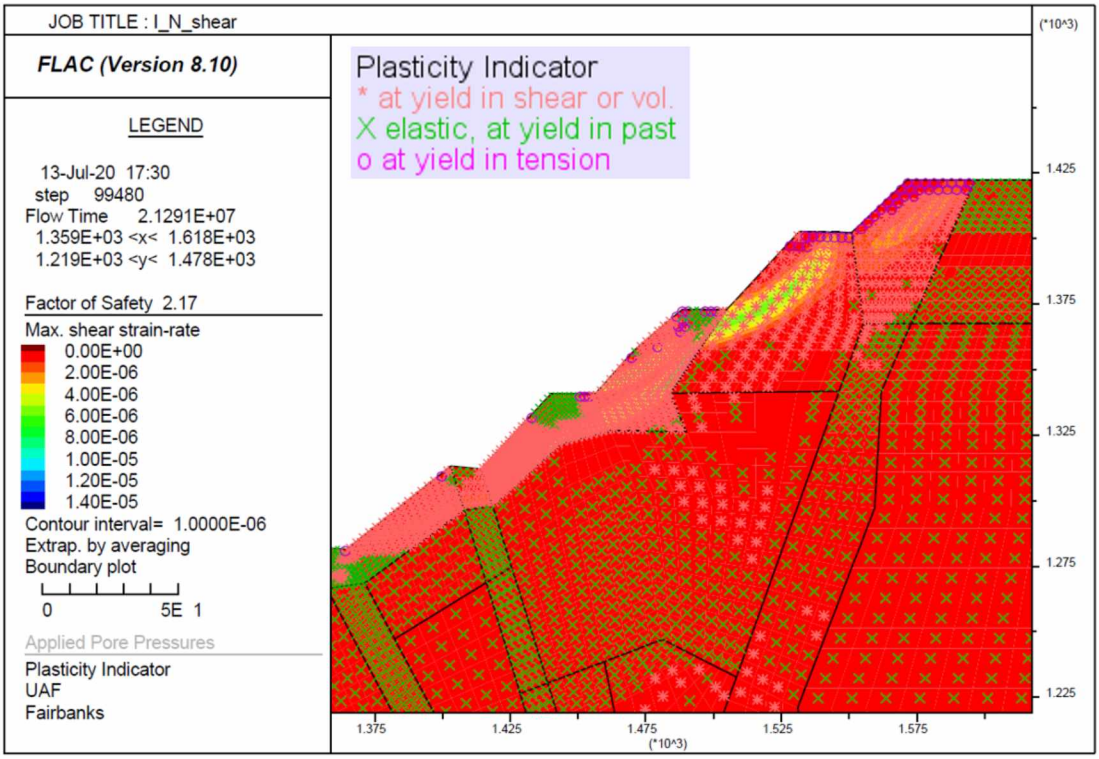

Figure 4. 10 Shear strain of I-I North cross-section

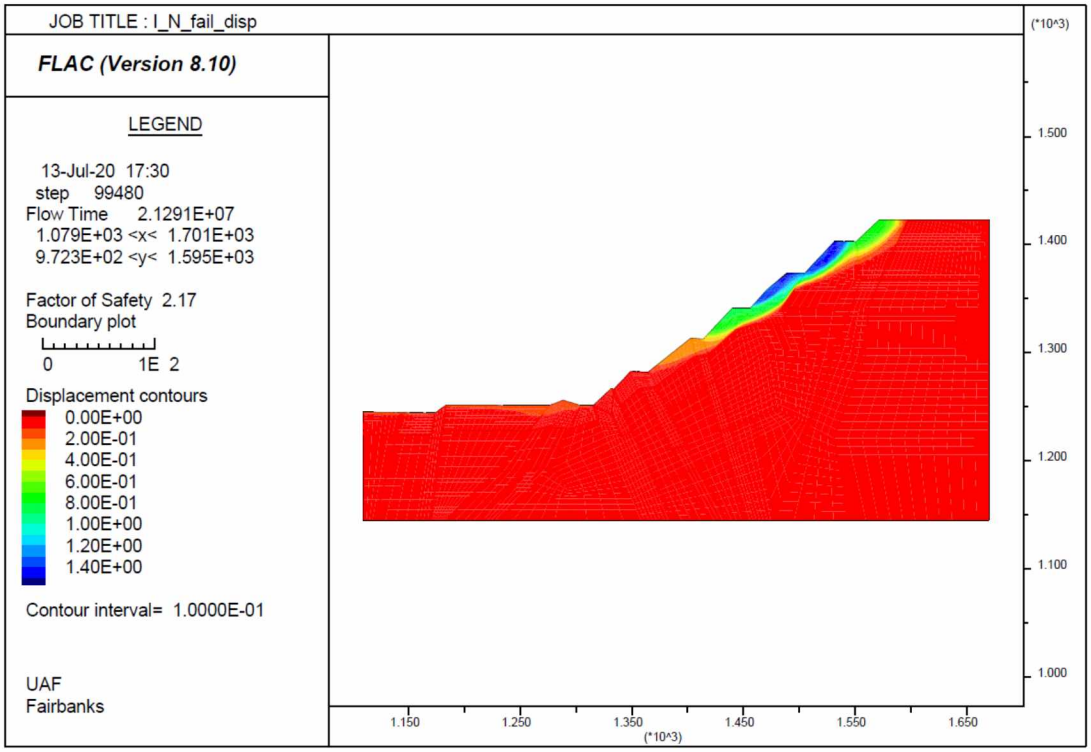

Figure 4. 11 Displacement at failure of I-I North cross-section

Another important cross-section is A-A East which has a height of 175 m and a FOS of 2.31. The second bench from the top has a potential failure as shown in Figure 4.12 (a) and it has a maximum displacement of 42.5 cm, as shown in Figure 4.12 (b). The displacement at failure increases from 42.5 cm to 170 cm with a magnitude of 0.165g earthquake, as illustrated in Figure 4.12 (b). The simulation result shows that A-A East cross-section stable enough with FOS of 2.31 (FOS 1.77 in 0.165g earthquake).

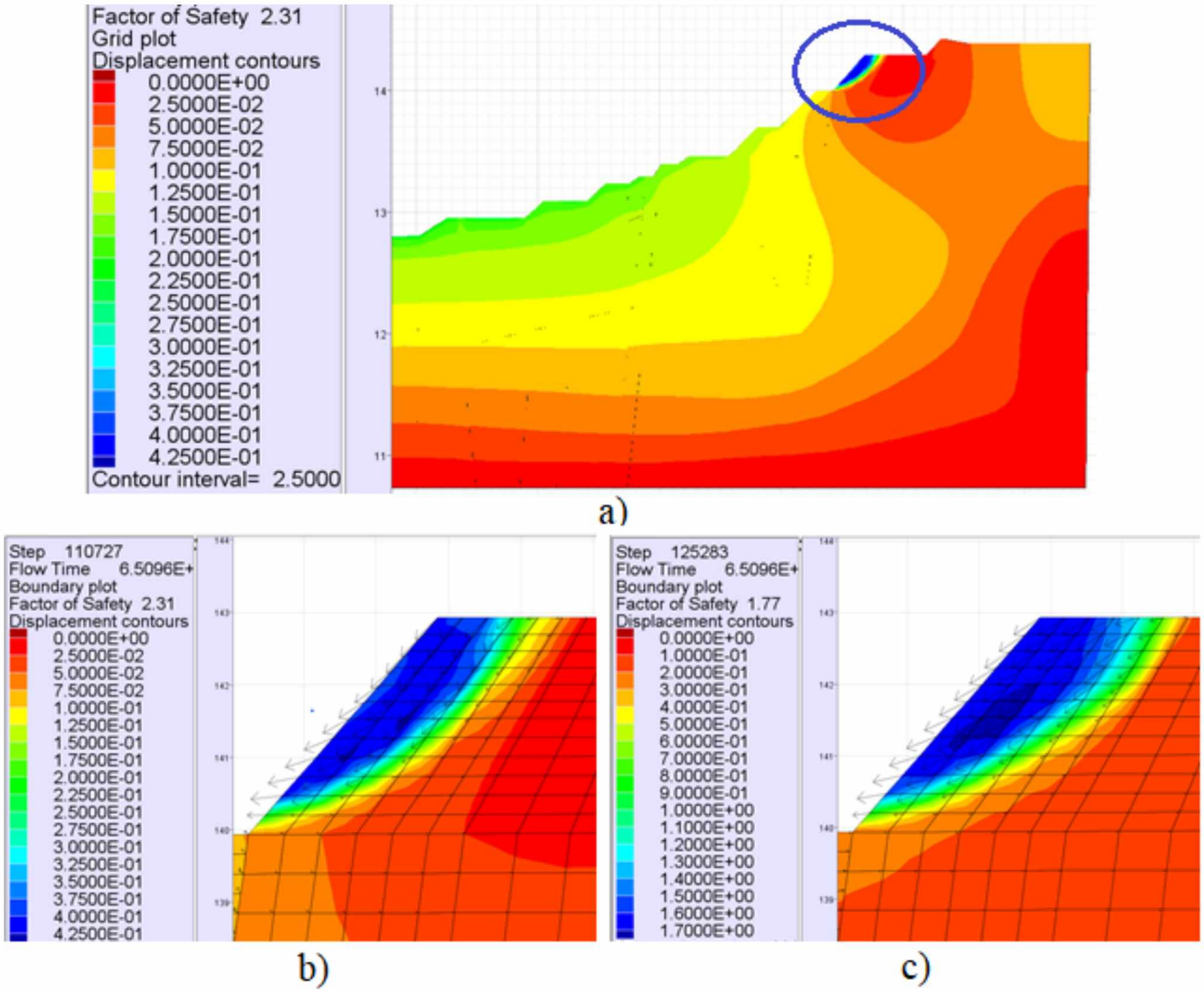

Figure 4. 12 Displacement at failure of A-A East cross-section a) position b) without earthquake c)with 0.165g earthquake

Another important result for the analysis of the slope instability is the shear strain contour. The current maximum shear strain reached 0.95 % (9.5E-3), as shown in Figure 4.13 (a), at the bottom of the pit. However, on the face of the bench slope, where it has the potential failure, the shear strain is only 0.25% (2.5E-3) less than the failure strain threshold presented in Table 3.3. The failure (Figure 4.13), would eventually develop as cohesion and friction angle reduced by SSR techniques. The location and shape of the failure surface is predicted by shear strain, and the failure mode is indicated by the velocity vector as shown in Figure 4.13 (b). The bench failure would be the combination of sliding and rotation. However, the main part of failure would slide down. The simulation result of the velocity vector as presented in Appendices Figure A.8 shows that the bottom part would be dominated by rotation along the failure surface.

Near the berm, with up to 1.25% shear strain, the rock materials yield in tension, and in the region with greater than 1.25% shear strain, they yield in shear. Also, the maximum shear strain increases when the PGA of the earthquake increases. In Figures 4.13 (b), (c), and (d), the maximum shear strain reached 4%, 11%, and 14% with no earthquake, 0.105g earthquake and 0.165g earthquake, respectively.

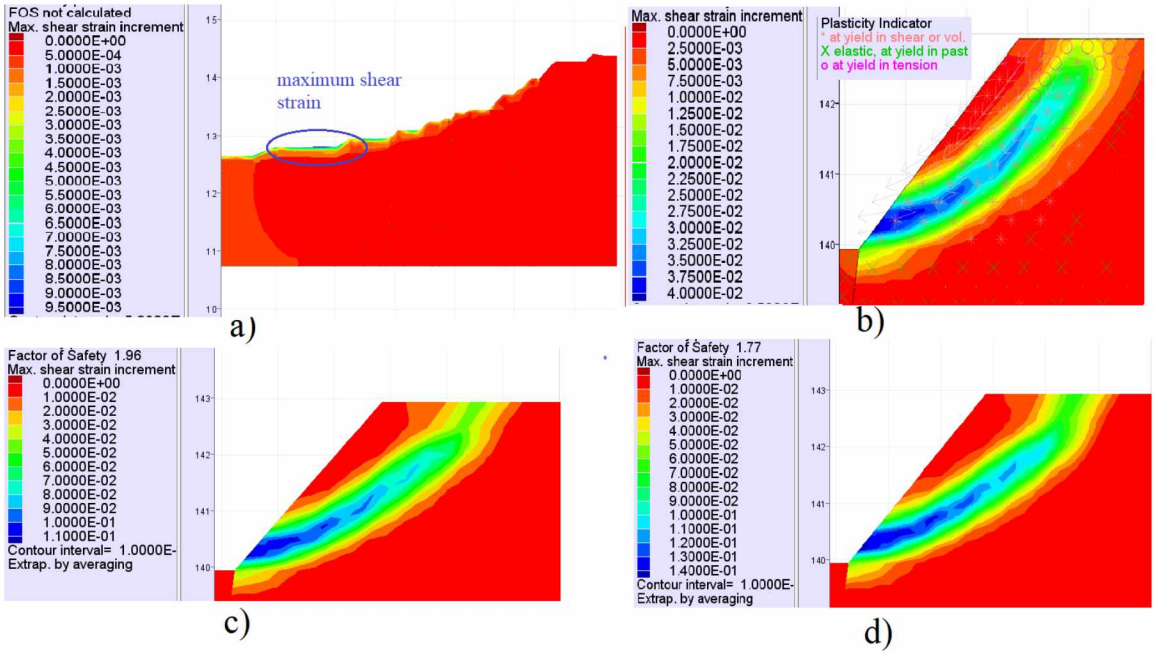

Figure 4. 13 Shear strain contour of A-A East cross-section a) current b) with no earthquake c) with 0.105g earthquake d) 0.165g earthquake

Most of the cross-sections' potential failure surfaces extend into a single bench or two benches, at maximum. Unlike the others, however, the IX-IX South cross-section has a large potential failure surface containing five consecutive benches. But this potential failure zone with high shear strain has a higher overall FOS of 2.78. The consequence of this failure can be severe due to its location which is just above the main haulage road as presented in Figure 4.14. The formation of such a potential failure surface is due to both natural and manmade causes. As shown in Figure 4.14, the upper part of the surface is along a natural discontinuity and the bottom part, which has the highest shear strain, is developed by steep toe angle, the results of excessive talus cleaning.

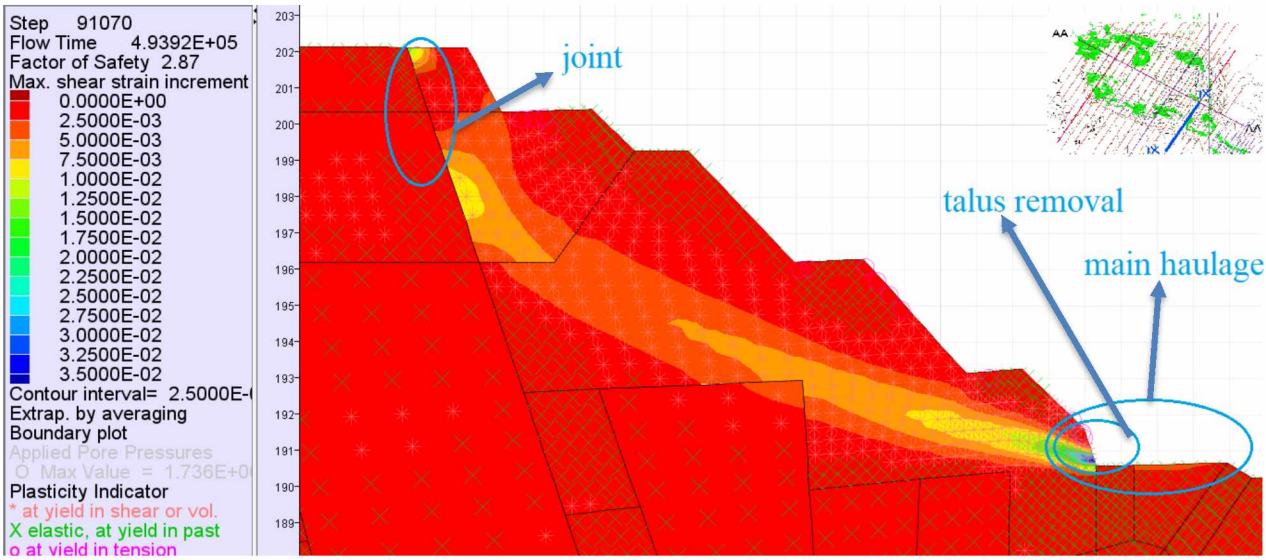

Figure 4. 14 Potential failure in IX-IX South cross-section

North-West pit slope stability simulation results (in the cases with magnitudes of 0.105g and 0.165g earthquakes) are listed in Table 4.6. The maximum and minimum FOS's are found to be 4.13 and 2.17 respectively.

Table 4. 6 Calculated slope FOSs

Cross-section	Side	No earthquake	Earthquake 0.105g, 1.03 m/s^2	Earthquake 0.165g, 1.62 m/s^2	Slope height (m)
A-A	East	2.31	1.96	1.77	175.00
	West	2.56	2.18	2.00	62.00
I-I	South	2.80	2.35	2.13	181.00
	North	2.17	1.78	1.57	178.00
XVIII-XVIII	South weak*	4.13	3.22	2.78	65.00
	North	3.29	2.85	2.60	65.00
IX-IX	South	2.87	2.31	2.05	170.00
	North	3.19	2.60	2.34	130.00
X-X	South	2.17	1.86	1.68	130.00
	North	2.26	1.86	1.66	90.00
	Max	4.13	3.22	2.78	
	Min	2.17	1.78	1.57	

In the case of a 0.105g earthquake, the maximum and minimum FOS drop to 3.22 and 1.78. The XVIII-XVIII South cross-section has the highest FOS values (see Figure A.9 in Appendices) in all cases due to having the shallowest slope depth of all cross-sections. The mining activity advances from the left to the right side of the North-West pit in several benches. That is why the east side of the pit has a lower slope depth and FOS than the west side. However, although the XVIII cross-section has a slope depth of 65m, only two benches reached the final wall. On the other hand, the I–I North cross-section has the lowest FOS value because of the steep overall angle and slope depth. The I–I cross-section is especially selected for the simulation because it passes through the bottom of the pit and the highest pit crest. The north wall has no haulage road, and ramps, and overall slope angles were found to be the deepest, ranging from 30° to 35°.

The north side of I–I North cross-section line (purple line), shown on the image of north highwall of North West pit, is illustrated in Figure 4.14.

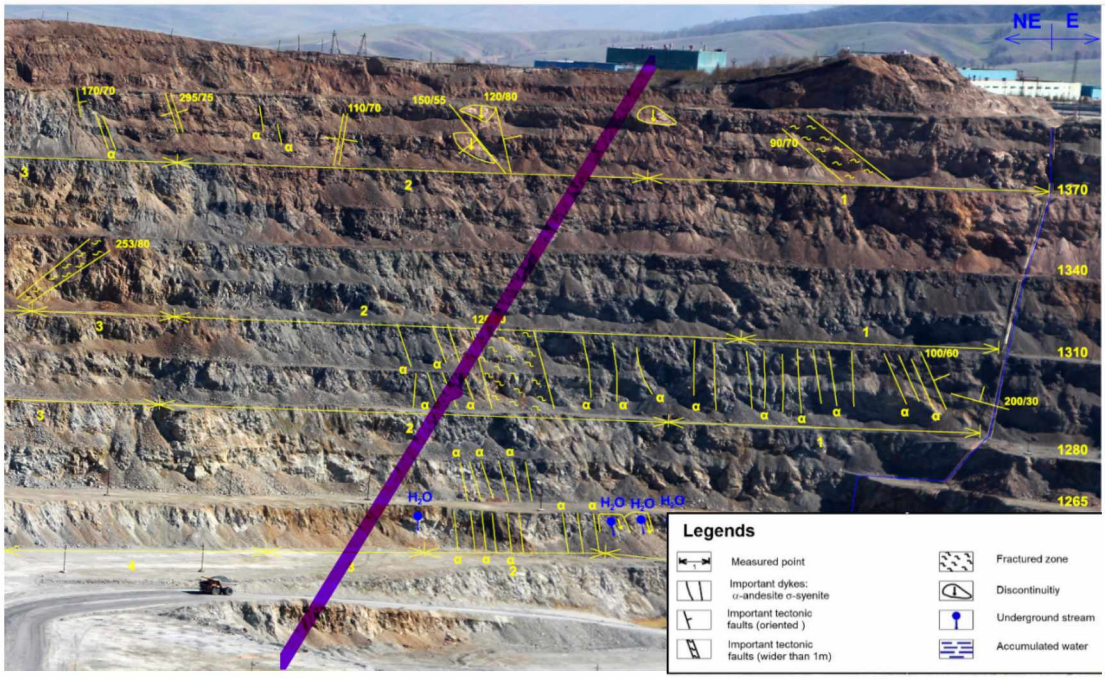

Figure 4. 15 I-I cross section on north highwall of the North-West pit (GEOtest, 2018)

4.4. FOS Comparison

The effects of a 10% modification of rock mass properties and slope angles, the two most important parameters of slope stability, on the slope FOS are investigated. This investigation is aimed to show how important these parameters are. It will also facilitate probabilistic analyses in the future as well as mine planning and optimizations. The effect of slope angle changes is particularly useful information for mine planning and optimization. Since rock mass parameters always contain uncertainties, the combination of FOS threshold values with failure probabilities will provide better design guidance for the mining industry.

To examine the sensitivity of the FOS, simulations are conducted with variations of the bench face angle, overall slope angle, and rock mass properties. The modified models are shown in Table 4.7. The simulation outcomes are presented in Table 4.8.

Table 4. 7 Input parameters of modified model

Cross-section	Model	Number of bench slopes modified*	Bench width kept same	Rock mass reduction**
I-I	North Flat	3	✓	
	North Flat1	5	✓	
XVIII-XVIII	South weak			✓
	South steep	6 (increased)		
IX-IX	North Flat	2		

***Number of bench slopes modified:** Bench angle is reduced by 10% of its original angle.

** **Rock mass reduction:** Cohesion, friction angle, young's modulus, and tension are reduced 10% of their original values.

Table 4. 8 The FOS comparison of original and modified model

Cross-section	Model	No earthquake	Earthquake 0.105g	Earthquake 0.165g
I-I	North	2.17	1.78	1.57
	North Flat *	2.21	1.81	1.61
	North Flat1 *	2.34	1.90	1.66
XVIII-XVIII	South	4.54	3.50	3.05
	South Weak *	4.13	3.22	2.78
	South Steep *	4.11	3.38	3.04
IX-IX	North	3.19	2.60	2.34
	North Flat*	3.32	2.68	2.40
	Max	4.54	3.50	3.05
	Min	2.17	1.78	1.57

*modified model

4.4.1 Comparison 1

The XVIII-XVIII cross-section's modified models, South Weak and South Steep, FOS value is compared with the original model XVIII-XVIII South, presented in Table 4.9 and Figure 4.16. The models' parameter modifications are listed in Figure 4.5.

Table 4. 9 FOSs and their differences of model S, South Weak, and South Steep of XVIII-XVIII cross-sections

Cross-section	Model	No earthquake		Earthquake 0.105g,		Earthquake 0.165g	
		FOS	Difference	FOS	Difference	FOS	Difference
XVIII-XVIII	S	4.54	-	3.5	-	3.05	-
	South Weak *	4.13	0.41	3.22	0.28	2.78	0.27
	South Steep *	4.11	0.43	3.38	0.12	3.04	0.01

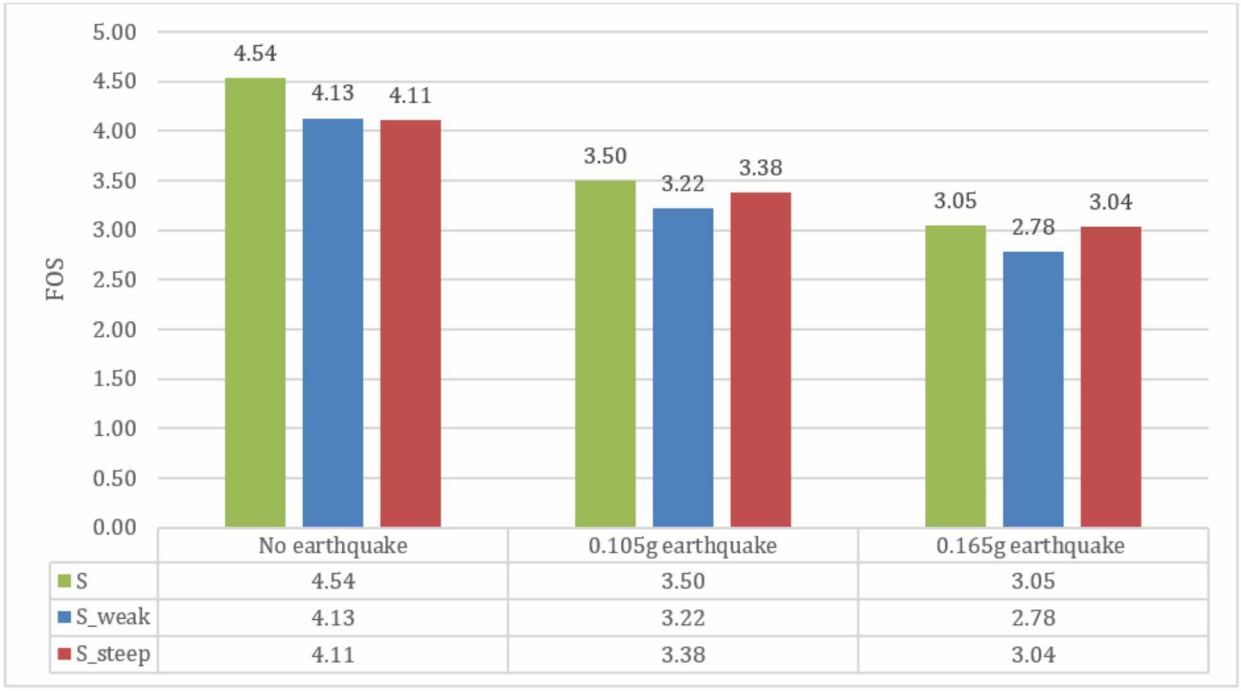

Figure 4. 16 FOS comparison of model S, South Weak, and South Steep of XVIII-XVIII cross-section

When no earthquake involved, FOS of S steep model is dropped by 0.43 unit from the original model and the South Steep has a slightly less FOS than South Weak has. With the increasing PGA of the earthquake, the FOS difference between S and South Steep model is getting less, and the difference is found 0.43, 0.12, and 0.01 in no earthquake, 0.105g, and 0.165g earthquake, respectively. On the contrary, the FOS difference of original model S and modified model South Weak is kept almost constant in earthquake cases. To sum up, although, South Steep model is found slightly less stable than South Weak model, it is more competent in earthquake cases.

4.4.2 Comparison 2

Comparison of FOS increments with a 10% reduction in face angle between the most stable cross-section, XVIII-XVIII South, and the least stable cross-sections, I-I North, are shown in Figure 4.17. The comparison includes cases with no earthquake (static), with a 0.105g horizontal earthquake and with 0.165g horizontal earthquakes.

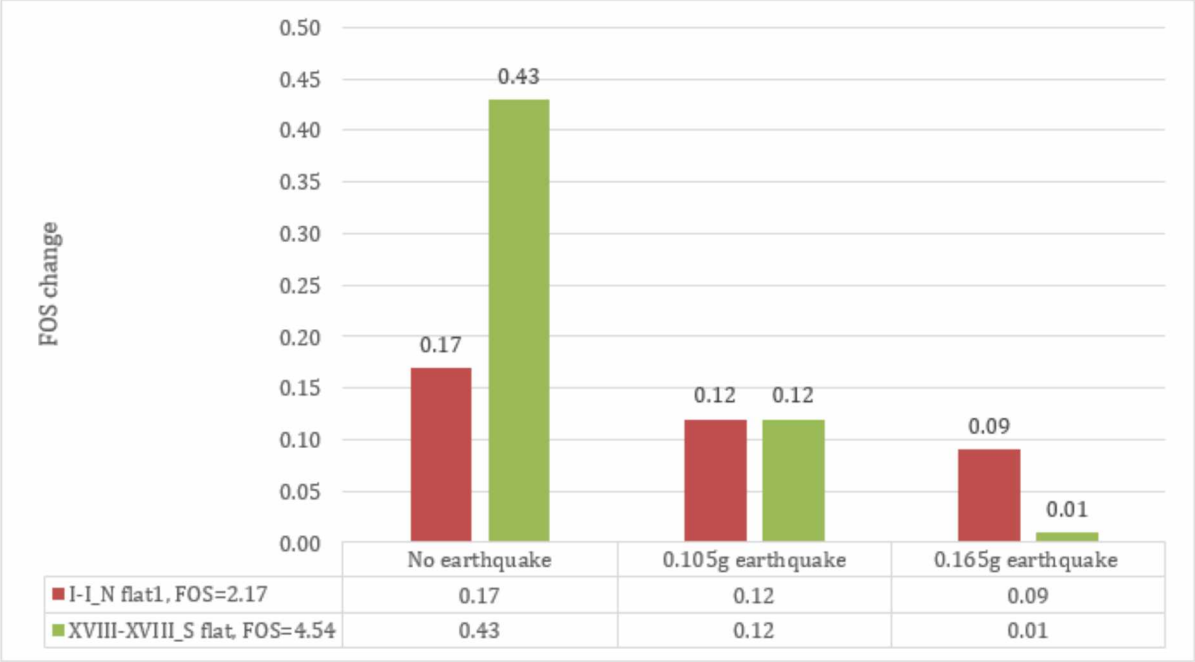

Figure 4. 17 FOS change comparison of the cross-sections which has the highest and lowest FOS value

The most stable cross-section, XVIII-XVIII South flat with a FOS of 4.54, has much greater FOS change when each bench slope angle is increased by 10% in no earthquake case.

However, FOS increment decreases for higher horizontal earthquake magnitudes. Also with a 0.105g horizontal earthquake, the FOS change due to flattening the slope are the same 0.12 for both cross-sections. Also, FOS changes significantly drops in the case of earthquakes.

4.4.3 Comparison 3

Figure 4.8 illustrates decreasing bench face angles by 10% and the original and reduced bench faces angles of I-I North Flat1 model.

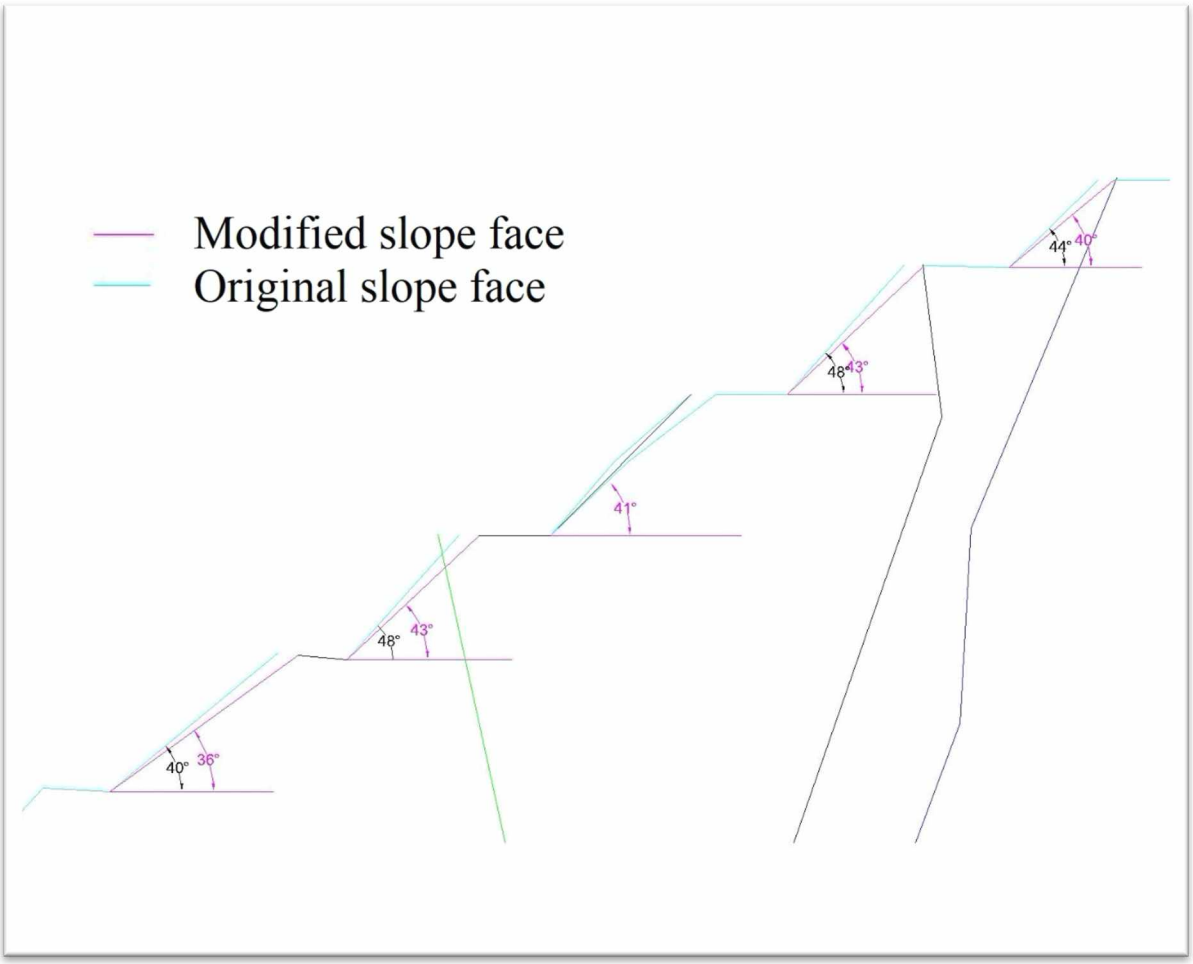

Figure 4. 18 I-I North flat1 cross-section profile with 10% lower bench face angles.

The slope angles of the top five benches of I-I North flat1 model are decreased by 10% from the original values, and bench widths are kept the same as shown in Figure 4.8. These modifications decrease the I-I North Flat1 model's overall slope angle from 33.84° to 32.42° and consequently, increased FOS from 2.17 to 2.34. Similarly, I-I North Flat model has a 33.46° overall slope and FOS reached 2.21. The original and reduced bench face angles of I-I North Flat and I-I North Flat1 model are shown in Table 4.10. The variation of FOS is investigated by reducing benches' face angles by 10% and the results are illustrated in Figure 4.19.

Table 4. 10 Angle change and corresponding FOS

cross-section	angle	bench face angle °					Overall slope angle °	FOS
		1st bench	2nd bench	3rd bench	4th bench	5th bench		
I-I North Flat	original	44	48	45	48	40	**33.84**	**2.17**
	reduced	39.6	43.2	40.5	same		**33.46**	**2.21**
I-I North Flat1	original	44	48	45	48	40	**33.84**	**2.17**
	reduced	39.6	43.2	40.5	43.2	36	**32.42**	**2.34**

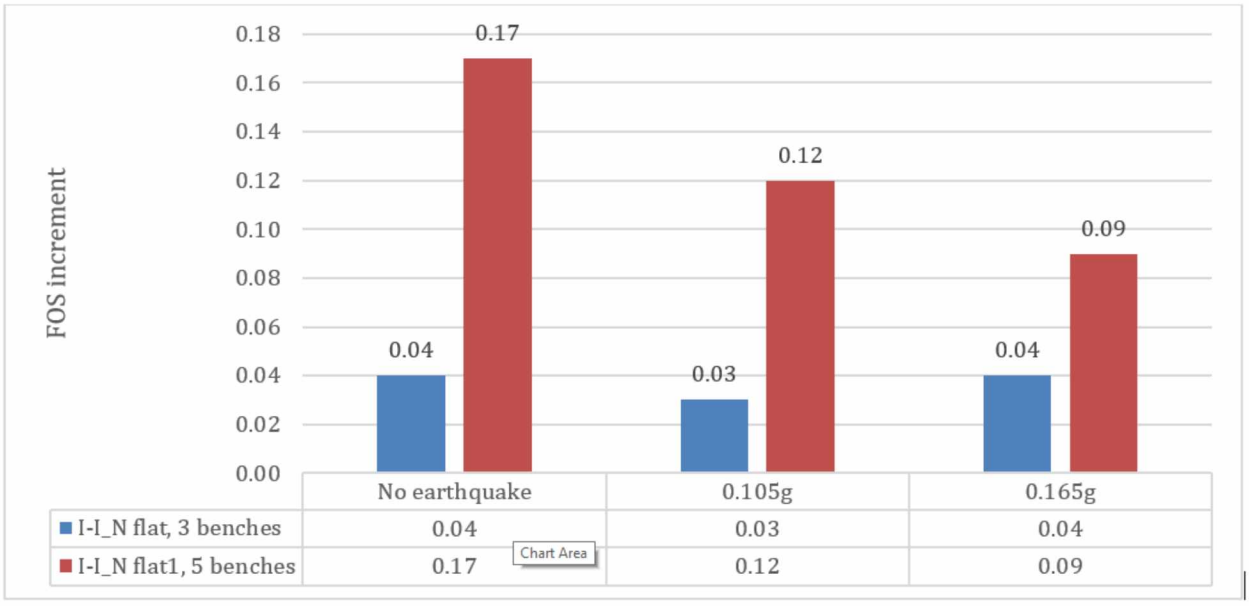

Figure 4. 19 FOS increment comparison of 10% reduction of different numbers of bench's face angles

The top benches are chosen to be modified due to their higher shear strain and, therefore, are more critical for potential failure. The face angles of the top 3 and 5 benches of I-I North Flat and I-I North Flat1 cross-section model, respectively, are decreased by 10% of their original values. Overall slope stability could be increased by 0.17 and 0.04 units of FOS by 10% reduction of 5 and 3 bench face angles, respectively. As expected, the above graph consistently shows that the more bench's face angle decreases, the more FOS value increases in all cases.

4.5 Summary

All FOS values of the ten cross-sections in the North-West pit are higher than allowable FOS of 1.5 with a magnitude of 0.165g PGA earthquake. The Erdenet mine's current North-West open-pit's maximum, minimum, and mean FOS values are calculated as 4.13, 2.17, and 2.78 respectively. In the most unlikely scenario, the case with a magnitude of 0.165g PGA of the earthquake, the mean FOS values of the ten different cross-section models dropped to 2.06. The model of the I-I North cross-section has the least FOS value of 1.57.

The slope stability is dependent on the slope geometry, namely the overall slope angle and slope height. A clear relation between FOS value and slope height is noticed. Unfortunately, there is no strong statistical correlation between the simulated FOS and the overall slope angle. FOS vs Overall Slope Angle (see Appendices Figure A.10) and FOS vs Slope Height (Appendices Figure A.11) have the coefficients of determination, R-squared, of 0.09 and 0.56, respectively, in linear regression. The reasons why the correlations are lower than expectation are listed below:

- The slope of the east side of the pit is shallow in depth, and most of the benches do not reach the final wall.
- The number of samples is insufficient.
- The geometries and rock mass discontinuities of each slope are different.

The high shear strain region reveals potential failure surface, which extends in most cases along with one or two benches in the simulations. Depending on the existing discontinuity orientation

and amount of excessive talus removal of the toe, the potential failure along IX-IX South cross-section may be very significant, as presented in Figure 4.14.

The effect of changing the rock mass properties and the slope angle by 10%, on the slope FOS is investigated and important findings are listed below:

- With a 10% of increase in slope face angles, the model of XVIII-XVIII South steep cross-section is found slightly less stable than that with 10% decrease of rock mass properties. But the XVIII-XVIII South steep slope is more stable in earthquake cases.
- The FOS increment with a 10% reduction in slope face angles is more significant for slopes with high FOS values than for slopes with low FOS values. FOS changes significantly drops in the case of earthquakes.
- I-I North cross-section's FOS increases from 2.17 to 2.34 and 2.21 when the overall slope angle drops by 1.42° and 0.38° respectively.

Charter 5

5. Effects on Mine Planning

The effect of the overall slope angle change in mine planning and pit optimization is investigated in this chapter. In the open-pit mine, the overall slope angle is the main parameter that directly defines the amount of waste rock to be striped and has a critical impact on highwall stability. As shown in Figure 5.1, EMC North-West pit mining advances in the direction of east to west. Currently, the lower benches have reached the north, west, and south sides of the highwall with overall slope angles of 29°, 21°, and 20°, respectively. More detailed dimensions of lines that represent the highwalls are presented in Appendices (Figure A.12). The effect of overall slope angles increase by 1° in indicated directions is calculated with Maptek Vulcan 10.1 mining 3D software and the pit digital terrain model is illustrated in Figure 5.1.

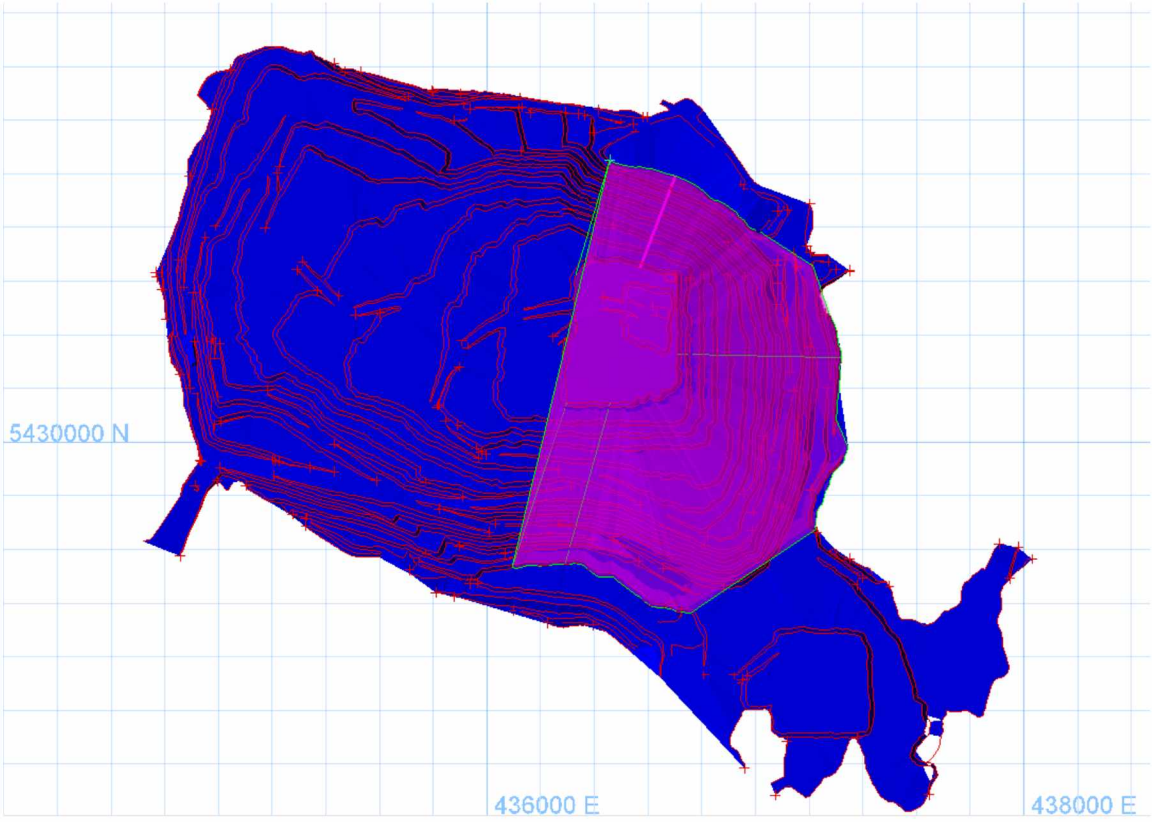

Figure 5. 1 Affected area in overall slope angle change

Due to the limitations of mining advances and pit geometry, the only portion of the less than half of the mine highwall overall slope angle is modified (pink color in Figure 5.1). The result shows that 5 M m3 (million cubic meter) earthwork could be saved with a 1° overall slope change from the North-West pit. The 5 M m3 earthwork represents $15 M, which is based on $2.98/m3 of mining cost, 2.6 months of work of 11 shovels, and 388 employees (EMC, 2017). The geometry of the north highwall is shown in Figure 5.2, which indicates an average overall slope angle of 28.97°, a height of 202.96 m, and a bottom length of 366.64 m.

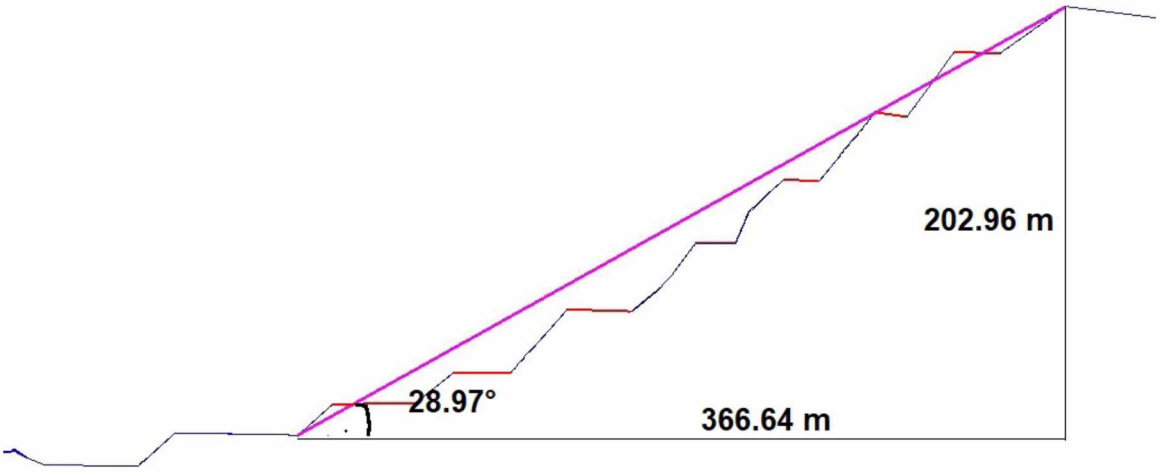

Figure 5. 2 Average overall slope angle and dimensions of north highwall

In order to increase the overall angle of north highwall by 1°, the average bench face angle should be increased by 4.8%, from 45.96° to 48.18°. The impact and sensitivity of this change on FOS have been discussed in Chapter 4. Based on the I-I North Flat1 cross-section model modification result, discussed in 4.4.3 Comparison 3, Chapter 4, a 1° increase of overall slope has an effect of decreasing 0.12 on FOS. Now there is an engineering trade of 0.12 on FOS for $15 million. Here its impact on the amount of mining earthwork converted to dollar amount is illustrated. Note that 5 M m3 earthwork ($15 M) can be saved from only a small portion of the open-pit. As mine depth increases in sixty and more years of mine-life, these values will be much more significant.

Charter 6

6. Summary and Suggestion

In this project, the slope stability of Erdenet mine's North-West open-pit is evaluated by dividing the pit into ten cross-sections of geological exploration. The FOS of each cross-section is calculated by *FLAC*, Fast Lagrangian Analysis of Continua, a 2D numerical modeling geotechnical software. The simulated overall FOS values of each cross-section are greater than the allowable mine FOS value of 1.5. However, individual bench stability was highly dependent on the loosened layer near the surface, which is damaged by production blasting. In addition to computer simulations for FOS analysis, real-time slope monitoring systems are introduced, and installation suggestions are provided. Any potential failure hazard found in either slope monitoring or computer simulation could be verified against each other. As a result, failure could be predicted to minimize the adverse effect.

Among all the cross-sections simulated in the study, the maximum, minimum and mean FOS values of Erdenet mine's current North-West open-pit are calculated as 4.13, 2.17, and 2.78, respectively. In the cases of 0.105g and 0.165g PGA earthquakes, the mean FOS values drop to 2.30 and 2.06, respectively. One of the deepest cross-sections, I-I North, is computed to have the least FOS value, 1.57 in 0.165g earthquake case, which is higher than suggested mine allowable FOS value. The fair correlation with 0.56 coefficient of determination, R-squared, between FOS and height of slope is found in linear regression. But FOS and overall slope angle have a poor correlation with 0.09 R-squared. The overall FOS could be increased by reducing individual bench angles, but its effect reduces in earthquake cases.

The effect of changes in the bench face angles and overall slope angles on slope stability and the amount of overburden removal is calculated. The result shows that just increasing the overall slope angle by 1° from the east half of the open-pit, approximately 5 million m3 overburden ($15 million cost work) removal could be saved. But the overall FOS drops by 0.12 unit. Therefore, the pit optimization in Erdenet Mine should be carried out by balancing slope stability and production profit improvement.

6.1 Suggestions for Erdenet Mining

- Pit slope optimization is strongly recommended.
- Sensitivity analysis should be conducted to optimize mine planning and overall slope angle.
- Controlled blasting techniques should be used to reduce highwall damage.
- A real-time monitoring system can be set to scan along the whole perimeter of the open-pit.
- A combination of slope monitoring and simulation is suggested. The observations from the monitoring process should be verified by the slope modeling simulation.
- The underground water level should be updated regularly to account for the effects of mining advance, drainage system, and the precipitation. It is one of the most critical factors defining the slope stability.
- The joint and discontinuity face mapping should be done simultaneously with the excavation. Right after the excavation, geological and geotechnical face mapping should be carried out on the fresh slope face. The more data is collected, the more knowledge we have about the rock mass.
- The mechanical properties of all types of rocks should be tested continuously.

6.2 Suggestions for future studies

- Three dimensional (3D) stability analyses should be conducted for a more representative and reliable result.
- A design simulation should be conducted for not only the current pit but also the final pit design of both North-West pit and central pit.
- The rock mass should be divided into local rock mass groups with more emphasis on the condition of joints and discontinuity.
- The discontinuities, tectonic faults, joints, and dyke should be tested and studied more to gain a better understanding of discontinuity condition.

- FOS does not give a linear scale of slope stability. Slope stability FOS does not correspond on a linear scale of the likelihood of failure. Due to uncertainties, larger FOS values are not always indicative of safer slopes. On the other hand, the probability of failure (PF) has a linear relationship with the likelihood of failure. For instance, a slope with a 10% PF is twice as stable as a slope with 20% PF. Thus, the acceptability criterion for slope stability should be represented by a combination of FOS and PF.

References

A New Rea in Slope Stability Analysis: Shear Strength Reduction Finite Element

Bye, A.R.& Bell, F.G. (April, 2001), Stability Assessment And Slope Design At Sandsloot Open-pit, South Africa. International Journal of Rock Mechanics and Mining Sciences, 38(3), 449-466. doi.org/10.1016/S1365-1609(01)00014-4

Cala,M. & Flisiak, J. (2001). Slope Stability Analysis with FLAC and Limit Equilibrium Methods. In Bilaux, Rachez, Detournay& Hart (eds.) *FLAC* and Numerical Modelling in *Geomechanics*: 111-114. A.A. Balkema Publishers.

Cala,M., Flisiak,J., Tajdus,A. (2004) Slope Stability Analysis With Modified Shear Strength Reduction Technique, Dept. Of Geomechanics, Civil Engineering & Geotechnics, State Committee for Scientific Research (Project No. 5 T12A 022 24) Retrieved from http://home.agh.edu.pl/~cala/papers/2004_7.pdf

Calderon, A.R. (n.d). The Application of Back-Analysis and numerical Modeling to Design a large Pushback In a Deep Open-pit Mine. [Master's thesis, Colorado School of Mines] Mountain Scholar, retrieved from https://mountainscholar.org/bitstream/handle/11124/170528/T5427.pdf?sequence=1

Carlà.T., Farinac.P., Intrierib.E, Ketizmend.E, Casaglib.N (2018). Integration Of Ground-based Radar and Satellite Insar Data for the Analysis of an Unexpected Slope Failure In An Open-pit Mine, doi.org/10.1016/j.enggeo.2018.01.021

Catanzariti.F. (13/06/2016), Slope Stability Analysis, Retrieved from https://www.geostru.eu/slope-stability-analysis/

Chen, G. (2019). MIN673-Advanced Rock Mechanics, Probabilistic Approach for the Analysis of Rock Excavation Stability. Session 10 notes [PowerPoint slides.]

Comparison to Other Methods. How does FLAC compare to the finite elements method of numerical modeling? (2019). Retrieved from https://www.itascacg.com/comparison-to-other-methods

Contreras, L.F.. (2015). An Economic Risk Evaluation Approach For Pit Slope Optimization. *Journal of the Southern African Institute of Mining and Metallurgy*, *115*(7), 607-622. https://dx.doi.org/10.17159/2411-9717/2015/V115N7A7

Donald.I.B., & Chen.Z. (1997), Slope Stability Analysis by the Upper Bound Approach: Fundamentals and Methods, Can.Geotech, Vol.34, Retrieved from https://www.nrcresearchpress.com/doi/pdf/10.1139/t97-061

EI-Ramly,H., Morgenstern,N.R., Cruden, D.M. (2002). Probabilistic Slope Stability Analysis for Practice, NRC Research Press Web Press Web, Retrieved from http://cgj.nrc.ca

EMC, (2018), Нэгдсэн Уурхайн Гидрогеологи Ба Инженер Геологийн Нарийвчилсан Судалгааны Тайлан, Ulaanbatar, Mongolia

EMC, (2017). Ил Уурхайн 2017 Оны Эхний Хагас Жилийн Үйлдвэрлэл, Эдийн Засаг, Аж Ахуйн Үйл Ажиллагааны Үр Дүнгийн Тайлан, Department of Open-pit, EMC

EMC, Production Index, Retrieved July 4, 2019 from https://erdenetmc.mn/en/operation/

Erdenet Mining Corporation. (2018). Feasibility Report of North-West and Central Pits of Erdenetiin-Ovoo Copper and Molybdenum Deposit, Ulaanbaatar, Mongolia

Fredlund D.G. & Krahn J. (April 4, 1977). Comparison of slope stability methods of analysis, Canadian Geotechnical Journal, 429-439, https://doi.org/10.1139/t77-045

FLAC 8 Basics, (2015), An Introduction to FLAC 8 and A Guide To Its Practical Application In Geotechnical Engineering

GEO-SLOPE, (2012). Stability Modeling With SLOPE/W. An Engineering Methodology November 2012 Edition, Retrieved from http://downloads.geo-slope.com/geostudioresources/8/0/9/books/slope%20modeling.pdf?v=8.0.10.6

GEOtest Final Report, (2018), Complex Research for Geotechnical Condition of Integrated Open-pit Mine, Prague and Brno, Czech Republic

Kashani,a.G., Olsen.M.J., Parrish.C.E., Wilson.N. (2015). a Review Of LIDAR Radiometric Processing: From Ad Hoc Intensity Correction To Rigorous Radiometric Calibration, Sensors 2015, 15. Doi:10.3390/S151128099

Kim, Y., Lee, I., Oyungerel, S., Jargal, L. (2018). Cu and S Isotopic Signatures of the Erdenetiin Ovoo Porphyry Cu-Modeposit, Northern Mongolia: Implications for Their Origin and Mineral Exploration, *Ore Geology Reviews, Retrieved from* doi.org/10.1016/j.oregeorev.2018.11.025

Krahulec, K. (September 2016), Bingham Canyon's Manefay Landslides and the Future of the Mine, Utah Geological Survey, Survey Notes, 48(3) Retrieved from https:// geology.utah.gov/map-pub/survey-notes/bingham-canyon-manefay-landslides/

Lidar Magazine. (2019). Sentry Safe, Continuous Mine Monitoring Extended to Cold Climates. https://lidarmag.com/2019/03/07/sentry-safe-continuous-mine-monitoring-extended-to-cold-climates/

Manga. M. Wang. C.-Y. (2015). 4.12 –Earthquake Hydrology. Treatise on geophysics (Second Edition). Vol.4. p 305-328. https://doi.org/10.1016/B978-0-444-53802-4.00082-8

Maptek I-Site, (2008). Laser scanning in extreme conditions. Case study. https://www.maptek.com/pdf/i-site/case_studies/Maptek_I-Site_diavik_diamonds_casestudy.pdf

Maptek. (n.d.). Maptek Drive https://www.maptek.com/products/scanners/drive.html

McHugh.E.L., Dwyer,J., Long.D.G., Sabine.C., (2006). Applications Of Ground-Based Radar To Mine Slope Monitoring, Report Of Investigations 9666. Retrieved from https://www.researchgate.net/publication/228700377_Applications_of_ground-based_radar_to_mine_slope_monitoring

Memon,M.Y. (2018). A Comparison Between Limit Equilibrium and Finite Element Methods for Slope Stability Analysis, ResearchGate. DOI: 0.13140/RG.2.2.16932.53124

Miller, S.M. (1984), Probabilistic Rock Slope Engineering. Washington, DC, Department of the Army US Army Corps of Engineers

Monserrat.O., Crosetto.M., Luzi.G. (2014). A Review Of Ground-based SAR Interferometry For Deformation Measurement, ISPRS Journal Of Photogrammetry And Remote Sensing, http://dx.doi.org/10.1016/j.isprsjprs.2014.04.001

Pagani, M., Garcia-Pelaez, J., Gee, R., Johnson, K., Poggi, V., Styron, R., Weatherill, G., Simionato, M., Viganò, D., Danciu, L., Monelli, D. (2018). Global Earthquake Model (GEM) Seismic Hazard Map (version 2018.1 - December 2018), DOI: 10.13117/GEM-GLOBAL-SEISMIC-HAZARD-MAP-2018.1

Phase2 8.0 Excavation &Support Design Software (n.d.). Retrieved June 23, 2019, https://www.rocscience.com/documents/pdfs/uploads/8481.pdf

Priest, S. D., & Brown, E. T. (1983). Probabilistic stability analysis of variable rock slopes. *Transactions of Institution of Mining and Metallurgy, Section A*, pp. A1-12.

Read, J., & Stacey, P. (2009). *Guidelines for Open-pit Slope Design.* Collingwood: CSIRO.

Rockslide Mapping in Norway by Means of Interferometric SAR Time Series Analysis –Scientific Figure on ResearchGate. Available from:https://www.researchgate.net/figure/Simplified-geometry-of-a-synthetic-aperture-radar-SAR-system_fig1_50280789 [accessed 27 Apr, 2019]

RS2, (2019) Rocscience Inc. retrieved fromhttps://www.rocscience.com/software/rs2

Ruijie, W., Chong, L., Jinhai, X., & Lijin, P. (2018). Development and verification of large deformation model considering stiffness deterioration and shear dilation effect in FLAC3D, *International Journal of Mining Science and Technology*, 28(6), 959-967, https://doi.org/10.1016/j.ijmst.2018.06.008

Singh, T.N., Gulati, A., Dontha, V., Bhardwaj, V.(2008), Evaluating Cut Slope Failure By Numerical Analysis-A Case Study, Nat Hazards, Springer Science+Business Media B.V. DOI 10.1007/s11069-008-9219-5

Technique (n.d.). Retrieved from https://www.rocscience.com/documents/pdfs/library/StrengthReduction.pdf

Turbide.S., Marchese.L., Terroux.M., Bergeron.A. (2014). Synthetic Aperture Lidar As A Future Tool For Earth Observation, International Conference On Space Optics—icso 2014 , Retrieved from https://www.spiedigitallibrary.org/conference-proceedings-of-spie

Valenta, J., Polák, M., Mrvík, O., Bláha, P., Pavlík, J., Zapletal, A.,Francírek, M.,Černý, M., (2018). Complex Research for Geotechnical Conditions of Integrated Open-pit Mine

Wesseloo, J. and Read, J. (2009). Chapter 9 - Acceptance Criteria. In: Guidelines for Open-pit Slope Design, J. Read and P. Stacey (eds), pp 221-236. CIRSO publishing. 496p.

Wessels.S.D.N., (2009), Monitoring And Management Of A Large Open-pit Failure, Retrieved from https://core.ac.uk/download/pdf/39667612.pdf

Yang, Y., Sun, G., Zheng, Z., Qi, Y. (2019), Investigation Of The Sequential Excavation Of A Soil-Rock-Mixture Slope Using The Numerical Manifold Method, *Engineering Geology*, 256 (2019) 93-109, Retrieved from https://doi.org/10.1016/j.enggeo.2019.05.005

Wyllie, D.C., & Mah,C.W. (2004). *Rock Slope Engineering.* (4th ed.). Spon Press. London and New York.

Appendices

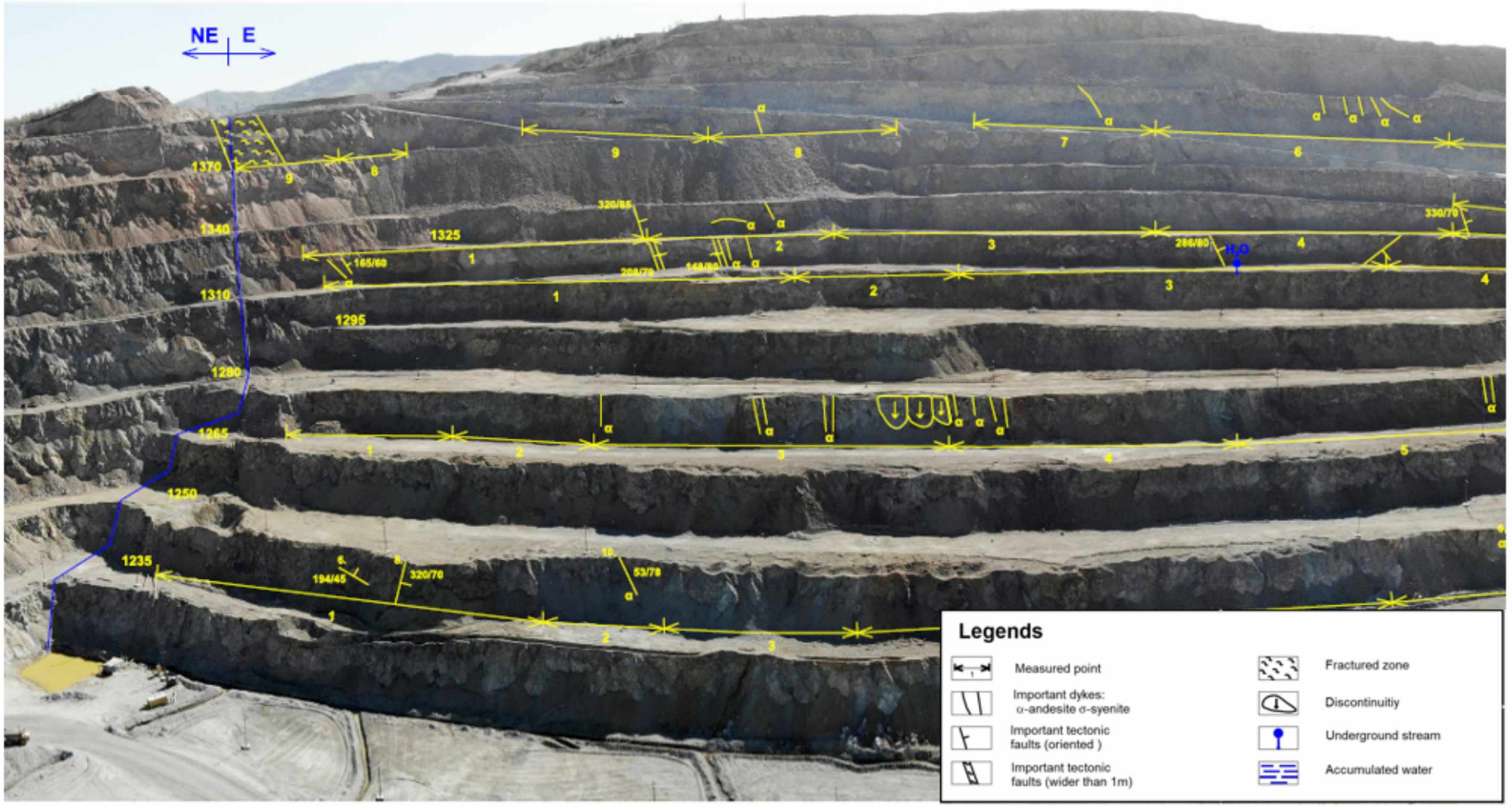

Figure A. 1 East highwall (GEOtest, 20018)

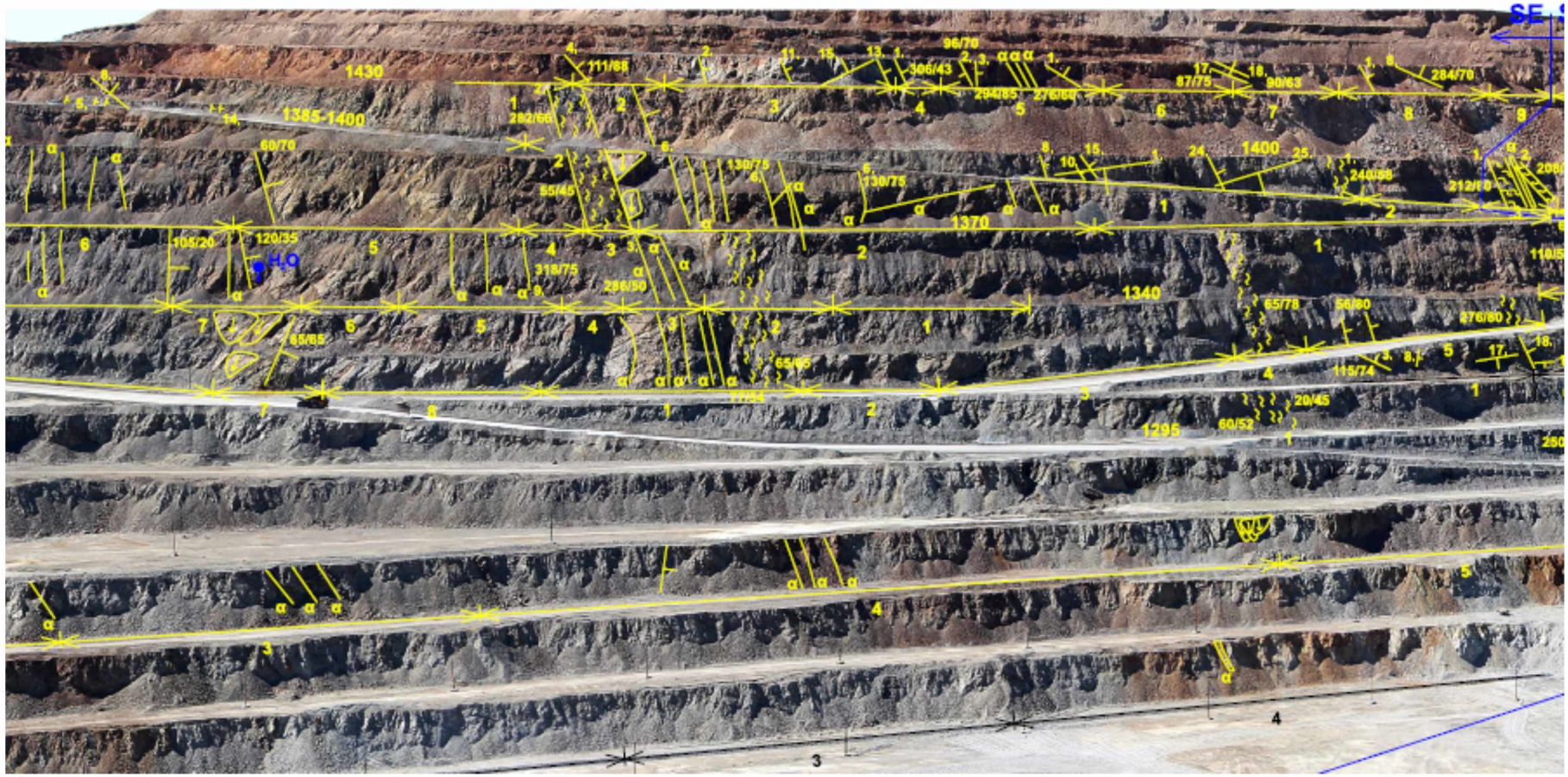

Figure A. 2 South highwall (GEOtest, 20018)

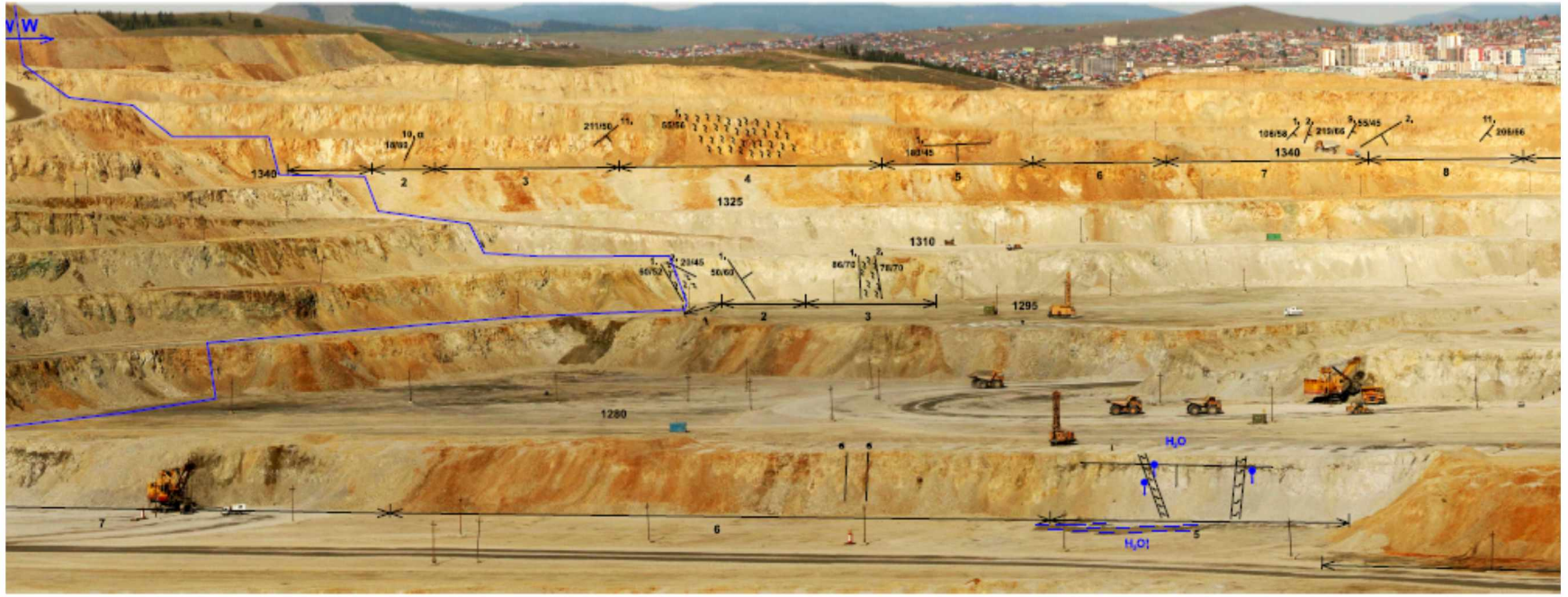

Figure A. 3 West highwall (GEOtest, 20018)

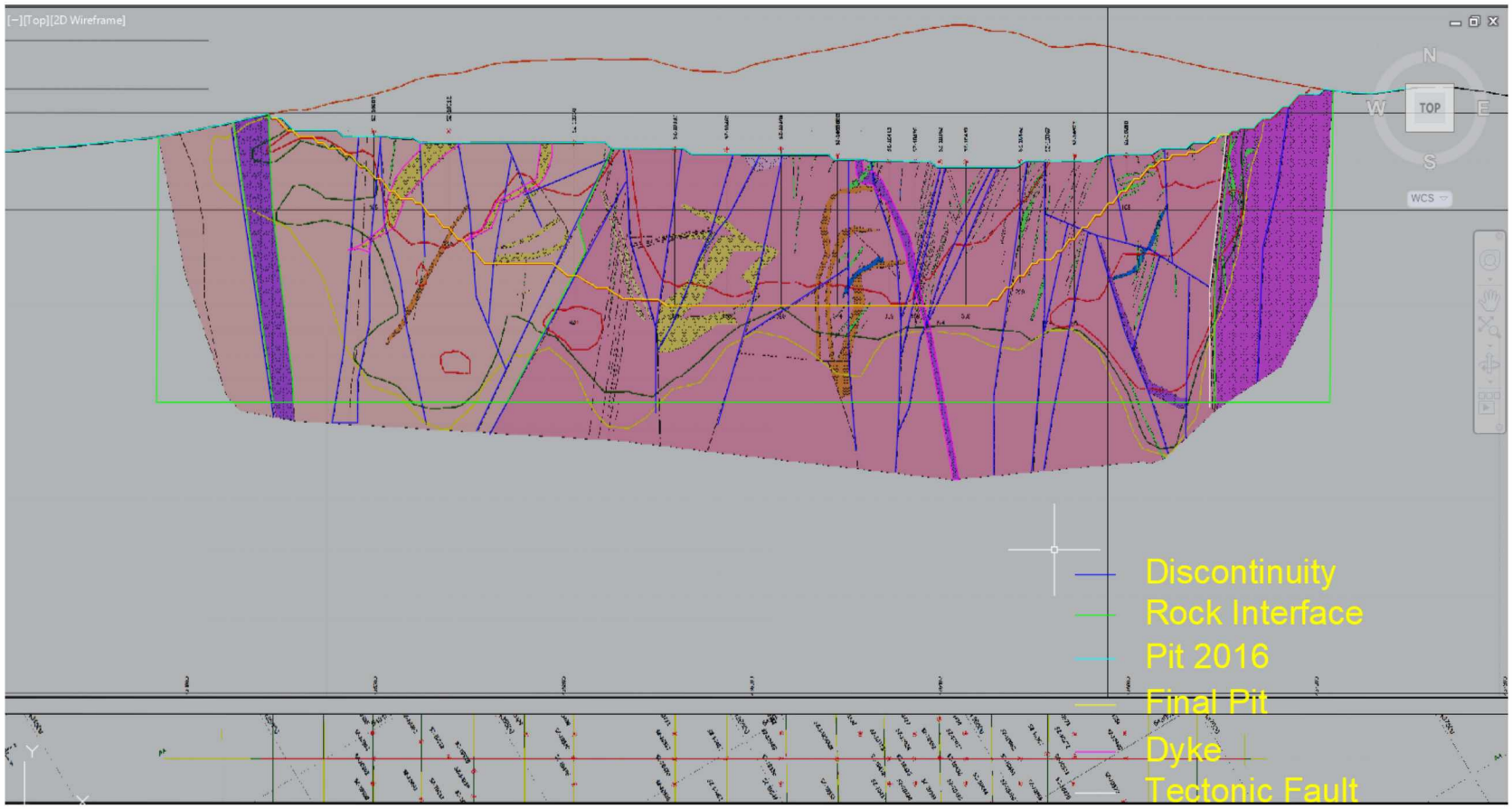

Figure A. 4 The A-A cross–section drawn by autoCAD 2018 program

Material 1	
Hoek Brown Classification	
intact uniaxial compressive strength	88 MPa
GSI	45
mi	29
disturbance factor	0
intact modulus	50000 MPa
Hoek Brown Criterion	
mb	4.067
s	0.002
a	0.508
Failure Envelope Range	
application	slopes
sig3max	3.785 MPa
unit weight	0.026 MN/m3
slope height	175 m
Mohr Coulomb Fit	
cohesion	1.675 MPa
friction angle	52.504 deg
Rock Mass Parameters	
tensile strength	-0.048 MPa
uniaxial compressive strength	3.945 MPa
global strength	23.266 MPa
modulus of deformation	11182.497 MPa

Figure A. 5 Rock mass tensile strength calculated by RocData 5.0 software

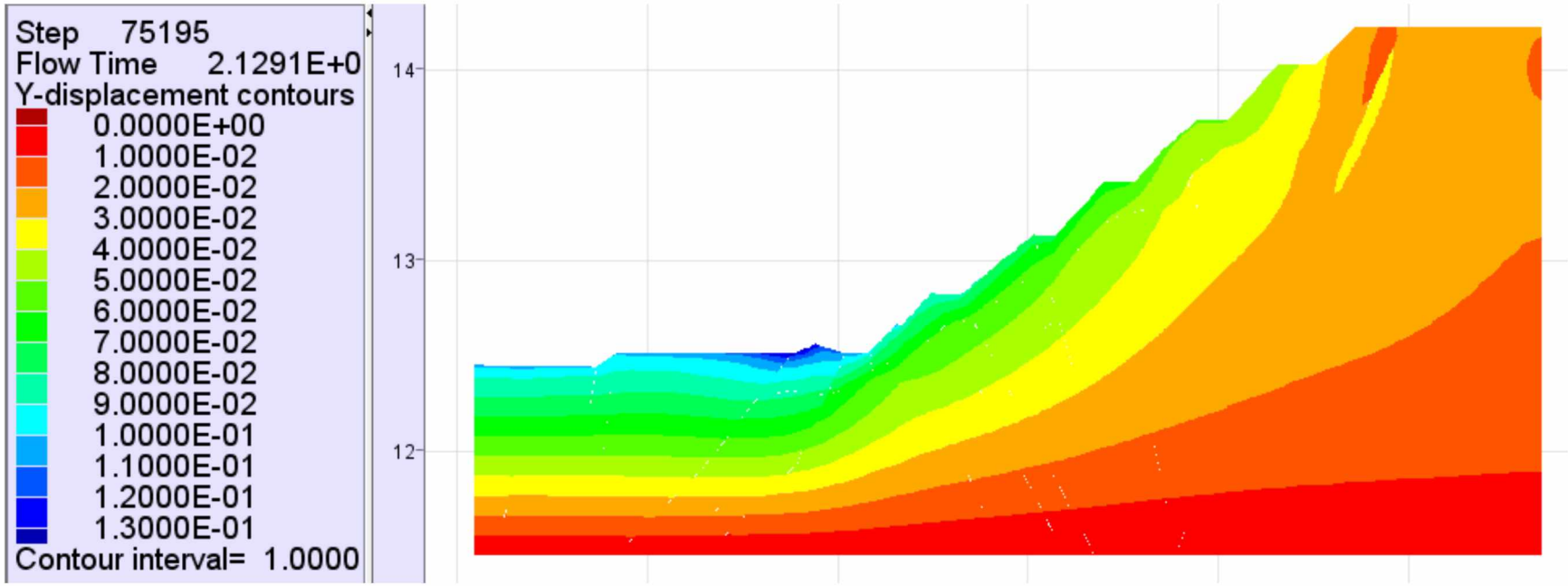

Figure A. 6 Actual Y-displacement contour of I-I North cross-section

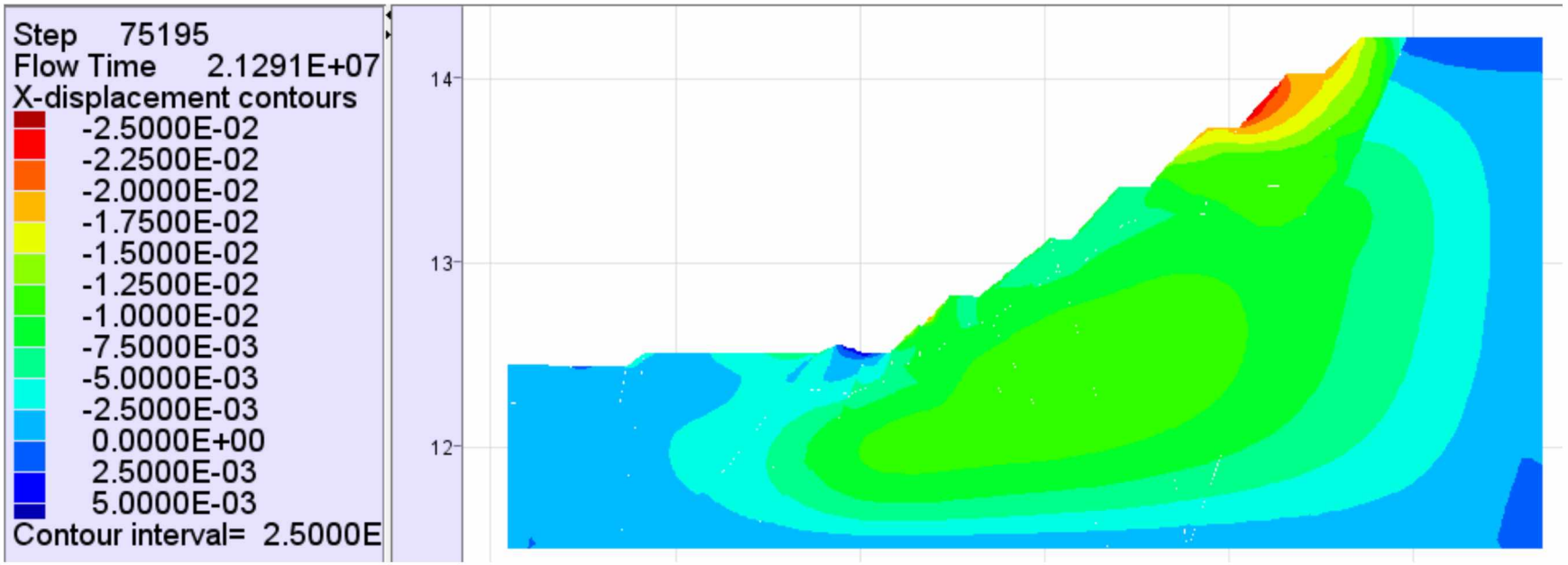

Figure A. 7 The actual X-displacement contour of I-I North cross-section

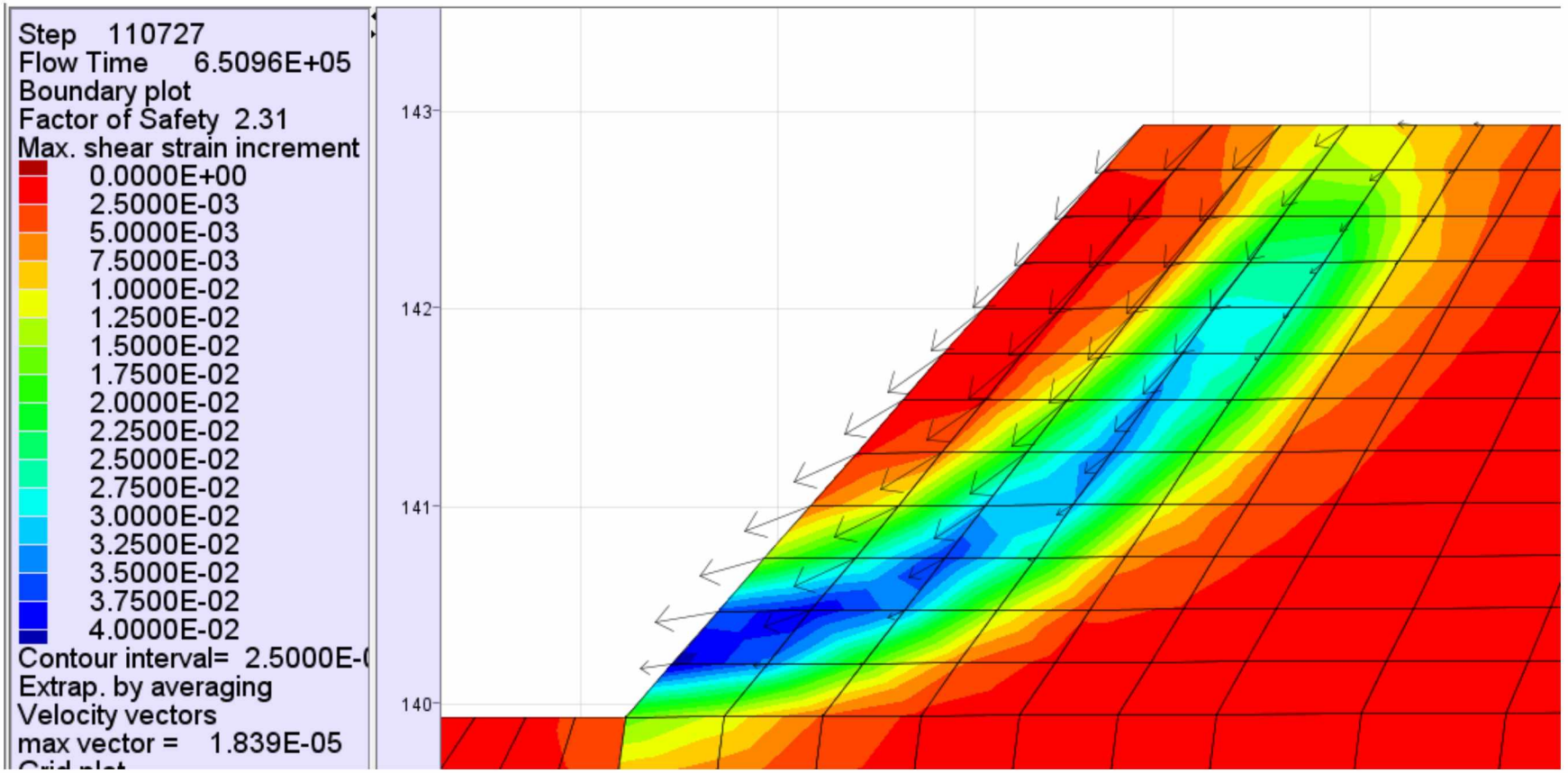

Figure A. 8 Velocity vector of A-A_E cross-section

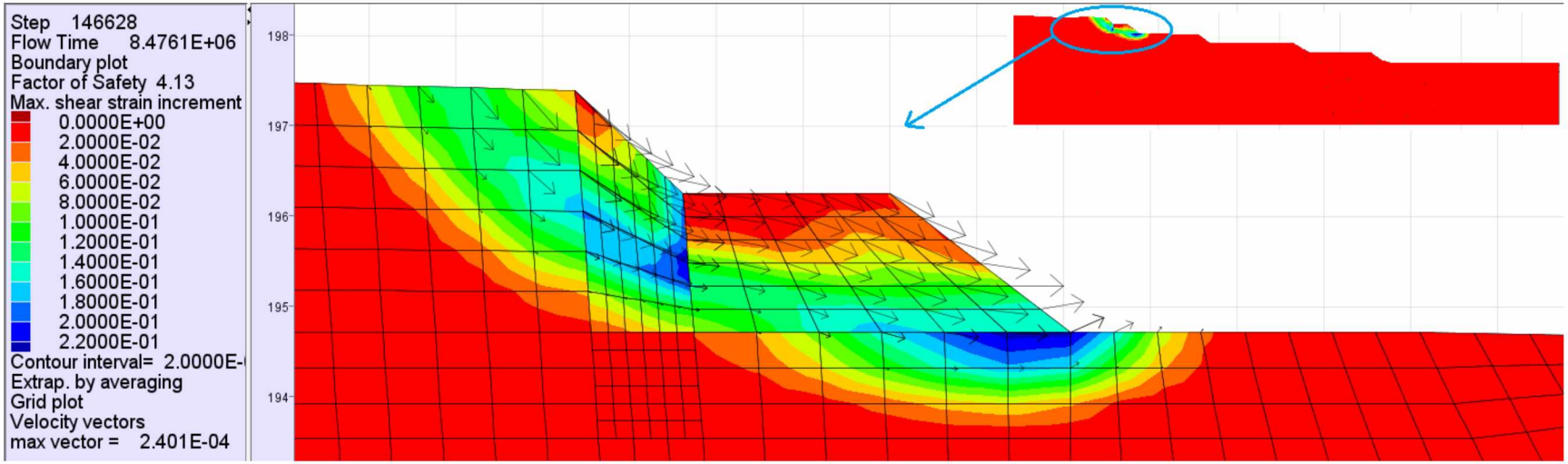

Figure A. 9 Potential failure of XVIII-XVIII South cross-section

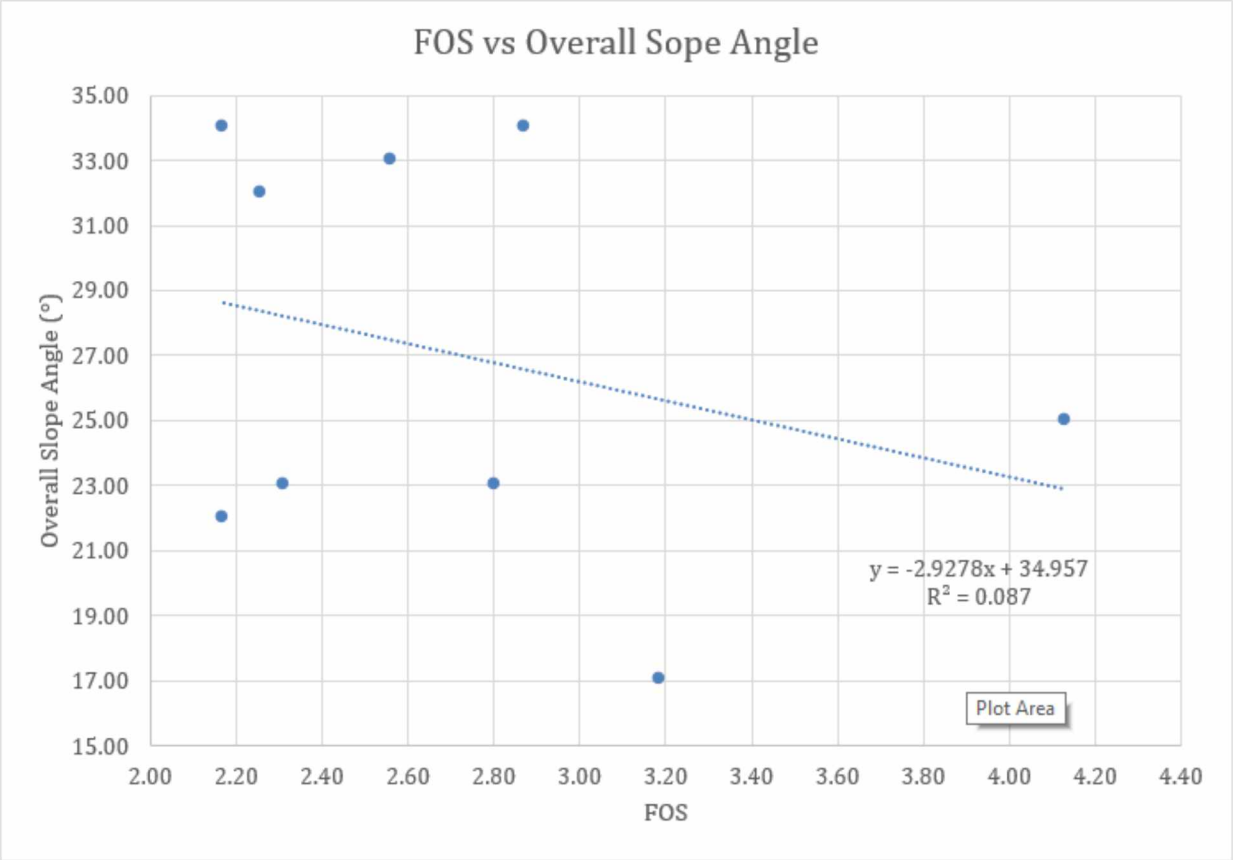

Figure A. 10 FOS vs Overall slope angle

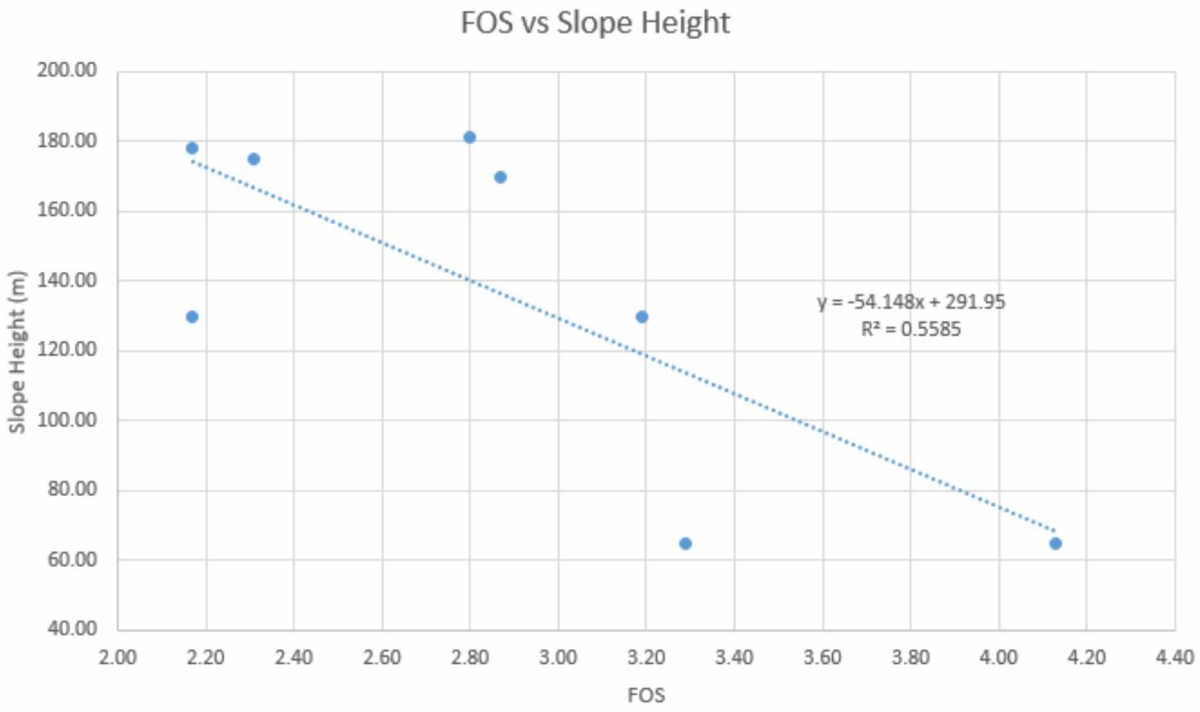

Figure A. 11 FOS vs Slope height

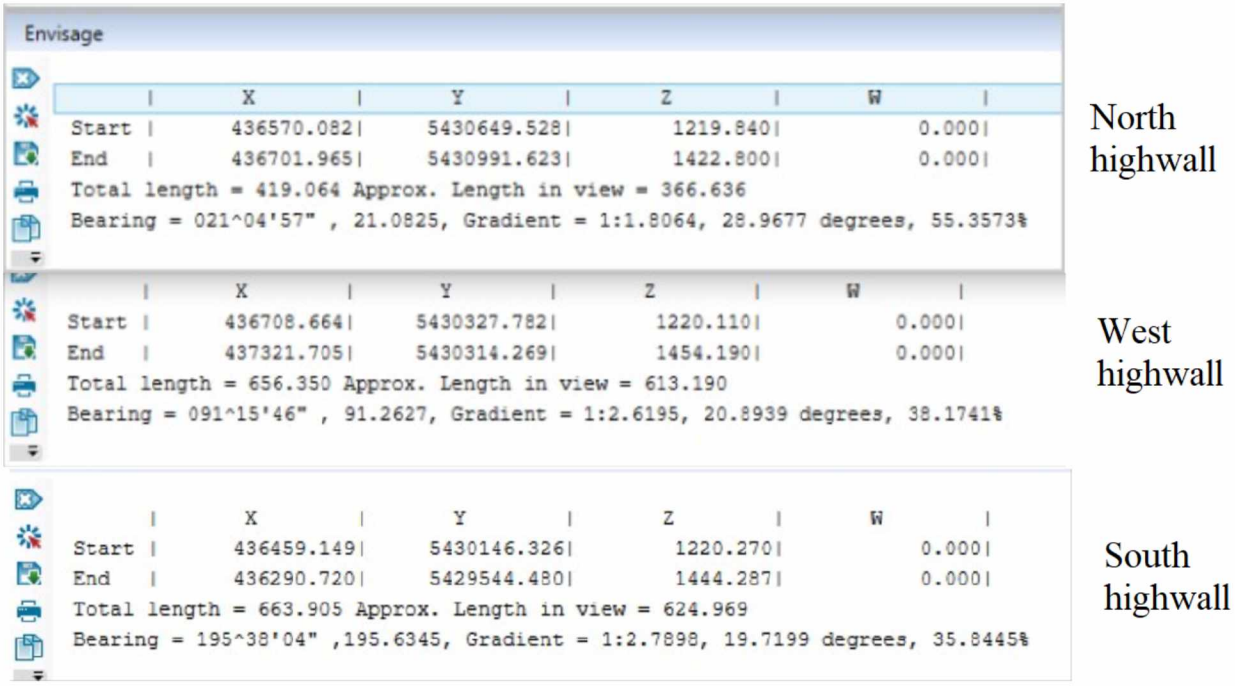

Figure A. 12 Geometrical dimensions highwalls used in volume calculation